Ph.D.

2011

H.Matsui

Investigation into the 3D structure of the developing human fetal heart

Hikoro Matsui, M.D.

Submitted in fulfilment of the requirements of the degree of Doctor of Philosophy,

Imperial College London, London, United Kingdom

Clinical Research Fellow

Perinatal Cardiology

Department of Surgery and Cancer

Faculty of Medicine

Imperial College of Science and Technology and Medicine

London

Supervisors:

Doctor Helena M Gardiner, Professor Siew Yen Ho, Doctor Timothy J Mohun, Doctor Sailesh Kumar

To Kanro, Takuro, Tomoro and Yumiko

Acknowledgements

I would like especially to thank the following people:

- Dr Helena M Gardiner, for her enthusiasm;
- Professor Siew Yen Ho, for her generous encouragements, significant suggestion and all supports in this research;
- Dr Timothy J Mohun, for his professional suggestions and superb supports in the most parts of this research;
- Dr Sailesh Kumar, for his suggestions in this research;
- Mr Michael Bennett and Mrs Louisa Dunlevy, for their great cooperation and help in all HREM processing and HREM study in the mouse;
- Mr Michael Stafford and Dr Claudine Domoney, for their kind help in collection of samples at Chelsea and Westminster Hospital;
- Professor Phillip R Bennett, for his kind help in collection of samples at Hammersmith Hospital;
- Mrs Wendy Weston, for her special supports in carrying out this research;
- Dr Liat Gindes, for her great cooperation in the clinical research;
- The staff of the developmental biology at National Institute of Medical Research, for their help in the basic research;
- The staff of the Cardiac Morphology Unit at Royal Brompton Hospital, for their help in the basic research;

And Finally:

- To the parents of all fetuses, and the fetuses themselves who kindly participate in this study.

Author's Declaration

I declare that the work presented in this thesis is original. I carried out all plans and have never applied to any other degree of this or other universities.

Funding

I am grateful for the financial support of:

Tiny Tickers (supported from October 2006 to August 2008) and

Richard and Jack Wiseman Trust (supported from September 2008 to September 2009)

for their generous support of this work.

Abstract

Investigating the developmental processes of the human fetal heart is a challenging task. Few reports describe the morphological features during the first stage of heart maturation and consecutive developmental periods after cardiogenesis. Reasons for this include the difficulty of collecting suitable samples and the limitations of investigating modalities. This research was proposed to clarify the detailed morphological features of normal human fetal hearts in early-stage maturation, using post-mortem samples. These samples were analysed using high-resolution episcopic microscopy (HREM), and compared with the latest clinical imaging taken by 3D fetal echocardiography and compared with mouse samples.

HREM, a newly-developed high-quality image modality, produces a computer-based 3D reconstruction which enables us to visualize detailed spatial structures of small specimens. HREM includes several procedural steps, which may affect the histological or morphological structures of samples, so I explored the potential effects. I found 12% shrinkage due to dehydration and polymerization. Therefore, while the general appearance of 3D reconstructed images looked identical to the pictures of the original heart samples, it is important to consider the effects of shrinkage when interpreting the morphological assessment by HREM.

Normal human fetal hearts from the 9th to 11th weeks of postmenstrual gestation demonstrated unique morphological findings. Ventricular walls and trabeculations showed thick and random cellular structures. Atrioventricular and semilunar valves were also thick but histological maturation was observed within a few

weeks after cardiogenesis. The great arterial walls were thick and comprised of dense cellular matrix. Morphologically, several characteristic findings, such as large atrial appendages, the developmental process of formation of the membranous ventricular septum and prominent coronary arteries, were recognised during this period. Heart size increased linearly with gestation. Normal human fetal hearts demonstrate geometrical development and histological and morphological maturation after the period of cardiogenesis.

In comparison with human fetal hearts, mouse hearts demonstrate dramatic morphological alterations during a short maturation period. Fetal mouse hearts show some similar morphological findings to the human fetal heart, such as large atrial appendages, lack of formation of the membranous septum, and thickened great arterial walls. This suggests a shared mechanism of fetal heart maturation in mammals.

Detailed clinical information regarding cardiac morphology is vital for accurate prenatal heart diagnosis in the first trimester. Fetal echocardiography in early gestation has become routine practice. However, the technical limitations of image acquisition and picture resolution make it difficult to visualize clear 3D images for fetal cardiac diagnosis. Current modalities for clinical investigation by 3D echocardiography do not have sufficient resolution to enable detailed morphological investigation of the human fetal heart between 10th to 12th weeks of postmenstrual gestation. Only the original data of the four-chamber view demonstrated no offsetting of the atrioventricular valves as seen on HREM. Further technical advances in 3D

echocardiography will be required to enable precise cardiac diagnosis in the first trimester.

This thesis describes morphological development in normal human fetal hearts for the first few weeks after cardiogenesis and contributes to a better understanding of the normal appearances in the first trimester which is vital for future investigation into the origin of congenital heart disease.

Table Content

1.0 Chapter One: Background and Literature Review

1.1 Introduction

1.2 Normal Heart Structure

1.3 Fetal Heart Development

1.3.1 Introduction

1.3.2 Cardiogenesis in the human

1.3.3 Heart maturation in the human

1.3.4 Difference between the human and the mouse

1.4 Morphological Investigation of the Fetal Heart

1.4.1 Conventional morphological examination of the human fetal heart in the first and early second trimester

1.4.2 Conventional computer based three dimensional reconstruction using histological sections

1.4.3 Episcopic image capturing

1.4.4 High Resolution Episcopic Microscopy

1.4.5 Other three dimensional imaging modalities for investigation of the heart in embryos

1.4.6 Comparison of image quality between HREM and other imaging modalities

1.4.7 Three dimensional reconstruction of the human fetal heart

1.5 Morphological Investigation by Three Dimensional Fetal Echocardiography

1.5.1 History of morphological investigation of cardiac structures by fetal echocardiography

1.5.2 Morphological assessment of fetal heart in the first trimester by 3D fetal echocardiography

1.6 Limitation and Issue of Investigation into the Developing Human Fetal Heart

1.6.1 Limitation of the investigation into the developing human fetal heart

1.6.2 Current issue of morphological investigation into the human fetal heart

1.7 Study Aim and Hypothesis

1.7.1 Study aim

1.7.2 Hypothesis

2.0 Chapter Two: Method (Research Facility, Ethical approval, Study Population and Technique)

2.1 Research Facility

2.2 Ethical Approval

2.3 Study Population

2.3.1 Study population for the research using human fetal hearts

2.3.1.1 Study population

2.3.1.2 Parent's consent and sample collection

2.3.1.3 Sample registration and transportation

2.3.1.4 Sample quality

2.3.2 Study population for the research using human fetal hearts from postmortem specimens

2.3.3 Study population for the research using mouse hearts

2.3.4 Study population for the clinical research

2.4 Technique

2.4.1 High Resolution Episcopic Microscopy

2.4.1.1 Principle

2.4.1.2 Trimming samples

2.4.1.3 Preparation

2.4.1.4 Embedding

2.4.1.5 System

2.4.1.6 Sectioning and capturing

2.4.1.7 Data processing

2.4.1.8 Qualitative 3D data assessment (volume rendering and multi-planar reconstruction)

2.4.1.9 Quantitative 3D data assessment (length and volume)

2.4.2 Measurement of length of morphological specimens by a microscope

2.4.2.1 Measurement of length by an eyepiece graticule

2.4.2.2 Measurement of length by digitally acquired pictures

2.4.3 Histological staining using plastic embedded sections

2.4.4 Three dimensional fetal echocardiography

2.4.4.1 Spatio-Temporal Image Correlation (STIC)

2.4.4.2 Data analysis

3.0 Chapter Three: Validation of Morphometry in High Resolution Episcopic Microscopy

3.1 Introduction

3.2 Subjects and Methods

3.3 Results

3.4 Discussion

4.0 Chapter Four: Qualitative and Quantitative Morphological Investigation of the human fetal heart

4.1 Introduction

4.2 Subjects and Methods

4.2.1 Qualitative 3D data assessment

4.2.2 Quantitative 3D data assessment of the heart

4.2.3 Quantitative 3D data assessment of the great arteries

4.3 Results

4.3.1 Qualitative assessment

4.3.2 Quantitative assessment

4.4 Discussion

5.0 Chapter Five: Morphological Difference of the heart between the human and the mouse

5.1 Introduction

5.2 Subjects, Methods and Results

5.3 Results

5.4 Discussion

6.0 Chapter Six: Comparing in-Vitro and in-Vivo "state of the art" imaging of the Human Fetal Heart

6.1 Introduction

6.2 Subjects, Methods

6.3 Results

6.4 Discussion

7.0 Chapter Seven: Conclusion

List of Tables

Chapter One

Table 1-1 Carnegie stage of the human and the mouse

Table 1-2 Comparison of 3D imaging modalities for cardiac investigation

Chapter Two

Table 2-1 Success rate of maternal consent and collecting heart samples

Table 2-2 Availability of normal and 1 abnormal hearts

Table 2-3 Solution for preparation and embedding

Table 2-4 Protocol and Time schedule for the preparation

Table 2-5 Details of products in HREM system

Table 2-6 Hardware and Software for data processing

Table 2-7 Protocol of Haematoxylin-Eosin stain for HREM sections

Chapter Three

Table 3-1 Protocol of Measurement of Mouse Heart Samples

Chapter Four

Table 4-1 List of measurement of length

Table 4-2 Cases of Offsetting of Atrioventricular valves

Table 4-3 Linear regression of parameters of the fetal heart by HREM

Table 4-4 Linear regression of external diameter and wall thickness of great arteries

Chapter Five No Table

Chapter Six

Table 6-1 Quality of four-chamber view by post-menstrual gestational weeks

List of Figures

Chapter One

Figure 1-1 Morphology of normal human hearts

Figure 1-2 Gestational period in human and difference between embryonic and post menstrual weeks

Figure 1-3 Timeline of cardiogenesis

Figure 1-4 Gestational difference in the mouse and the human

Figure 1-5 Pictures of human Fetal Hearts in the early second trimester

Figure 1-6 Images of multiple sectioned human fetal heart

Figure 1-7 Pictures of human fetal heart at 9 post menstrual weeks

Figure 1-8 Conventional 3D reconstruction of the heart using histological slides in embryos

Figure 1-9 Flowchart of conventional image capturing of histological slides and Episcopic image capturing

Figure 1-10 3D Volume rendered images of the mouse fetal heart by EFIC

Figure 1-11 Volume rendered 3D images of the mouse fetal heart

Figure 1-12 Comparison image quality between micro MRI and HREM

Figure 1-13 Computer-based 3D reconstruction of the human heart in early days

Figure 1-14 Pictures and cardiac 3D images of normal (upper) and abnormal (lower) human embryos

Figure 1-15 Pictures of EFIC images of the human fetal heart

Chapter Two

Figure 2-1 Flowchart of HREM processing

Figure 2-2 Sample before and after dissection and unnecessary tissue

Figure 2-3 Flowchart of HREM preparation

Figure 2-4 Embedding moulds and embedded samples

Figure 2-5 HREM system

Figure 2-6 Flowchart of HREM data acquisition

Figure 2-7 Flowchart of optimisation of digital images

Figure 2-8 Calibration of voxel data to create a volume dataset

Figure 2-9 Examples of various image setting of 3D VR image of a human fetal heart

Figure 2-10 Examples of VR image and MPR image of the human fetal heart

Figure 2-11 Geometrical measurement of 3D images

Figure 2-12 Flowchart of the microscopic measurement using graticule in the eyepiece

Figure 2-13 Example of digital measurement

Figure 2-14 Standard planes of MPR image in 3D echocardiography

Chapter Three

Figure 3-1 Microscopic measurement in each step during HREM process

Figure 3-2 Appearance of 10 fetal mice hearts (E18.5) before and after HREM

Figure 3-3 Results of microscopic measurement and comparison of each step of HREM process

Chapter Four

Figure 4-1 Measuring points in each standard image

Figure 4-2 Images of morphometry of great arteries

Figure 4-3 Atrial morphology in the first trimester

Figure 4-4 Offsetting of Atrioventricular valves

Figure 4-5 Images of Atrioventricular Junction

Figure 4-6 Fetal ventricular morphology in the first trimester

Figure 4-7 Images of semilunar valves

Figure 4-8 Thickened great arterial wall

Figure 4-9 Coronary arteries in the late first trimester

Figure 4-10 Graphs of morphometry of length parameters in four chamber view

Figure 4-11 Morphometry of the inlet and the outlet components in the right and the left ventricles

Figure 4-12 Ventricular mass volume

Figure 4-13 Graphs of external diameter and wall thickness in the pulmonary trunk and the aorta

Chapter Five

Figure 5-1 Additional measuring points for morphometry

Figure 5-2 External feature of the mouse fetal heart

Figure 5-3 Atrial structure in the mouse fetal heart

Figure 5-4 Atrioventricular junction in the mouse fetal heart

Figure 5-5 Ventricular structure of the mouse fetal heart

Figure 5-6 Structure of the semilunar valves and great arteries

Chapter Six

Figure 6-1 Visual quality of original images of 3D volume data by echocardiography

Figure 6-2 Quality of images

Figure 6-3 Comparison of MPR images acquired by HREM and 4DTV

Figure 6-4 The level of the atrio-ventricular valves by 4DTV

Figure 6-5 Comparison of measurement of ventricular length and width using 4DTV echocardiography and HREM

Figure 6-6 Four chamber view of 14 weeks' of human fetal heart from clinical practice

1.0 Chapter One

Background and Literature Review

1.1 Introduction

Investigation into the developmental processes of heart growth in the human is a challenging task. Knowledge of phenotype in the normal and the abnormal developing heart could be the first step for understanding the mechanism of heart development. Furthermore, elucidating its regulatory factors may be vital for the treatment of heart diseases in paediatric patients because almost all heart diseases affecting children are congenital structural malformations resulting from abnormal morphogenesis. There are two major periods regarding the abnormal morphogenesis during fetal life. (O'Rahilly and Muller 1987) The first is the embryonic period when the organogenesis of the cardiovascular system is almost established within about 50 embryonic days in the human (approximately nine weeks of post-menstrual gestation). The cellular segmentation from zygote results in transformation and construction of the complex heart during this period. The second is the maturational stage, which continues for more than 30 weeks after the embryonic period in the human. The maturation occurs during this stage and the heart increases in size by the end of pregnancy. Cardiac function matures during this period as well.

However, it is not easy to investigate the developmental features of the human fetal heart because of the following four reasons. The first is the difficulty in obtaining parental consent to collect samples of human fetal hearts. These samples need to be collected from cases at termination of pregnancy (TOP) or fetal demise with the consent of the mother for whom it may be a difficult time emotionally to donate fetal tissue for research. The second is that collecting samples is technically difficult in

certain gestational weeks when TOP is surgically possible (in general from about six to seventeen post menstrual weeks of gestation) because the damage to the fetal heart by the surgical procedure is sometimes too severe to obtain a useful sample for research. Bullen et al reported their failure to collect human fetal samples by aspiration during TOP in the first 38 cases. (Bullen, Robson et al. 1998) The third problem is medical TOP makes the heart insufficient for morphological or molecular investigations because long period from fetal demise to delivery causes lysis of organs. The fourth issue is the technical limitation of assessment of the heart structure, especially in small samples. The conventional method for investigating a small heart in the first trimester is histological sectioning, resulting in difficulty of three-dimensional (3D) investigation although the basic morphological assessment is 3D observation. Thus, few reports regarding detailed heart morphology in the early maturational stage of the human fetus are available to date in spite of the many animal models and reports.

In some congenital heart diseases it is believed that altered growth patterns after embryogenesis effect growth of the heart and result in ventricular hypoplasia, myocardial hypertrophy or hypoplasia of vessels. Hypoplastic left heart syndrome (HLHS), one of the most severe forms of congenital heart disease, shows a variety of phenotypes, which suggests a cessation of growth at one of several points after embryogenesis. (Hornberger, Sanders et al. 1995) Although there are many reports regarding embryogenesis of the heart in the human, few reports regarding the heart structure after organogenesis in early gestation are available because of the inherent

difficulties of investigation. One report by Allan et al described the utility of the morphological assessment of early human hearts by manual handling. (Allan, Santos et al. 1997) Therefore, detailed documentation of normal morphological features in the early fetal heart is an essential first step towards establishing the origins of the abnormal development of fetal cardiac malformations.

Recent advanced digital technology has allowed us to analyse the detailed structure of the heart in experimental samples. Therefore, I propose in this research to document morphological investigation of the normal human heart in early gestation (from nine to seventeen post-menstrual weeks) using High Resolution Episcopic Microscopy (HREM), which is a newly-developed analysing technology producing 3D digital capture of small samples. Documenting the morphological features at each step of the developing heart will be an essential first step towards understanding the origins of fetal cardiac abnormalities and devising potential therapies.

1.2 Normal Heart structure

Knowledge of the normal heart structure in children and adults is essential for proper understanding of abnormal or fetal heart anatomy. Morphological investigation of the heart is a fundamental skill for the diagnosis of a normal heart or a wide variety of congenital cardiovascular diseases. Proper description of the structure and understanding of the morphological features in the normal heart will be the first step in the assessment of heart anomalies. Combining an accurate morphological description with haemodynamic assessment will contribute to the appropriate surgical strategy in patients with congenital heart defects. Thus, morphological assessment of the heart is the most vital skill for children with congenital heart malformations.

Morphology of the heart has to be described by accurate terminology and classification. Historically, many classifications of congenital heart disease described by Edwards and his group at the Mayo Clinic in early days, has had a profound affect on current morphological description. (Edwards and Chamberlin 1951; Edwards 1953) They reported some cases with cardiac malformation and aortic arch anomalies suggesting that disturbance of prenatal embryogenesis or abnormal fetal circulation resulted in congenital heart disease. Under the influence of Edwards' group, two major nomenclatures of morphological terminology describing detailed structure of congenital heart disease has been established, one is the work of Van Praagh's group and the other is by Anderson's group.(Tynan, Becker et al. 1979; Anderson and Ho 1997) To emphasize precise description of morphology, not to deny the importance of the science of embryology, the terminology based on the somewhat shifting sands of

embryology has been avoided as much as possible. (Kouchoukos, Blackstone et al. 2003) and succinct and comprehensive description using precise terminology has been proposed.(Shinebourne, Macartney et al. 1976; Becker and Anderson 1983)

There are particular features in each component of the normal heart. (Ho, Baker et al. 1995) The right atrium is divided into four parts: the right atrial appendage, the venous component, the septum, and the vestibule. (Figure1-1A) The right atrial appendage shows a triangle structure, which contains pectinate muscles branching from the terminal crest dividing the venous component and the appendage. The junction of the right appendage is wide and the pectinate muscles extend around the atrioventricular junction. The venous component receives the superior and the inferior caval vein and the junction between appendage and the venous component is particularly wide. The fibrous creases in the region of the openings of the inferior caval vein and the coronary sinus form the venous valves, which are commonly called the Eustachian valve and the Tehebesian valve, respectively. The septal surface is smooth and the vestibule supports the attachment of the leaflets of the tricuspid valve in the normal heart.

The left atrium is also divided into four components like the right atrium, however the structure is relatively smooth-walled, with a much smaller tubular appendage while the right atrium is dominated by an extensive array of pectinate muscles within the extensive appendage. (Figure 1-1B) (Ho, Anderson et al. 2002) The left atrial appendage has a hooked and narrow shape with less pectinate muscles, which mostly limits within the appendage. The venous component receives four

pulmonary veins and no formation of venous valves is found. The septal surface of the left aspect is rough. The vestibule supports the attachment of the mitral valve in the normal heart.

The ventricles consist of three parts: inlet, apical and outlet components. (Figure 1-1C) In the right ventricle, the inlet component supports the leaflets of the tricuspid valve. The tendinous chords of the septal leaflet of the valve attach to the ventricular septum. The apical component has remarkably coarse trabeculations. In the outlet component, the pulmonary valve is supported by a muscular infundibulum, which has complex trabeculations forming the Y-shaped septo-marginal trabeculation and the supraventricular crest separating the tricuspid from the pulmonary valves.

In the left ventricle, the inlet component of the left ventricle supports the mitral valve, which has two large papillary muscles, but no chordal attachments to the ventricular septum. The apical part of the left ventricle has fine trabeculations and the surface of the ventricular septum is smooth. In the outlet component, the aortic valve is partially supported by muscular walls, but is posteriorly supported by a fibrous structure, which is a part of the mitral valve (mitral-aortic continuity) and the membranous ventricular septum.

The ventricular septum has muscular and membranous components and the latter is quite small. The mitral and the tricuspid valves are separated by the ventricular septum in an off-set arrangement where the tricuspid valve is positioned slightly closer to the apex than the mitral valve. (Figure1-1D)

The aortic valve has three leaflets with each sinus. Two sinuses, which have the orifices of coronary arteries, face to the pulmonary trunk and the commissure between the two facing valves aligns to the commissure of the pulmonary valves. Leaflets in both semilunar valves are thin, smooth and fibrous. The position of the pulmonary artery is insensibly higher than the aortic valve. Great arteries (the aorta and the pulmonary artery) form spiral relationship and the walls of both great vessels have three layers.

Figure 1-1: Morphology of normal human hearts. A: The right atrium consists of four components; venous component, the vestibule, the septum and the appendages. B: The right atrial appendage shows wide junction and the left appendage demonstrates narrow junction to the atrial cavity. C: The right ventricle is divided into three components; inlet, outlet and apical part. The aorta is visible through the supraventricular crest removed. The supraventricular crest inserts into the septal trabeculation forming Y-shaped septomarginal trabeculation (arrow). D: Four-chamber section shows off-set arrangement of the atrioventricular valve (arrow).

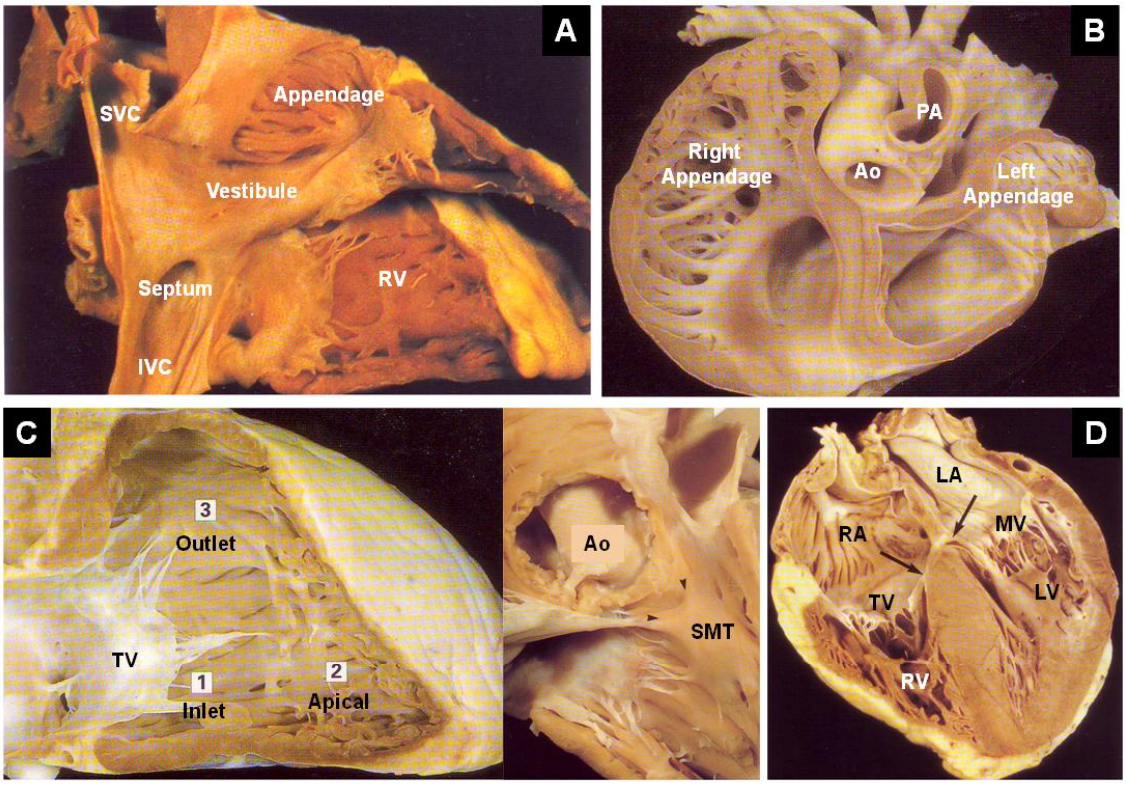

Ao: aorta, LA: left atrium, LV: left ventricle, MV: mitral valve, PA: pulmonary artery, RA: right atrium, RV: right ventricle, SMT: septomarginal trabeculation, TV: tricuspid valve
These pictures are from "*Color Atlas of Congenital Heart Disease.*"

1.3 Fetal Heart Development

1.3.1 Introduction

Understanding the steps of heart development during the fetal period is important for investigation into the structure of the human fetal heart. After fertilisation the zygote proliferates dramatically. The first step of heart development after fertilisation is the heart organogenesis during embryonic period, so-called "cardiogenesis", relating to formation of basic structures of the heart.(O'Rahilly 1971) Not only morphological differentiation of each component of the heart including chambers, coronary arteries, valves or vessels, but also histological differentiation of the heart, such as myocardium, endocardium, conduction system or cardiac nerve system, is mostly established during this period which ranges about from 20 to 56 embryonic days. After this the heart grows in size and weight and its structure and function matures after cardiogenesis until the end of the pregnancy.

Figure 1-2 demonstrates each period and approximate weeks through the gestation period in the human.

Figure 1-2: Gestational Period in human and difference between embryonic and post menstrual weeks.

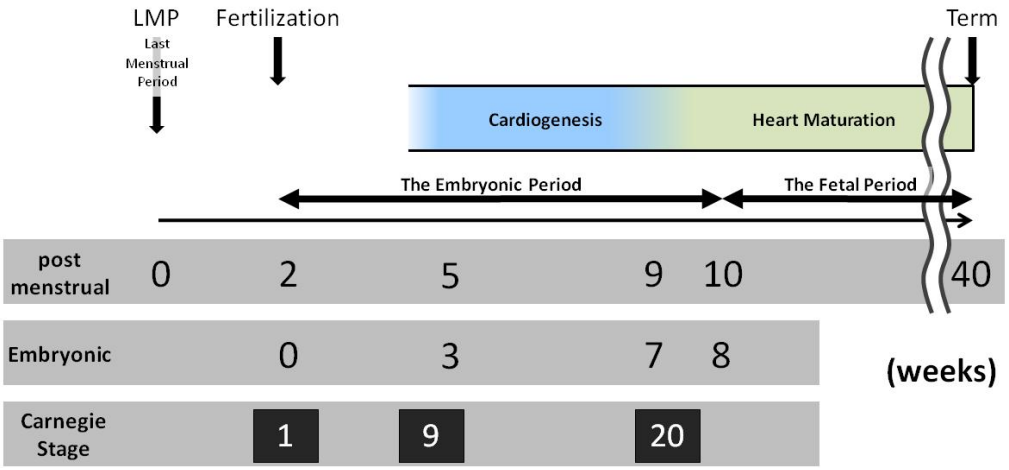

The gestational period from fertilisation to birth is usually from two to 40 weeks (38 weeks) of post-menstrual gestation; this is generally used in daily clinical practice for dating human gestational age. In contrast, embryonic week continues approximately eight weeks from fertilisation, during which most of the major organ systems are formed. There are consistent differences of approximately two weeks between embryonic and post-menstrual weeks calculated as the fertilisation day being on the 14th day after the last menstrual period.(Moore 2003) The period during embryonic weeks is generally called the 'Embryonic Period.' followed by the 'Fetal Period' which continues for about 30 weeks until birth.(Larsen 2001)

Embryonic period is commonly used in medical science, however it was arbitrarily defined by Streeter. He described the period of "the onset of marrow formation in the human" was adopted as the conclusion of the embryo and it occurred in specimens about 30 mm in length. (Streeter 1949) The term "cardiogenesis", the

definition is formation of the heart in the embryonic period, starts at about three embryonic weeks and major heart structures finish forming by around 8 embryonic weeks (five to ten post-menstrual weeks). Following the end of the embryonic period, the heart grows in size without major structural changes during the fetal period although there is no common term relating to this period. Therefore, in this thesis, I would like to use the term “Heart Maturation” as a term for this period after cardiogenesis to the end of pregnancy to clarify this period (while some people call the later period the “Developmental Stage” or “Fetal Period”.

Furthermore, before discussing cardiogenesis and heart maturation, it is important to understand the standard staging of fetal embryogenesis in human, which was originally proposed by Streeter and consolidated by O'Rahilly at the Carnegie Institute. (Streeter 1951; O'Rahilly 1979; O'Rahilly 1987) This classification, known as “the Carnegie Stage,” uses the embryonic day of the human fetus and is divided into 23 stages from fertilisation to the end of organogenesis. Table 1-1 shows the difference between the Carnegie Stages and gestation in the human and the mouse. The heart starts to form at Carnegie Stage 9 and most components finish forming by Carnegie Stage 23.

Table 1-1: Carnegie stage of the human and the mouse.

		Carnegie Stages	Human		Mouse
			Post Embryonic Days (weeks)	Post Menstrual Week	Post embryonic Days
Embryogenesis	Cardiogenesis	1	1		
		2	2		
		3	4		
		4	5-6		
		5	7-12		
		6	13-14		
		7	15-16		
		8	17-18		
		9	19-20 (2.7-2.9)	4.7-4.9	9
		10	21-22 (3.0-3.2)	5.0-5.2	9.5
		11	23-25 (3.3-3.6)	5.3-5.6	10
		12	26-27 (3.7-3.9)	5.7-5.9	10.5
		13	28-30 (4.0-4.3)	6.0-6.3	11
		14	31-34 (4.4-4.9)	6.4-6.9	11.5
		15	35-36 (5.0-5.2)	7.0-7.2	12
		16	37-41 (5.3-5.9)	7.3-7.9	12.5
		17	42-43 (6.0-6.2)	8.0-8.2	13
		18	44-47 (6.3-6.8)	8.3-8.8	13.5
		19	48-50 (6.9-7.2)	8.9-9.2	14
		20	51-52 (7.3-7.5)	9.3-9.5	14.5
		21	53 (7.6)	9.6	15
		22	54-55 (7.7-7.9)	9.7-9.9	15.5
		23	56 (8.0)	10	16

1.3.2 Cardiogenesis in the Human

Most major components of the heart are complete by approximately 50 embryonic days (nine weeks post-menstrual gestation; Carnegie Stage 20) in human and E14.5 (14.5 days) in mouse. Figure 1-3 shows the timeline of cardiogenesis in human.

Figure 1-3: Timeline of Cardiogenesis.

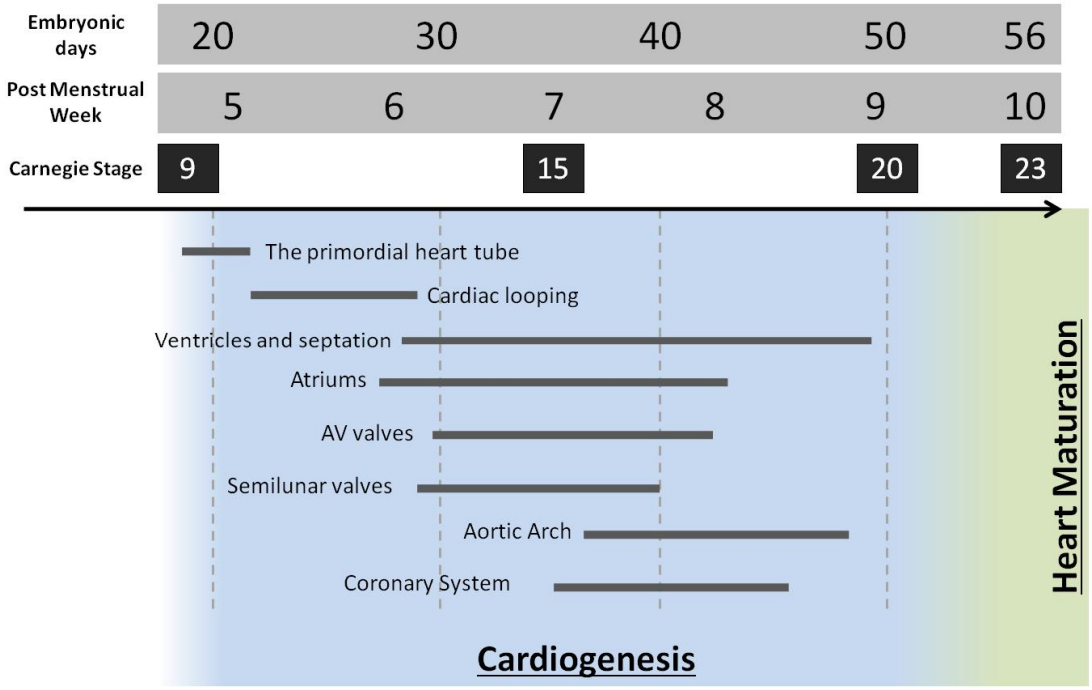

The first sign of cardiogenesis is vasculogenesis, which is blood vessel formation originated from the mesoderm, in the cardiogenic region of the embryo at about 19 embryonic days (late four post-menstrual weeks, Carnegie Stage 9). After this sign, endocardial tubes form in the thoracic region resulting in the primitive heart tube at approximately 21 embryonic days (five post-menstrual weeks, Carnegie Stage 10). By the period of formation of the primitive heart tube, some cells, which may contribute to form the right ventricle and its outflow tract, have migrated to the cranial end of the heart tube from the anterior heart field located posterior to the dorsal wall of the developing pericardial cavity.(Zaffran, Kelly et al. 2004) The primordial cardiac tube begins to beat from around this period whilst the movement of the blood merely flows and ebbs.

On around embryonic day 22 (early five post-menstrual weeks, Carnegie Stage 10-11), the primitive heart tube begins to elongate and simultaneously to loop and fold. The cardiac tube has already formed a myocardial layer with myocardial cells proliferating during cardiogenesis and heart maturation. This cardiac looping is usually held to be the first visual evidence of asymmetry in the embryo.(Moorman, Webb et al. 2003) The looping is complete by around day 28 (early six post-menstrual weeks, Carnegie Stage 13). By the time the cardiac looping has finished, the primary heart tube is divided into an outflow tract and the primordial atrium and ventricle with inflow and outlet components. The primordial atrium and ventricle are separated by the atrioventricular (AV) canal.

Formation of some components simultaneously occurs and overlaps during cardiogenesis. Ventricular formation, including septation by the interventricular septum, is the longest process, which continues for about three weeks after the end of the cardiac looping (six to nine post-menstrual weeks, Carnegie Stage 13 to 19). Toward the end of the cardiac looping, three significant processes simultaneously occur for formation of the ventricles. One is realignment of the heart where the primordial ventricle shifts to the right to align the AV canal with the truncus arteriosus. The second is the formation of the endocardial cushion dividing the AV canal into the right and the left AV canals. The third is a formation of the primordial interventricular septum, which grows and becomes the most part of the interventricular septum. Then, two endocardial cushions, ventral and dorsal, fuse and develop and the primordial interventricular septum grows toward the endocardial cushion to fuse together with

the outlet septum at roughly 50 post-embryonic days (nine post-menstrual weeks, Carnegie Stage 19)

The primordial atrium starts to be divided into right and left atrium at around 27 embryonic days (late five post-menstrual weeks, Carnegie Stage 12) and the right and the left atrium formed by the formation of two types of atrial septum (the septum primum and the septum secundum) at about 43 post-menstrual weeks (eight post-menstrual weeks, Carnegie Stage 17). Both AV valves, originating from a part of AV sulcus and endocardial cushion, form during four to six embryonic weeks (six to eight post-menstrual weeks, Carnegie Stage 14 to 18). Two semilunar valves, whose origins are from three creases of subendocardial tissue between the truncus and conus, are formed along with the septation of the outflow septum at approximately 40 embryonic days (late seven post-menstrual weeks, Carnegie Stage 16). The aortic arch exists bilaterally in both right and left sides at about 37 embryonic days (early seven post-menstrual weeks, Carnegie Stage 16) and the right aorta dorsalis is obliterated, followed by the arterial duct connecting to the aortic arch just distal to the left subclavian artery at approximately 44 embryonic days (late eight post-menstrual weeks, Carnegie Stage 18).

The coronary system develops from a different origin compared to other components of the heart.(Hutchins, Kessler-Hanna et al. 1988) The blood islands on the epicardium of the interventricular sulcus near the apex of the heart forms coronary capillaries at about 35 embryonic days (seven post-menstrual weeks, Carnegie Stage 15) before the establishment of the coronary venous connection to the coronary sinus

at around 42 (eight post-menstrual weeks, Carnegie Stage 17). Then the coronary system is established by about 45 embryonic days by the arterial connection to the epicardial plexus with retrograde formation of the coronary artery ostia of the Valsalva (middle eight post-menstrual weeks, Carnegie Stage 18).

Thus, most organogenesis of the cardiovascular system is completed by around 50 embryonic days in the human (the end of eight weeks of post-menstrual gestation) and no major structural formation occurs after Carnegie Stage 20 (about nine post menstrual weeks). The period from Carnegie Stage 20 to 23 is transitionary phase between cardiogenesis and heart maturation and then, cardiogenesis shifts to heart maturation which continues from about 10 post-menstrual weeks until birth.

1.3.3 Heart Maturation in the Human

The heart is an exceptional organ, which seems to be functional from early embryonic days. Although all the organ systems are present by 10 post-menstrual weeks, most organs are not properly functional and some organs do not finish maturing until after birth, such as the reproductive system and associated sexual characteristics, or the brain. However, the heart starts to beat and to circulate blood at about six post-menstrual weeks.

The heart shows histological and functional maturation during the fetal period. Aikawa et al described that, after cardiogenesis, increase of collagen content and decrease of cell density in the human aortic valve demonstrates the process of heart maturation from early to late fetal stages.(Aikawa, Whittaker et al. 2006) DeAlmeida et

al reported an experimental hemodynamic effect on myocardium in the chick embryo by increasing preload which results in myocyte proliferation in the left ventricle.(deAlmeida, McQuinn et al. 2007) Sanchez-Quintana et al reported a progressive change in the direction of the muscle fibres in the superficial layer throughout heart maturation in 22 human fetal hearts suggesting the structural maturation contributes to the functional improvement in the fetus.(Sanchez-Quintana, Garcia-Martinez et al. 1995) Spencer et al mentioned that rapid changes in the calcium handling capacity of the cell (as smooth endoplasmic reticulum develops) increase the ability to generate force during heart maturation.(Spencer, Botting et al. 2006)

Geometrical increase has been described in the human fetal heart. Cook described that the length of the ventricle is less than 3 mm at first, followed by dramatic growth in size to more than 10 times this size by term.(Cook 2001) Guihard-Costa et al reported dramatic increase of cardiac weight which grows about 100-fold from 0.24 grams at 12 post menstrual weeks to 24 grams at term from 635 post-mortem human fetal heart and Maroun et al also described similar growth from 759 posmortem human fetal heart. (Guihard-Costa, Menez et al. 2002; Maroun and Graem 2005) Thus, the heart shows significant growth and maturation after the embryonic period in the human.

1.3.4 Difference between the Human and the Mouse

The mouse is a commonly used species for an experimental model of diseases. Cardiogenesis starts from E 7.0, the heart finishes forming at around E14.5 and the final term of pregnancy is at about E18.5. (Theiler 1972) Figure 1-4 shows the difference in the ratio over the period of cardiogenesis and heart maturation to pregnancy in the mouse and the human.

Figure 1-4: Gestational Difference in the mouse and the human.

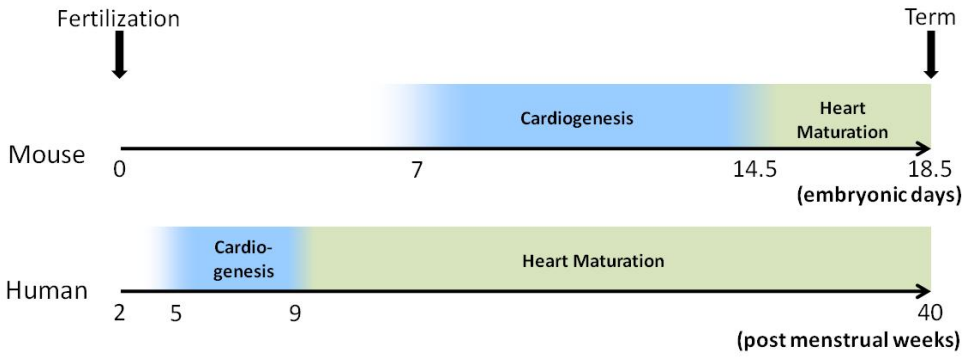

The duration of heart maturation after cardiogenesis is only about four days and the ratio of heart maturation to the period from fertilization to term is 0.22 (4 divided by18.5) in the mouse. In contrast, the human has approximately 30 weeks in 38 weeks from fertilisation to term and the ratio is 0.79 (30 divided by 38). The duration of heart maturation is more than six times that of cardiogenesis in the human (30 divided by 5) whilst it is approximately half in the mouse (4 divided by 7.5). Thus, the ratio of the heart maturation is significantly longer in the human than the mouse, suggesting that the mouse heart may have limitations in terms of being an experimental model of heart maturation after cardiogenesis.

1.4 Morphological Investigation of the Fetal Heart

1.4.1 Conventional Morphological Examination of the Human Fetal Heart in the First and Early Second Trimester

Manual manipulation of the fetal heart is not easy, especially in the first and early second trimester in humans, because the size of the heart is small and the tissues are relatively soft and fragile although morphological investigation of the human heart is generally performed by hand in fetuses after the first trimester, children and adults. Although comprehensive description of the cardiac phenotype is the essential first step in analysing the process of the heart development in normal or mutant organs, histological investigation is still generally used for morphological evaluation of fetuses in the first and early second trimester, while it has an inherent limitation for morphological assessment, which is two-dimensional.

Morphological observation using histological sections in the Carnegie collections by Streeter and O'Rahilly has been used as the standard of the process of human cardiogenesis by interpreting 2D histological information into 3D embryogenesis. (Streeter 1942; Streeter 1945; Streeter 1948; Streeter 1951; Heuser and Corner 1957; O'Rahilly 1973; O'Rahilly 1979; O'Rahilly 1987; O'Rahilly and Muller 1996) Following the work at the Carnegie Institute, several reports assessed the morphological features using histological sections of the human fetal heart. In1970, Goor et al described morphological observation of process of interventricular septation during cardiogenesis using histological sections in 54 normal human embryos. (Goor, Edwards et al. 1970) Anderson et al pointed proliferation of specific myocardial cell in

17 human fetal hearts (Crown-Rump Length 7 -190mm) in the area of the atrioventricular canal suggesting different cellular origin of atrioventricular canal compared to the ventricle. (Anderson and Taylor 1972) His team also reported establishment of outflow septum in 17 normal human fetal hearts (Carnegie Stage 14 to 22) in 1974 and suggested differential bulbar absorption and truncal rotation resulted in bulboventricular malformation during cardiogenesis. (Anderson, Wilkinson et al. 1974) Orts-Llorca et al in 1982 showed the step of septation in the arterial trunk using histological sections in 24 human embryos. (Orts-Llorca, Puerta Fonolla et al. 1982) Barteling et al observed the process of outlet septation in 20 human fetal hearts (Carnegie stage 14 to 23). (Bartelings and Gittenberger-de Groot 1989) In 1992 Lamers et al reported different origin of ventricular septum using immunohistochemistry in eight human fetal hearts. (Lamers, Wessels et al. 1992) Coronary development during human cardiogenesis were also examined in 52 samples in 1984 (Hirakow 1983), in 32 samples in 1984 (Conte and Pellegrini 1984) and in 351 fetal hearts in 1988 (Hutchins, Kessler-Hanna et al. 1988) describing detailed observation of the development of the coronary system using 2D histological sections.

Morphological measurements using histological sections in the human fetal hearts have been reported. In 1962, Grant et al described measured cardiac components linearly using sectioned 16 human fetal hearts and described dramatic growth of both ventricles from 4 to 7 post embryonic weeks. (Grant 1962) In 1991, Mandarim-de-Lacerda et al reported increase of growth ratio of fetal myocardial mass volume after Carnegie Stage 20 in 27 human fetal hearts suggesting the effect by

circulatory demand of peripheral circulation. (Mandarim-de-Lacerda 1991) Wenink et al, in 1992, estimated myocardial mass volume in each ventricle using histological sections by Cavalieri's principle in 32 human embryos (4.0-42.0mm in Crown-Rump Length; 5 to 11 post menstrual weeks) (Gundersen, Bendtsen et al. 1988) and suggested that the trabeculation in each ventricle might be changed during the period of valve formation. (Wenink 1992) Recently, Arraez-Ayba produced a normogram of estimated myocardial volume from histological slides in 30 human fetuses (Carnegie Stage 15 to 23) and proposed its utility as a reference for cardiac development. (Arraez-Aybar, Turrero-Nogues et al. 2008) Thus, quantitative assessment of the structures of human fetal hearts has been performed. Importantly , however, all these investigations are limited by the two-dimensional origin of the component parts from histological investigation.

Morphological measurement of ventricles by manual handling in the human fetal heart has been undertaken in some reports as well. In 1983, Leslie et al reported hypertrophy of the ventricular septum in the second trimester in the 153 normal fetuses by measuring the ventricular wall, suggesting the effect of increased vascular afterload in placental circulation in the second trimester.(Leslie, Shen et al. 1983) Alvarez et al, in 1987, estimated ventricular volume by measuring inner diameter of each ventricular cavity in 281 fetal hearts (15 to 40 post menstrual weeks) and described linear growth of each ventricular cavity by anatomical morphometry. (Alvarez, Aranega et al. 1987) Recently in 2009, Arteaga-Martinez et al reported the detailed external and internal measurement of ventricular segments by morphometry

measured by stereoscopic microscopy in 103 fetal hearts ranging from 13 to 20 post menstrual weeks.(Arteaga-Martinez, Halley-Castillo et al. 2009) They demonstrated liner cardiac growth and illustrated pictures of whole appearance of fetal heart (Figure 1-5), however they focused on quantitative measurements and there is no morphological description in the report.

Figure 1-5: Pictures of Human Fetal Hearts in the early second trimester. (modified figure2; Arteaga-Martinez 2009) Basic appearances of the hearts are normal. Atrial appendage is prominent in both sides, especially the left appendage. Inside structure is unkown.

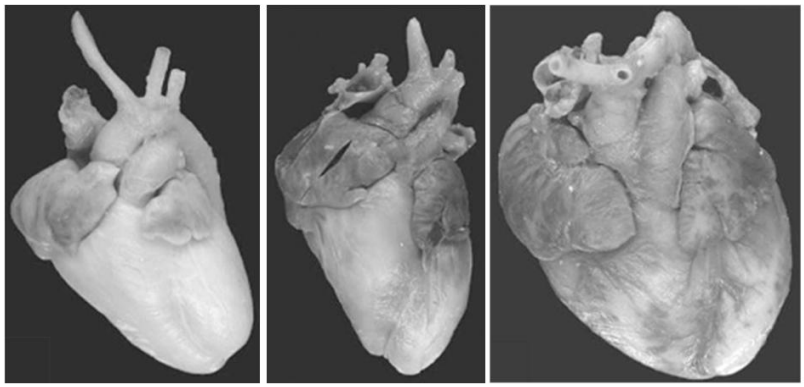

Morphological measurement of great arteries and valves by manual handling also has been performed. Hyett et al reported external diameter of several points of the aortic and the ductal arch by dissecting with a microscope in 61 fetal hearts from 9 to 18 post menstrual weeks and proposed linear formulas of each parts of growth in great arteries. (Hyett, Moscoso et al. 1995) In 2005, Castillo et al measured the external diameter of great arteries as a morphometric reference for fetal

echocardiography in 103 fetal hearts from 13 to 20 post menstrual weeks.(Castillo, Arteaga-Martinez et al. 2005) Gielecki et al also reported external measurements of the aortic arch in 80 human fetuses between 17 and 27 post menstrual weeks suggesting that the aortic isthmus becomes narrower during heart maturation. (Gielecki, Syc et al. 2006) Szpinda in 2007 reported growth of aortic arch by measuring external diameter and volume of the aorta and showed similar growth to previous reports. (Szpinda 2007) However, all reports regarding morphometry focused on quantitative growth by measuring the size of ventricles, valves or great arteries and there is a lack of information of detailed morphological description of structures of each component of the fetal heart.

Investigation of myocardial architecture in the human fetus is another approach for structural investigation of the development fetal heart. In 1990, Sanchez-Quintana et al reported abnormal myocardial arrangement of a patient with Tetralogy of Fallot compared to 5 normal fetal hearts by manually peeling layers of myocardium followed by characterising normal 3D myocardial structure in 25 normal fetal hearts in 1995 (13 to 32 weeks post-menstrual gestation). (Sanchez-Quintana, Garcia-Martinez et al. 1990; Sanchez-Quintana, Garcia-Martinez et al. 1995) They described a progressive change in the direction of the muscle fibers in the superficial layer and age-related differences on the sternocostal and diaphragmatic aspects, which were more evident in the right ventricle. In 2000, Ohayon and Jouk et al demonstrated detailed myocardial architecture using polarised light through sectioned specimens embedded in a resin of methyl methacrylate in 18 normal human fetal hearts (14-27

post menstrual gestation) and emphasized utility of their 3D models of myocardial layer arrangement. (Ohayon, Usson et al. 1999; Jouk, Usson et al. 2000) However, these reports focused on structures of myocardial fibres and there was no description of fetal cardiac morphology.

The importance of morphological assessment of the fetal heart in the first stage of heart maturation was emphasized. Klinkenbijl et al reported structural assessment by sectioning two human fetal hearts (Carnegie stage 23) in various angles in 1988. They traced the edge of cardiac sectioned surface in different angulations and described internal morphology in the human fetal heart. (Klinkenbijl and Wenink 1988) They particularly emphasized usefulness of understanding morphology for fetal echocardiography. (Figure 1-6)

Figure 1-6: Images of multiple sectioned human fetal heart. (modified 5-7, Klinkenbijl 1988) Traced pictures show cardiac structure and shape of myocardium and great vessels.

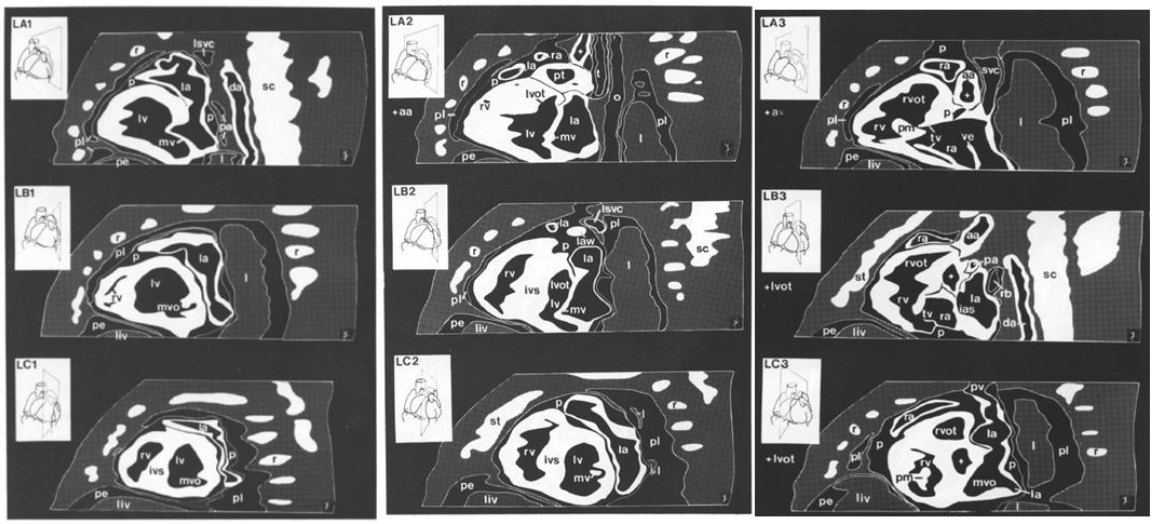

In 1997, Allan et al described the qualitative features of general geometrical structures of the heart and great arteries in fetal heart specimens from abortion followed by a validation study in which they compared 200 fetal echo images with 25 normal fetal heart specimens (5-12 post menstrual weeks). (Allan 1995; Allan, Santos et al. 1997) Figure 1-7 demonstrates the pictures of the human fetal heart from the report. They suggested visualisation and description of normal characteristics and the sequence of cardiac development might enable us to notice abnormalities and help to identify factors contributing to malformations.

Figure 1-7: Pictures of human fetal heart at 9 post menstrual weeks. (modified figure 4; Allan 1997) In the frontal view (left) the aorta is running almost parallel to the pulmonary trunk and coronary arteries are prominent. In the lateral view (right), the arterial duct joins the descending aorta at an acute angle and its diameter is less than that of the pulmonary trunk.

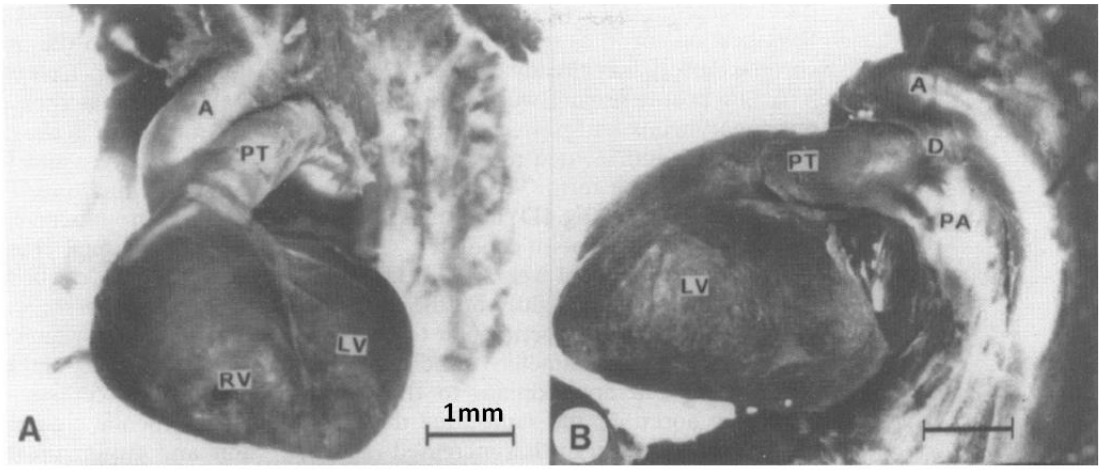

A; aorta, D; arterial duct, LV; left ventricle, PA; pulmonary artery, PT; pulmonary trunk, RV; right ventricle

Despite conventional morphological investigations in the human fetal heart, there is still a lack of detailed information because conventional histological or morphological assessments cannot provide sufficient 3D morphological information of small human fetal hearts. To overcome this fundamental problem, some researchers have reconstructed embryonic structures physically using various materials and techniques such as the wax plate method (Born 1883; Thompson 1907; Licata 1954; Vernall 1962), plastic reconstruction (Licata 1954), plaster (De Vries and Saunders 1962), cardboard (Cooper and O'Rahilly 1971), graphic reconstructions from photographic pictures (Payne and Hutchins 1973; Braverman and Ken-Yen 1983) or cast by orthodontic compound (Hoffman and Ritman 1985) , however, they are technically difficult to duplicate and may only provide a restricted view of the structures under investigation.

1.4.2 Conventional Computer Based 3D Reconstruction using Histological Sections

Computer-based 3D reconstruction has been performed using a series of digitised images from slide-mounted histological sections of small specimens instead of 2D histological methods. The principle of this technique is 3D reconstruction by volume rendering captured digital images of consecutive histological slides like 3D computed tomography (CT) or 3D magnetic resonance image (MRI). However this technique is time-consuming because image capturing and adjustment of each image is not automatic. Nevertheless this technique was a standard to assess 3D structure because no other efficient methods were available.

There are two fundamental and serious difficulties using 2D histological digital images. The first is distortion of each section. The sectioning process itself causes variable distortions of individual sections, such as stretching and squashing, which frequently occur with paraffin-embedded specimens. Captured images mounted on slides may cause malaligned reconstructed images because each section shows different deformation. The second issue is displacement of sections. The precise alignment or registration of consecutive sections is lost by the sectioning and mounting processes resulting in low quality of the 3D model. Thus correcting distortion and image realignment are the key problems of 3D reconstruction from histological sections as Streicher et al emphasized. (Streicher, Donat et al. 2000)

The problems of malalignment were noticed very early on by Willhelm His, the inventor of the rotary microtome in the 19th century, who described the problem using images of serial sections of embedded embryos. (His 1887) Many modifications have been described to tackle these problems: to realign the images of consecutive sections there are two ways for vertical reorientation of images. One is using internal reference markers which may result in many artefacts of 3D images because they are generally an independent structure of the sectioned samples. Another is using external reference markers generated for example by drilling holes adjacent to samples within the embedding medium. External marker may have fewer artefacts than internal markers, however, the marker must lie perpendicular to the section plane within the embedded sample block. Thus, loss of 3D information led to numerous numbers of reconstruction methods, however, the initial images produced poor 3D quality because

volume rendering of histological images were manually traced by a digitizing panel, not digitally captured as serial pictures. (Sjostrand 1958; Arnolds 1978; Sundsten and Prothero 1983; Wong, Thompson et al. 1983; Braverman and Braverman 1986; Huijsmans, Lamers et al. 1986; Prothero and Prothero 1986; Meyer and Domanico 1988; Brandle 1989) After the first report of 3D reconstruction of digitized sectioned images in 1987 (Hibbard, McGlone et al. 1987) and introduction of commercially available charge coupled device (CCD) cameras, digitized image capturing has become the mainstream for images of 3D reconstruction for various tissue in embryos with many modifications. (Moss, Jenkinson et al. 1990; Reisner, Bucholtz et al. 1990; Rydmark, Jansson et al. 1992; Skoglund, Pascher et al. 1993; Stockley, Cole et al. 1993; Rude, Anderson et al. 1994; Verbeek, Huijsmans et al. 1995; Kaufman, Brune et al. 1997; Streicher, Weninger et al. 1997; Streicher, Donat et al. 2000; Soufan, Ruijter et al. 2003)

Figure 1-8 shows images of conventional 3D reconstruction using histological sections. Conventional reconstructed 3D images using histological slides are not satisfactory and are very time-consuming. There has been no fundamental change in these problems for about a century, and researchers are still facing the same difficulty first tackled by His.

Figure 1-8: Conventional 3D reconstruction of the heart using histological slides in embryos. The left image shows a 3D picture of the semilunar valves in chick embryo by manual tracing edge of the sectioned slides. The image is terraced and non-aligned. The right picture shows 3D surface volume rendered image of the mouse heart (E14.5). The image is based on smoothing function in isosurface rendering which eliminates variation and looses detail in the same process.

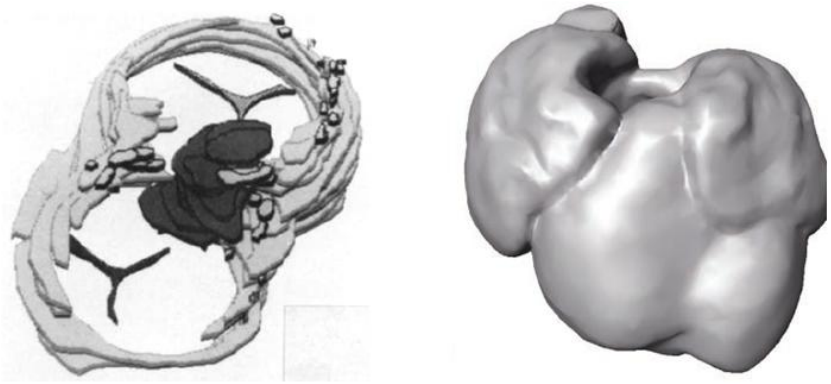

Wong 1983 Soufan 2003

1.4.3 Episcopic Image Capturing

The episcopic method is an alternative image capturing of sectioned samples by an episcope, a projector for images of an opaque object. Figure 1-9 shows the comparison of flowcharts between conventional image capturing of histological slides and episcopic image capturing.

Figure 1-9: Flowchart of Conventional image capturing of histological slides (upper) and Episcopic image capturing (lower). In conventional image capturing of histological slides, the image is taken from each mounted slide. In contrast, in Episcopic image capturing the image is taken from surface of sectioned block in each sectioning process.

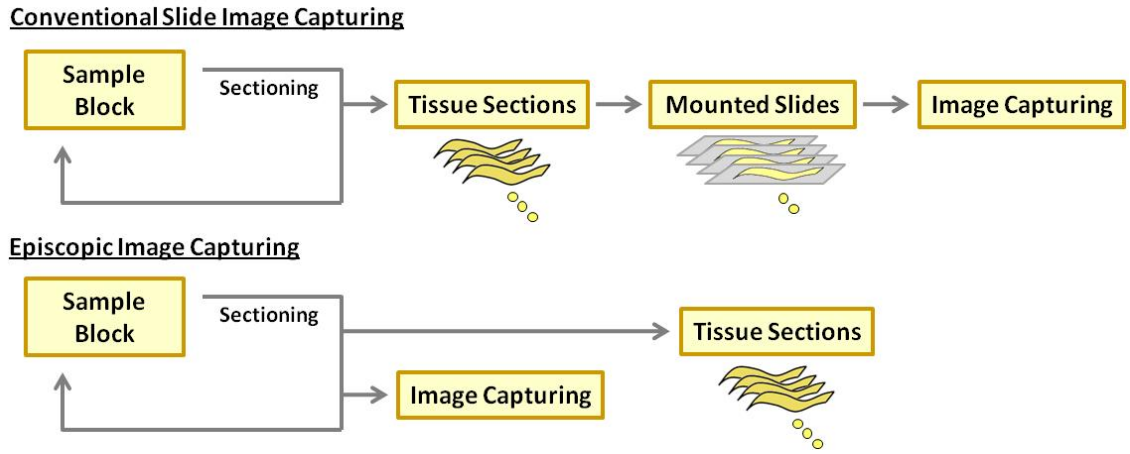

Hegre and Breshear firstly reported block-surface imaging in the 1940s, but the image was not digitally captured and its quality was poor. (Hegre and Breshear 1946; Hegre and Breshear 1947) Laan et al investigated cardiogenesis in the rat using 3D reconstructed models created by episcopic capturing technique in 1989. They adjusted each image by graphic software, but quality of images was still unsatisfactory. (Laan,

Lamers et al. 1989) Odgaard et al proposed a new computer-based image processing system for direct digitization of the cut surface of a sample block embedded in epoxy resin (Odgaard, Andersen et al. 1990) followed by demonstrating 3D reconstruction of cancellous bone. (Odgaard and Gundersen 1993) Following the progress of computer technology Episcope image capturing has been developing, but images in early days were not suitable for detailed investigation of structure of samples.

Despite the limitations of digitising technology in the early episcopic methods, problems regarding insufficient image quality and malalignment of consequent images have been improved. In 1998, Weninger et al first reported a fast method for an acceptable 3D reconstruction using regular paraffin-embedded mouse fetus.(Weninger, Meng et al. 1998) This technique consists of consecutive images captured from the cutting surface of the block by a rotation microscope and an episcope. In 2000, Mohun et al reported morphological change and 3D distribution of cardiac gene expression using episcopic image capturing in Xenopus laevis. (Mohun, Leong et al. 2000) Then, in 2002, Weninger and Mohun proposed episcopic fluorescence image capturing (EFIC), a new method for detecting specific signals of small samples demonstrated high resolution 3D images of mouse hearts.(Weninger and Mohun 2002) Rosenthal et al reported further EFIC images of mouse fetal hearts and demonstrated 3D structure of cardiac trabeculation. (Rosenthal, Mangal et al. 2004) EFIC is good for older samples, but very poor for young samples because of the very low levels of autofluorescence, however, tissue contrast by EFIC is still not sufficient to observe detailed tissue architecture because of weak fluorescence while EFIC is good to detect specific signals

by virtue of their ability to suppress such fluorescence. (Figure 1-10) (Rosenthal, Mangal et al. 2004; Weninger and Mohun 2007)

Figure 1-10: 3D Volume Rendered images of the mouse fetal heart by EFIC. (upper, modified figure 2, Weninger and Mohun 2002) (lower, modified figure 6 and 9, Rosenthal 2004) (A) Connections of cardiac chambers and great arteries are confirmed by coloured internal cavities of atriums, ventricles and great vessels. Myocardial and arterial walls are not clearly shown. (B) Heart trabeculation is shown in the lower images. Trabeculation in the chambers show less contrast and weaker tissue architecture (left and b).

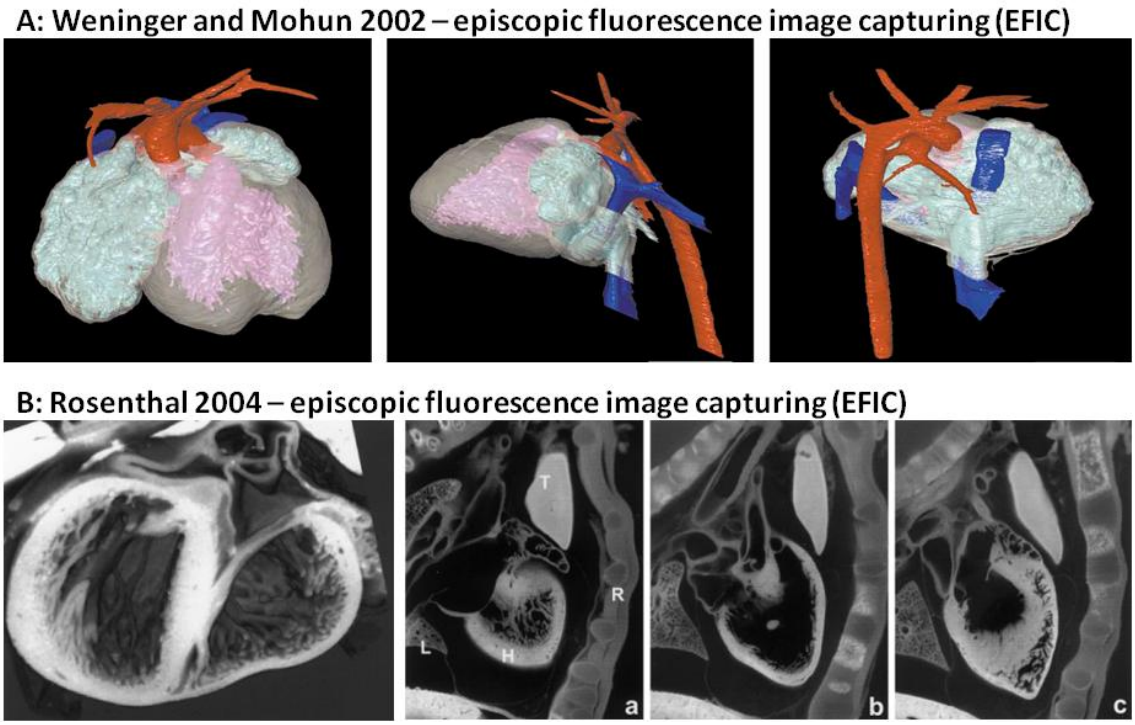

1.4.4 High-Resolution Episcopic Microscopy

High-resolution episcopic microscopy (HREM) is a newly-developed episcopic image capturing which assesses the 3D tissue structure of small samples.(Weninger, Geyer et al. 2006) HREM is a process to create a voxel dataset of consecutive high-quality images by repeating automatic capturing from the cutting surface of the block by an episcope with episcopic light during each sectioning process. Weninger et al embedded samples into the plastic embedding medium instead of paraffin wax for the following two reasons: (a) to avoid distortion of captured images by the sectioning process and to create non-aligned digital volume datasets, and (b) to detect tissue architecture at the surface of the sectioned block using the intrinsic and strong fluorescence illumination of resin-embedding media and histological stain “eosin” for providing morphology. A series of consecutive digital images of each freshly-cut block surface is obtained using a microscope and digital camera during the sectioning process. These images retain complete alignment with the position controlled by a sliding microtome and are ready to be converted to volume data sets.

HREM can provide high quality 3D images from voxel data and original volume datasets are almost histological quality with a resolution of minimum 1 □mm, but 2 to 3 micrometer is satisfactory for 3D analysis and sections can be retained and mounted on glass slides for further subsequent light microscopy viewing. (Weninger, Geyer et al. 2006; Pieles, Geyer et al. 2007)

There are some issues in the HREM method. HREM cannot be applied to living specimens because tissue samples or specimens need to be fixed by fixative solution

and stained with dye and are destroyed. The second is that large samples are still difficult to process because equipment has upper limitation of the size of samples. Thirdly the influence of processing on histological and morphological findings is still unclear. This might cause limitation or unexpected changes in histological or morphological investigation. Furthermore, because the size of volume dataset of digital images is very large (more than 20 GB in large sample in one case) data storage, including the backup system, needs to be large, or the number of HREM sections needs to be kept as low as possible to focus on the specific regions. (Pieles, Geyer et al. 2007)

Several tissues, including human adult skin, pig adult liver, frog tadpole, chick embryo, quail embryo and mouse fetus, have been examined by HREM.(Weninger, Geyer et al. 2006; Pieles, Geyer et al. 2007) In terms of investigation of the heart, Weninger et al first examined the heart of a transgenic mouse by HREM describing 3D morphological features and protein expression (myocardial LacZ) in a developing mutant mouse. In 2007, Pieles et al examined mouse fetus at the stage E15.5 (about 5 – 6 mm in length; similar size of the human fetal heart at about 11 post menstrual weeks (Gembruch, Shi et al. 2000)) and demonstrated sufficient quality of the heart morphology and tissue architecture in greyscale HREM images. (Pieles, Geyer et al. 2007) Recently in 2009, Weninger et al proposed quantitative assessment of HREM by measuring areas, perimeter and diameter of the lumen of the aorta in the mouse fetus at the stage of E15.5 and showed its reliability and reproducibility. (Weninger, Maurer et al. 2009) These reports suggest that HREM has a significant potential for 3D assessment of the detailed structure of the human fetal heart.

1.4.5 Other Three Dimensional Imaging Modalities for Investigation of the Heart in Embryos

Non invasive 3D modalities, which do not require the sectioning process and enable us to obtain non-destructive imaging of specimens or in vivo, have demonstrated considerable potential for investigation of the structure and molecular factors of the embryo although expensive specialist equipment is required.

Several modalities have been used for structural investigation of the heart in embryos. Following the first report of MRI microscopy by Johnson et al in1989 (Johnson and Maronpot 1989), micro-MRI has been applied to examine the structure of cardiovascular system in embryos. Smith et al first described 3D images of thoracic vasculature in chick embryos at resolution of 80 micrometer in 1992 (Smith, Effmann et al. 1992) and they preliminarily reported 3D structure during cardiogenesis in the mouse by micro-MRI in 2001. (Smith 2001) In 2003, Yelbuz et al also reported 3D evaluation of cardiac development by micro-MRI at resolution of 25 micrometer in the chick embryo and reported advantage of 3D cardiac analysis in the embryo. (Yelbuz, Zhang et al. 2003) Schneider et al first reported cases of cardiac malformation in the mutant mouse fetus confirmed by micro-MRI. (Schneider, Bamforth et al. 2003; Schneider and Bhattacharya 2004; Schneider, Bose et al. 2004) In 2008, Petiet et al published a 4D atlas and morphologic database in the mouse fetus and neonate created by micro-MRI at resolution 19.5 micrometer. (Petiet, Kaufman et al. 2008) Recently, Hogers et al reported the first 3D reconstructed images in vivo of avian embryonic heart at resolution about 80 micrometer and showed its utility. (Hogers,

van der Weerd et al. 2009) Thus, micro-MRI has shown important progress in 3D image construction although its resolution is still about 20 micrometers to date.

Micro-CT has provided significant possibilities and potential for detailed morphological assessment of cardiovascular structures in embryos. Heinzer et al reported feasibility of micro CT in 2006 by demonstrating qualitative and quantitative assessment of 3D vasculature of the mouse brain with theoretical resolution less than 1 micrometer. (Heinzer, Krucker et al. 2006) Johnson et al in 2006 described the 3D reconstructed images of the mouse heart by micro-CT with 8 micrometer resolution and reported on a potential of micro-CT for of assessment of cardiac structure. (Johnson, Hansen et al. 2006) Butcher et al demonstrated cardiogenesis in the chick embryo by qualifying cardiac lumens at resolution 10.5 micrometre. (Butcher, Sedmera et al. 2007) Recently, Martinez illustrated pathologic images of atherosclerosis in mutant mice by micro-CT with resolution 6 micrometer voxel and showed potential of virtual histology by micro-CT. (Martinez, Prajapati et al. 2009)

High-frequency ultrasound was first applied to the mouse heart to assess the structure in vivo with 2-D images in 2002 (Foster, Zhang et al. 2002; Zhou, Foster et al. 2002) followed by Dawson's study validating cardiac volume in the mouse in vivo between micro-MRI and 3D high-frequency ultrasound, but its resolution was 100 micrometer.

Optical projection tomography (OPT) was another approach applied to assess the structure of the heart in embryos using light transparency. (Sharpe, Ahlgren et al. 2002) This method is 3D reconstruction of captured images from illuminating light

through rotating specimens at resolution 5 to 10 micrometer. Vinegoni et al described whole heart imaging by OPT by adjusting images, however inside of the heart was still not clear because translucent samples cause light attenuation resulting in less detailed information of images. (Vinegoni, Razansky et al. 2009) (Vinegoni, Razansky et al. 2009)

These modalities applied to cardiac investigation, may still have important limitation for analysing structures of heart in embryo despite technological advances. Table 1-2 shows comparison of resolution of each method including EFIC and HREM and Figure 1-11 illustrates 3D volume rendered image from micro-MRI.

Table 1-2: Comparison of 3D imaging modalities for cardiac investigation

Modality	Resolution (micrometer)	Principle of image capturing
Micro-MRI	20-25	Reconstruction of signal from nuclear magnetic resonance
Micro-CT	6-8	Tomography from radiation signal
High-frequency ultrasound	50-100	Reconstruction of ultrasound signal
OPT	5-10	Tomography from data of translucent light
EFIC	0.5-5	Direct image capturing by a CCD camera
HREM	0.5-5	Direct image capturing by a CCD camera

Figure 1-11: Volume rendered 3D images of the mouse fetal heart. (modified figure Schneider 2003) Inner cavities of ventricle, atriums and great arteries were shown, however no information of atrial wall, ventricular wall and arterial wall was shown.

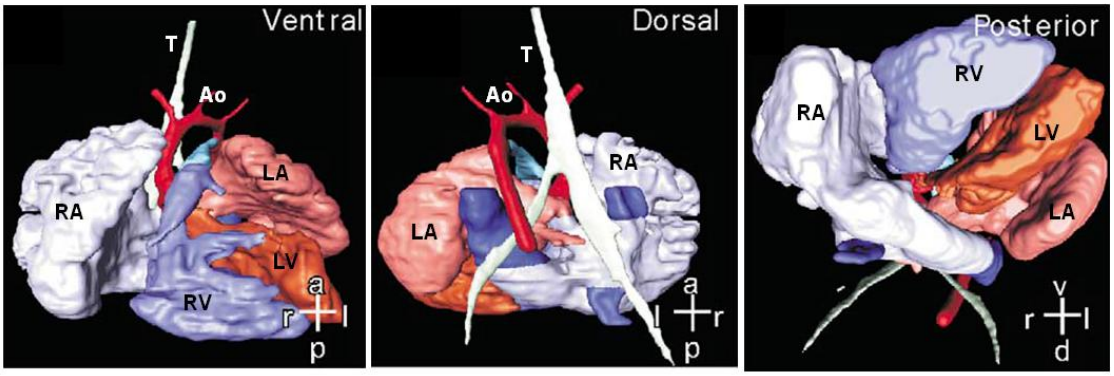

Ao; aorta, La; left atrium, LV; left ventricle, RA; right atrium, RV; right ventricle, T; trachea

One of the limitations is that original 2D images reconstructed from wave signals (wave of nuclear magnetic resonance in micro-MRI, radiation in micro-CT, ultrasound in high frequency ultrasound, translucent light in OPT) may cause more artefact than a direct image-capturing method like EFIC or HREM. The second is that fundamental low resolution may result in less precise visualised information on overall morphology in histological detail or on tissue architecture. OPT has significant restriction of samples, such as difficult optimisation or small and transparent samples. These limitations make it difficult to distinguish different tissues, and may cause loss of essential morphological information in small samples. Furthermore, the heart appearance is difficult to observe by volume rendered images because cardiac surface was not clearly detectable for difficult separation the heart from other tissue surrounding the heart, like lung or diaphragms, in each digital image. (Figure 1-10)

1.4.6 Comparison of Image Quality between HREM and Other Imaging Modalities

Pieles et al reported comparison study between HREM and micro-MRI in the murine embryo (E15.5) in 2007. They demonstrated higher quality of 3D images by HREM at resolution 1 to 2 micrometer than by MRI at resolution about 25 micrometer. (Pieles, Geyer et al. 2007) Figure 1-12 shows comparison of images between micro-MRI and HREM from Pieles.

Figure 1-12: Comparison image quality between micro MRI (left) and HREM (right). (modified figure 4, Pieles 2007) In the same level of digital sectioning (upper and lower images), image contrast and density of myocardium in HREM is much clearer than in micro-MRI. Resolution is 2 micrometer in HREM and 25 micrometer in micro-MRI.

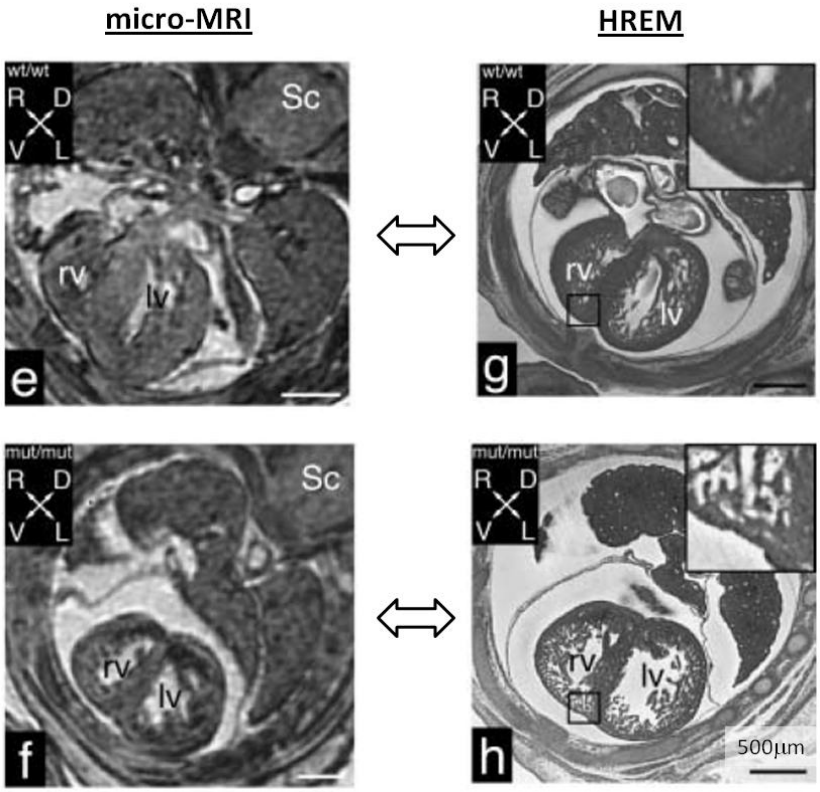

The voxel dataset (more than 5G bites of greyscale) in HREM was approximately 65 times larger than in micro-MRI and HREM data includes much larger 3D digital information than in other in or ex vivo imaging methods. Thus, HREM has more potential to illustrate the precise image of cardiac structure in embryos than other modalities.

1.4.7 Three dimensional Reconstruction of the Human Fetal Heart

Some reports are available on 3D reconstructed images of the human fetal heart using serial histological sections to date or episcopic image capturing. In 1987, McLean et al reported a single case of 3D reconstructed image of a large human heart (more than 7 cm) by episcopic image capturing. The specimen was not fetal heart, however they embedded the heart into plastic resin (JB4) and demonstrated the potential of episcopic image capturing with a sample embedded by plastic resin. (McLean and Prothero 1987)

In 1990, Blausen et al first applied computer-based 3D reconstruction to the human fetal hearts and demonstrated volumetric analysis in 8 human embryos ranging from 9 to 23 Carnegie stages.(Blausen, Johannes et al. 1990) They showed about thousand-fold cardiac growth during the stages by quantifying total cardiac volume using histological sections and described utility and potential of their method. Scarborough et al reported 3D reconstructed images by conventional capturing histological slides using original software in four human fetal hearts (Carnegie stage 10 - 17) in 1997. (Scarborough, Aiton et al. 1997) They described 3D structure of atrium,

however, image quality was still not satisfactory. In 1998, Whiten et al reported another computer-based 3D reconstruction of the human fetal heart describing a potential of virtual models for investigation of cardiogenesis. (Whiten, Smart et al. 1998) Figure 1-13 illustrates 3D models of human hearts (1 infant's and 3 fetal) in 1980-90s.

Figure 1-13: Computer-based 3D reconstruction of the human heart in early days (modified figure 4 in Mclean, figure 5 in Blausen, figure 4 in Scarborough and figure 8 in Whiten). All images were traced manually. (A) 3D reconstructed image of ventricles in infants. Coloured cavities and ventricular surface can be seen. (B) Orthogonal trace of a 3D image in the human embryonic heart (Carnegie Stage 23). (C) 3D reconstructed image of both atrias. (Carnegie Stage 17) two parts of atrial septum (SP and SS) were illustrated. (D) 3D reconstructed model from edge trace of embryonic heart. (Carnegie Stage 19) Image quality of all images is unsatisfactory for detailed structural investigation.

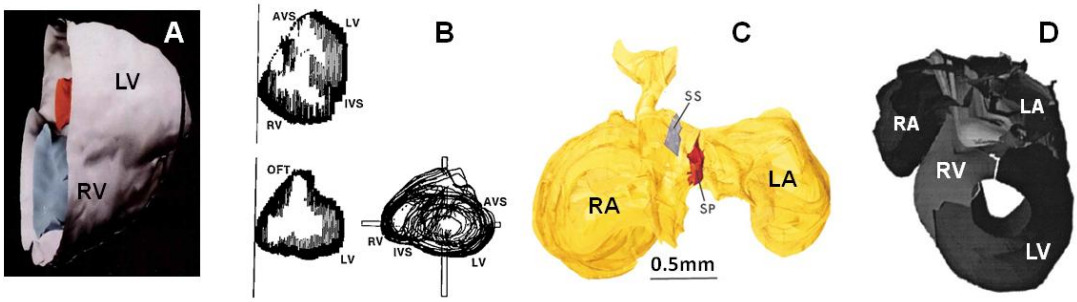

AVS; atrioventricular sulcus, IVS; interventricular septum, OFT; outflow tract, LA; left atrium, LV; left ventricle, RA; right atrium, RV; right ventricle, SP; Septum Primum, SS; Septum Secondum

In 2007, Yamada et al described 3D reconstructed images of eight normal and two abnormal human fetal hearts by the conventional method using histological slides (Carnegie stage 11 - 20). (Yamada, Itoh et al. 2007) Figure 1-14 shows pictures and 3D reconstructed images of a normal embryo and a embryo with holoprosencephaly and double outlet from the right ventricle. (Carnegie stage 20; about nine post-menstrual weeks) Their 3D images, which demonstrate inner cavities of heart chambers created by internal references using histological slides, show a non-aligned and jagged appearance (B-D and F-H). Segmental description of the morphological diagnosis is difficult because of its low quality.

Figure 1-14: Pictures and cardiac 3D images of normal (upper) and abnormal (lower) human embryos. (modified figure 5; Yamada 2007) Normal embryo (A) and its 3D cardiac images (B–D) and holoprosencephaly embryo (E) and its cardiac 3D images (F–H). B and F: Anterior views of the heart. Ventriculo arterial connection is double outlet of the right ventricle with a ventricular septal defect (arrow) in the abnormal heart (H) although great arteries arise normally in the normal embryo (D). Atrioventricular connection is not clearly shown.

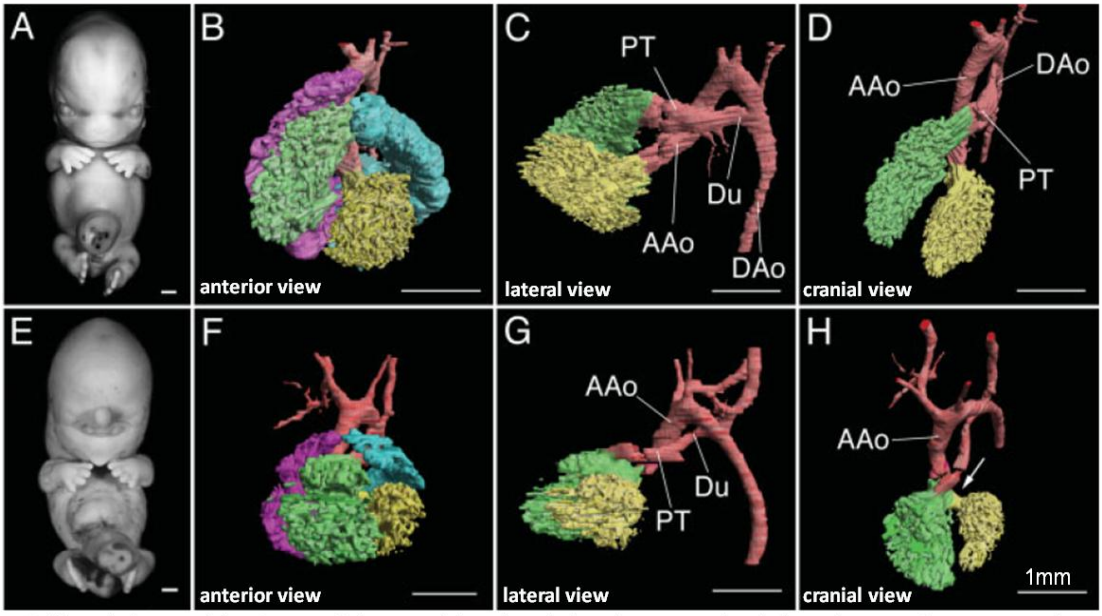

Yellow; left ventricle, Green; right ventricle, Blue; left atrium, Purple; right atrium, Red; great arteries
AAo; ascending aorta, DAo; descending aorta, Du; arterial duct, PT; pulmonary trunk

Recently, Dhanantwari et al reported investigation of cardiogenesis using 3D reconstructed images of 42 human fetal hearts (Carnegie stage 13-23, 6-9 post menstrual gestation) by micro MRI and EFIC and proposed series of digital images as an atlas of cardiogenesis in the human. (Dhanantwari, Lee et al. 2009) EFIC was successful in 11 of 22 fetal hearts and described major anatomical finding of the developing human fetal heart (Figure 1-15), however no detailed cardiac components were described, including ventricles, atriums, valves or great arteries, because EFIC was not sufficient to observe detailed tissue architecture because of weak fluorescence. (Weninger and Mohun 2002) Furthermore, they did not demonstrate 3D appearance of whole hearts suggesting it is difficult to distinguish the heart from other tissue, like lung or diaphragms, surrounding the heart and cardiac surface was not clearly detectable for 3D volume rendering.

Figure 1-15: Pictures of EFIC images of the human fetal heart. (modified figure 4; Dhanantwari 2009) 3D structures of endocardial cushion (* in A) and well-formed atrioventricular junction (arrowhead in B and C) were shown, however tissue architecture is not clear because of less contrast and weak fluorescence of this technique.

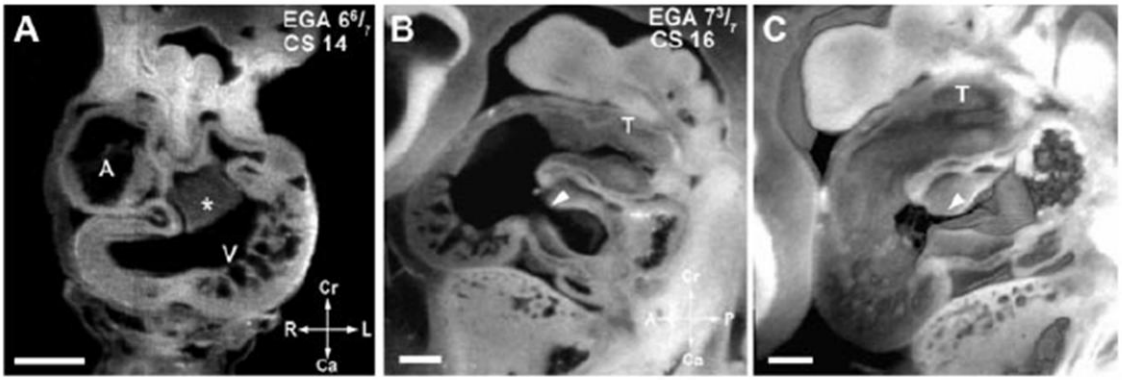

R; right, L; left, Cr; cranial, Ca; caudal, EGA; estimated gestational age, CS; Carnegie stage
A; primitive atrium/venous confluence, V; ventricular chamber, T; truncus arteriosus.

Thus, no detailed morphological assessment of the normal fetal heart in the human has been available.

1.5 Morphological Investigation by Three Dimensional Fetal Echocardiography

1.5.1 History of morphological investigation of cardiac structures by fetal echocardiography

Fetal echocardiography is the most useful tool to assess the fetal cardiac structure in the living human. The first description of images by 2D images of the human fetal heart was reported by Garrett et al in 1970 (Garrett and Robinson 1970) and their early images were still pictures illustrating the image of morphological structures of the human fetal heart, however, preliminary images required skills for analysing information and were difficult for most cardiologists to interpret. In the 1980s, many reports described the feasibility of two dimensional fetal echocardiography for morphological assessment. Lange demonstrated high success rate of cardiovascular images after 19 weeks of gestation in 111 normal hearts and proposed the possibility of diagnosis of major congenital heart diseases. (Lange, Sahn et al. 1980) Allan reported the success rate of standardised planes and the accuracy of diagnosis of structural heart malformation in fetuses in the second trimester. (Allan, Tynan et al. 1980; Allan, Chita et al. 1989) Three dimensional (3D) echocardiography was firstly applied to the fetus in 1996. (Nelson, Pretorius et al. 1996; Zosmer, Jurkovic et al. 1996) Their 3D echo data needed to be analysed off-line and the image quality of cardiac planes captured by manual sweeping was not clearly focused, however they described the potential to use 3D fetal echocardiography in clinical practice.

1.5.2 Morphological assessment of fetal heart in the first trimester by 3D fetal echocardiography

Morphological assessment of the human fetal heart in early gestation by 3D echocardiography is still challenging even using the high quality transvaginal probes available for 3D echo scan of small fetal hearts. Vinals et al first reported the usefulness of 3D echocardiography recorded by transvaginal probe at 11- to 13- week fetuses for the purpose of screening by telemedicine (Vinals, Ascenzo et al. 2008) Achiron et al demonstrated cases of thoracic anomalies by 3D echocardiography using either transvaginal or transabdominal probe. (Achiron, Gindes et al. 2008) Bennasar et al reported feasibility of 3D transvaginal fetal echocardiography for assessment of major cardiac structures. (Bennasar, Martinez et al. 2009) However, no morphological assessment of detailed structure of the fetal heart is yet available.

1.6 Limitation and Issue of Investigation into the Developing Human Fetal Heart

1.6.1 Limitation of the Investigation into the Developing Human Fetal Heart

Molecular investigation of human fetal hearts is difficult although investigating regulatory factors is essential for understanding the process of the heart's development. However, the molecular factors regulating heart development are largely unknown in humans because of the degradation and the decomposition of the heart tissue caused by prolonged delivery time after fetal death. This problem makes it more difficult to investigate molecular factors in the human, especially transcriptional factors where a short processing time is important.

1.6.2 Current Issue of Morphological Investigation into the Human Fetal Heart

No detailed morphological 3D investigation into the developing human fetal heart in the first and early second trimester after cardiogenesis has been performed despite 3D evaluation. Morphological differences of the heart between the human and experimental models, such as the mouse, are unclear. Documenting normal morphological structure and distinguishing between normal and abnormal phenotypes by high quality 3D modality at each step of the developing heart will be a fundamental first step towards the origins and therapies of fetal cardiac abnormalities with impaired heart development. To this end, comparison of high quality in-vitro imaging with the latest 3D echo modality will be the first step for detailed diagnosis in early human fetal hearts.

1.7 Study Aim and Hypothesis

1.7.1 Study Aim

The aim of this thesis is to clarify the morphological features of the human fetal heart in the early stages of fetal heart maturation using HREM, a newly-developed high-quality image modality.

1.7.2 Hypothesis

In this study I propose the following hypotheses:

Main hypothesis:

Morphological development in normal human fetal hearts for few weeks after cardiogenesis can be described in detail resulting in contribution into basic and clinical diagnosis of human fetal hearts in the first trimester.

Hypothesis in chapters

- No important morphological deformation of fetal hearts has occurred in the process of HREM.
- No significant difference of measurement of length in fetal hearts has occurred by the process of HREM for quantitative assessment.
- Morphological assessment of the normal human fetal heart from nine to seventeen weeks post-menstrual gestation can be achieved by HREM.

- Geometrical quantification of the heart, including length and volume measurement, can be achieved by HREM.
- Reconstructed images by HREM can show specific morphological features of the human fetal heart from 9 to 17 post menstrual weeks of gestation.
- Quantitative cardiac growth of the human fetal heart from 9 to 17 weeks of post menstrual gestation can be shown by morphometry.
- Great arterial measurement during the heart maturation can be described by HREM.
- Maturation of specific components of the human fetal heart can be qualified by HREM.
- Difference in fetal cardiovascular structures between the human and the mouse after cardiogenesis, can be detected by HREM.
- Fetal echocardiography can demonstrate 3D structure for morphological investigations in human fetal hearts.

2.0 Chapter Two

Methods (Research Facility, Ethical approval, Study Population, Sample Collection and Technique)

2.1 Research Facility

The research in this thesis is a collaborative work between four facilities:

- Institute of Reproductive and Developmental Biology (IRDB), Department of Surgery and Cancer, Faculty of Medicine, Imperial College, London

  Paperwork and data-processing mainly have been done in this facility.

- Division of Developmental Biology, National Institute of Medical Research (NIMR), Mill Hill, London

  HREM process has been done in this facility.

- Cardiac Morphology Unit, Royal Brompton and Harefield Hospital (RBHH), London

  Morphological and histological investigations of fetal samples have been done in this facility.

- Department of Obstetrics and Gynaecology, Chaim Sheba Medical Centre, Tel Hashomer, Israel

  All clinical images of fetal hearts were collected in this facility.

2.2 Ethical Approval

This research is a part of the project approved by the Hammersmith and Queen Charlotte's and Chelsea Hospitals, Imperial College NHS Trust, Research Ethics Committee. (2003/6496, Title: "Investigation into the narrowing of the components of the left side of the heart and its outflow vessels leading to obstruction of blood flow during human fetal cardiac development." Primary investigator: Dr Helena Gardiner)

- Approved Date: 11th November 2003
- Amendment 1: Approved on 9th August 2006
    - Collecting samples at Chelsea & Westminster Hospital NHS Trust was approved.
- Amendment 2: Approved on 29th March 2007
    - Analysing using new imaging modality (HREM) was approved.
- Amendment 3: Approved on 18th December 2007
    - Change of the information sheet and the consent form was approved. This amendment is to combine those of this study with that of another group (Haematology, Principal Investigator; Professor Irene Roberts, Ethics Ref numbers: 04/Q0406/145) to obtain the maximal number of tissues.

2.3 Study Population

2.3.1 Study Population for research using human fetal hearts

2.3.1.1 Study Population

Singleton pregnancies undergoing surgical termination of pregnancy (TOP) from six to 17 weeks have been recruited under clause C or E of the 1967 Abortion Act.(AbortionAct 1967) All mothers were given time to consider co-operating in the research after a full explanation from the information sheet (Appendix 1C for normal hearts and 1D for abnormal hearts). Written consents were obtained from all mothers who agreed to participate in the study. Each original consent form was put into the patients' note.

2.3.1.2 Patient's Consent and Sample Collection

Cardiac samples were retrieved from fetuses following TOP. Recruited patients were attending obstetric clinics for surgical TOP at two hospitals; one was at the general obstetric clinic at QCCH and the other was at the gynaecology clinic at Chelsea & Westminster Hospital (CWH). Patients' gestation ranged from six to 17 weeks. Each gestational age was confirmed by crown-rump length or by bi-parietal diameter at both clinics. All the mothers who agreed to donate fetal tissues had the information sheet fully explained (Appendix 1C in normal and 1D in abnormal hearts) before consenting to the research project and parental written consents were obtained.

Samples were collected at the surgical theatre in Hammersmith Hospital, Imperial College Healthcare Trust, or at the treatment centre in CWH. Surgical TOP was

performed by suction or forceps at each facility. Hearts and lungs were isolated in the laboratory at the IRDB or at the laboratory in RBHH. Table 2-1 shows the success rate of maternal consent and collection of samples.

Table 2-1: Success rate of maternal consent and collecting heart samples.

	Maternal Consent				Sample Collection	
Post menstrual week at TOP	Number of Cases	Number of Consent	Rate (%)		Number of Success	Rate (%)
6	13	11	85		0	0
7	19	16	84		0	0
8	17	12	71		0	0
9	35	27	77		8	30
10	12	10	83		4	40
11	17	14	82		10	71
12	10	6	60		2	33
13	14	8	57		5	63
14	12	9	75		5	56
15	2	1	50		0	0
16	6	2	33		2	100
17	12	4	33		4	100
	169	120	66		40	33

The period of sample collection was from August 2006 to June 2008 (total 22 months). In April 2007 sample collection was stopped before nine post-menstrual weeks because these cases are too soft to preserve the heart structure against surgical TOP and no heart tissue could be retrieved. I obtained 40 samples of human fetal

hearts from nine to 17 weeks post-menstrual gestation in 120 attempted collections (successful rate of retrieval 41%; 55% after nine post-menstrual weeks). Retrieved fetal hearts were immediately fixed with 10% formalin. After collection, the rest of the tissues were taken back to the surgical theatre in each hospital to dispose of them appropriately.

2.3.1.3 Sample Registration and Transportation

All tissues were legally registered on Itemtracker for storage at the Cardiac Morphology Unit, Royal Brompton Hospital NHS Trust. All samples were transported to NIMR for HREM processing by medical courier under Material Transfer Agreement. Human tissues were kept strictly in the storage refrigerator. After the HREM process, all the samples were transferred back to the Cardiac Morphology Unit, RBHH and registered in the same way.

2.3.1.4 Sample Quality

Within the 40 cases of collected heart samples, some were used for other preliminary molecular research by cutting the ventricular apex, and some were damaged by the TOP procedure itself and only partly available for research because of this. Finally, I obtained 36 normal samples and one abnormal heart with hypoplastic left heart syndrome for the research. Table 2-2 shows the availability of samples for the research.

Table 2-2: Availability of normal (left) and 1 abnormal hearts (right).

	Normal Heart (36 cases, 9 - 17 weeks)			Abnormal Heart (Hypoplastic Left Heart Syndrome)
	Intact	Partly available	Not available	
Left Atrium	16	7	13	Intact
Right Atrium	17	7	12	Intact
Left Ventricle	16	19	1	Intact
Right Ventricle	18	17	1	Intact
Aortic Valve / Aorta	26	0	10	Intact
Pulmonary Valve / Trunk	25	1	10	Intact
Aortic Arch	12	1	13	Not Available
Ductal Arch	8	2	26	Not Available

2.3.2 Study Population for the research using human fetal hearts from post-mortem specimens

Post-mortem specimens of normal fetal hearts stored at the Cardiac Morphology Unit at RBHH were used for the research. All samples have agreement with written consent for post-mortem scientific survey. All tissues have already been registered by Itemtracker at RBHH under Human Tissue Regulations.

2.3.3 Study Population for the research using mouse hearts

Wild type mouse fetal hearts from stage E14.5 to E18.5 were used for the HREM at NIMR. All mice were obtained from the Biological Services Division at NIMR. Mouse fetal hearts were immediately retrieved by dissection before fixation with 4% paraformaldehyde (PFA). All fetal mouse samples were kept in the refrigerator or the cold room at the Department of Developmental Biology at NIMR.

2.3.4 Study Population for the clinical research

Singleton fetuses with normal nuchal translucency, healthy mother and no detectable malformation from 9 week 6 days to 12 weeks 6 days postmenstrual gestation were enrolled at the department of Obstetrics in the Chaim Sheba Medical Centre, Israel. All mothers were given time for co-operation of the research and written consents were obtained from all mothers who agreed with participating in the research. All written documents were kept in the centre in Israel. Original 3D images of fetal hearts were digitally stored in the echo machine and data was securely transferred to IRDB in London and analysed. Normal cardiac morphology was confirmed in all fetuses later in pregnancy and after delivery.

2.4 Technique

2.4.1 High Resolution Episcopic Microscopy (HREM)

2.4.1.1 Principle

The principle of HREM is to create 3D images by reconstruction of digital images of sections of samples. This concept is similar to 3D reconstruction of CT or MRI. Tomographic images are taken by digital capturing the surface of the sectioned sample by a charge-coupled device (CCD) camera. Figure 2-1 shows a flowchart of the step of HREM processing. After trimming and preparing specimens, samples needed to be embedded into plastic resin (JB4 Embedding kit which consists of solution A and B, Polysciences Inc) for hardening the block of a sample to avoid the problems of the distortion. The plastic resin is mixed with dye for staining tissue dark and making background. Volume dataset of digital images is obtained by automatic sectioning and capturing of the embedded sample. Then, high quality digital images or 3D images are created by processing the volume dataset using graphics programmes.

Figure 2-1: Flowchart of HREM processing.

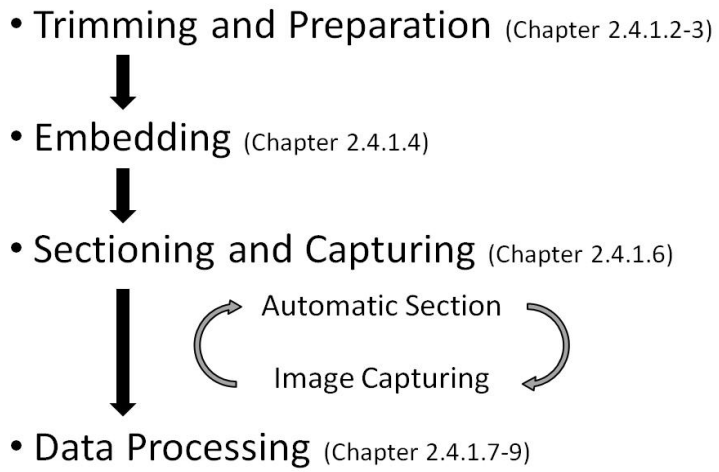

2.4.1.2 Trimming Samples

Before preparation of samples for HREM processing, samples must first be trimmed manually, using a microscope to remove unnecessary tissues from the cardiovascular system. Figure 2-2 shows an example of sample before and after trimming of unnecessary tissues. Before trimming, the heart is covered by pericardium, there are many connective tissue surrounding great arteries and the lung is attached to the pulmonary arteries and veins (left). After trimming, each component of the heart is clearly visible including ventricles, atria and great arteries (middle). Unnecessary tissues (right) are gathered and taken back to the surgical theatre for appropriate disposal.

Figure 2-2: Sample before (left) and after (middle) dissection and unnecessary tissue (right). The heart was covered by endocardium and lung. After trimming the sample, heart structure is clear.

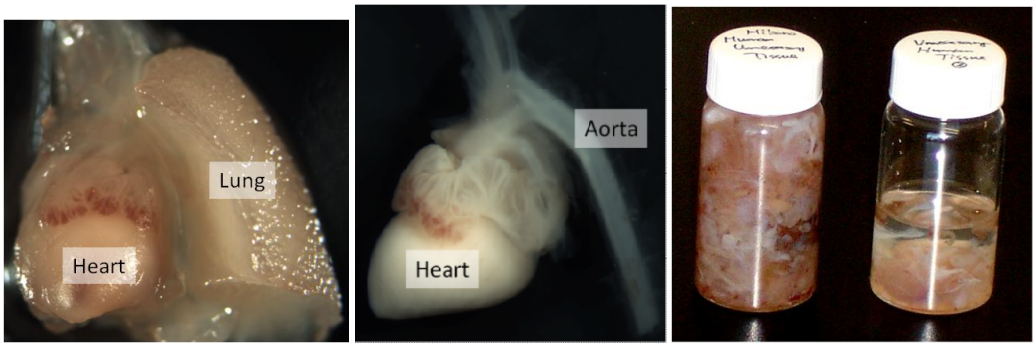

2.4.1.3 Preparation

Preparation of samples is the most vital step in the process of HREM. The embedding medium for HREM is a JB4 solution, which includes glycol methacrylate

(GMA) as its main plastic substance. JB4 solution consists of solution A and B. JB4 solution A contains monomer GMA, which converts to polymer GMA by adding enhancer (solution B). (Weninger, Geyer et al. 2006)

Figure 2-3: Flowchart of HREM preparation.

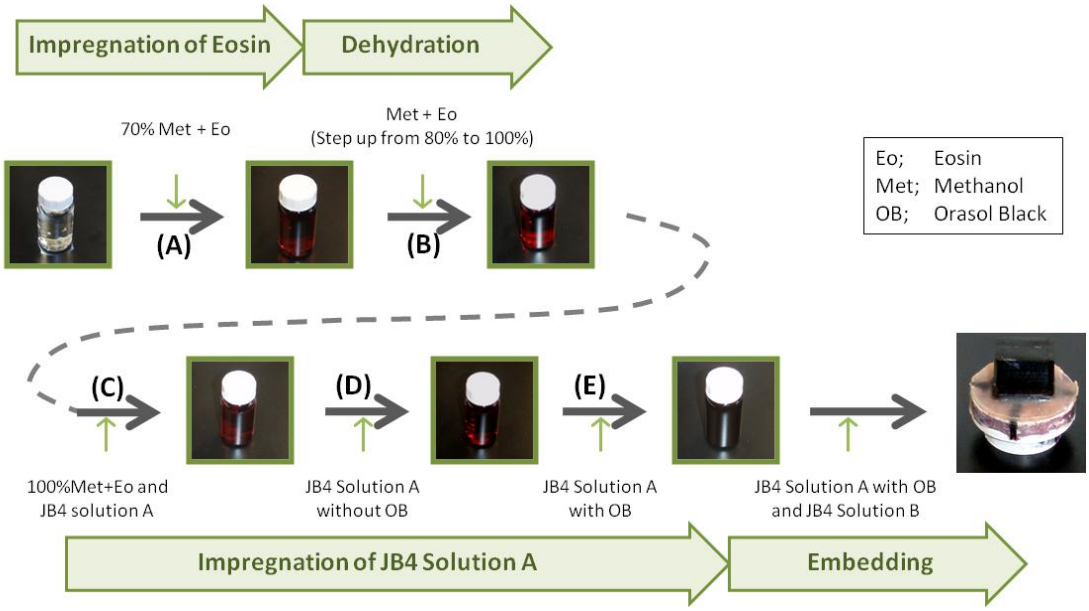

Figure 2-3 demonstrates the flowchart of preparation for HREM processing. There are two purposes in this step. The first is staining samples with dye. In order to capture clear images of the surface of the sectioned block, the sample needs to be stained by eosin, producing good contrast of images between samples and plastic resin. If tissues are not stained by eosin well, the tissue images become significantly bright because of fluorescence. The staining with eosin has another roll which is making background to minimise “bleedthrough” of data from below the surface. Therefore, sample tissue must be stained with eosin well enough in HREM steps (A).

Impregnation of eosin into cardiac tissue can be helped by agitating sample bottles on a bottle roller. The other purpose is for dehydration and impregnation of primary solution for samples to avoid softening the plastic resin. Dehydration is important because GMA is hydrophilic and excess water inside samples blocks polymerization resulting in soft blocks (B). Consistently, the primary solution of plastic resin (JB-4, solution A) needs to be impregnated enough into samples before embedding to harden the sample itself (C-D). JB4 solution A used to contain dark dye (Orasol Black) to create further contrast of captured images, but we have stopped using it since June 2009 (E). Table 2-3 shows each solution for the step of preparation in HREM.

Table 2-3: Solution for preparation and embedding.

	Solution	**Purpose**	**Ingredient**	**Amount**
Preparation	**70% Methanol + eosin**	Staining tissue by eosion	70% Methanol	100ml
			Eosin B	0.275g
	80% - 100% Methanol + eosin	Dehydration	80 – 100% Methanol	100 ml
			Eosin B	0.275g
	Half and Half solution	Impregnation of JB4 solution	100% Methanol + eosin (Same as above)	
			JB4 solution A without Orasol Black (Same as below)	
	JB4 solution A without OB		JB4 Solution A	100ml
			Eosin B	0.275g
			Acrydine Orange	0.055g
			Catalyst	1.25g
	JB4 solution A with OB	Impregnation JB4 solution and Embedding	JB4 Solution A	100ml
			Eosin B	0.275g
			Acrydine Orange	0.055g
			Catalyst	1.25g
			Orasol Black	0.1g
Embedding	**JB4 Solution B**	Embedding	JB4 Solution B	

Table 2-4 shows a time schedule of the preparation of the fetal heart in the human and the mouse. The preparation of the human fetal heart for HREM takes several weeks. Larger samples generally require longer time for dehydration or impregnation of eosin or JB4 solution than smaller ones because of their size. The duration varies from 2 to 50 days in the human while the preparation normally finished within one day in the mouse. Bigger samples require longer duration for preparation for the human fetal heart. It is impossible to capture clear images without sufficient impregnation of eosin in this step in HREM. Thus, appropriate preparation is vital for the HREM process in the human fetal heart.

Table 2-4: Protocol and Time schedule for the preparation.

<table>
<tr><th colspan="2" rowspan="2"></th><th colspan="3">Human Fetal Heart</th><th rowspan="2">Mouse Fetal Heart</th></tr>
<tr><th>9-11 weeks</th><th>12-14 weeks</th><th>15-17 weeks</th></tr>
<tr><td rowspan="2">Staining with eosin</td><td rowspan="2">70% Methanol + eosin</td><td rowspan="3">1 days</td><td>14 to 27 days</td><td>30 to 40 days</td><td rowspan="3">Half day</td></tr>
<tr><td rowspan="2">dehydration</td><td rowspan="2">80-100% Methanol + eosin</td><td rowspan="2">5 days</td><td rowspan="2">5 days</td></tr>
<tr><td rowspan="3">Impregnation of JB4 solution A</td><td>Half and Half solution</td><td rowspan="3">1 days</td><td rowspan="3">4 days</td><td rowspan="3">5 days</td><td rowspan="3">Half day</td></tr>
<tr><td>JB4 solution A without OB</td></tr>
<tr><td>JB4 Solution A with OB</td></tr>
</table>

2.4.1.4 Embedding

After the first step of preparation, a sample is embedded in a mould with hardening process by mixing solution A with B. For embedding the samples original large moulds are required because a commercially available mould is too small to embed the human fetal heart. There are several sizes of the original moulds which are produced for embedding large samples. Figure 2-4 shows different types of moulds (upper figure) and plastic embedded samples (lower figure). A sample and a mould need to be matched in size.

Figure 2-4: Embedding moulds and embedded samples. From the left hand side, depth of the mould is 8, 12, 15 and 20 mm, respectively. Embedded samples are dark wine red.

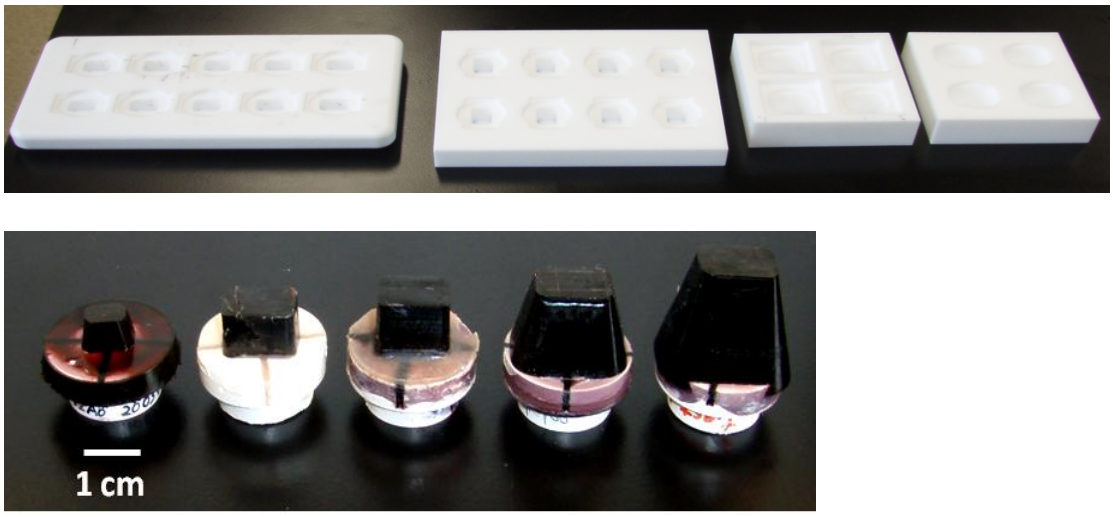

Plastic resin in a large mould, experimentally, tends to harden less than in a small mould, resulting in a soft sample block. Some samples embedded in the large

mould were too soft for sectioning. To overcome this difficulty we found a new method to harden the soft blocks. In cases of soft sample blocks after embedding, they were kept in the heater for two days at 90°C followed by cooling down in a refrigerator for one day. This step was repeated four times for each sample. Every sample then became hard enough for sectioning.

2.4.1.5 Capturing System

The equipment of HREM is shown in the Figure 2-5. There is no commercially available system of HREM. The HREM process is controlled by signalling between the microtome, the shutter control unit and the capturing software. Table 2-5 shows the list of equipment.

Figure 2-5: HREM system.

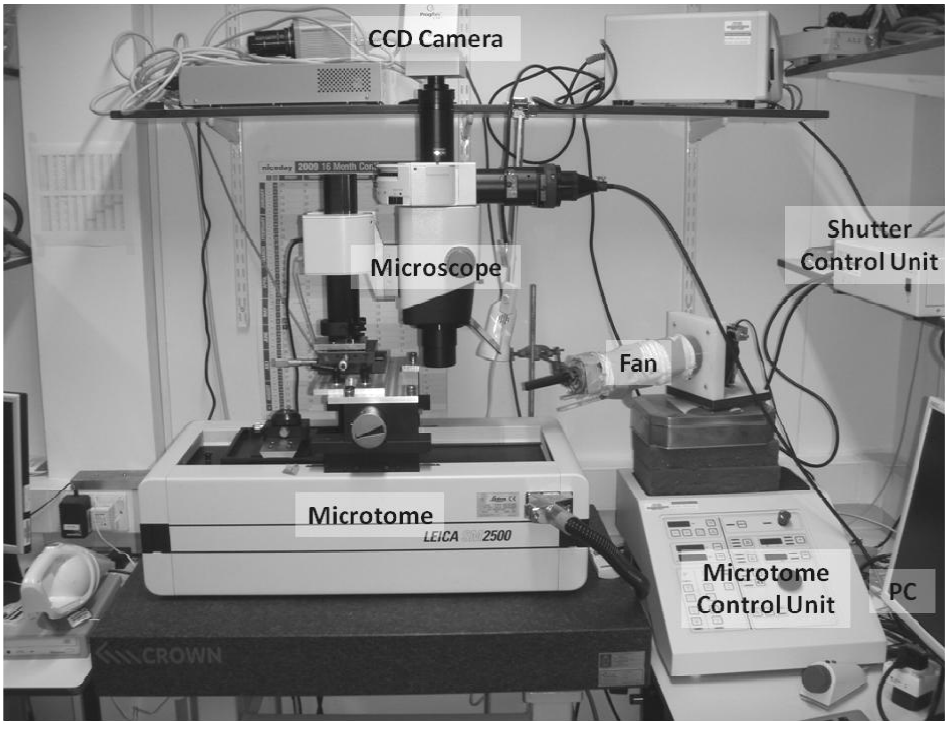

Table 2-5: Details of products in HREM system.

Product Name	Company	Country		Purpose
SM2500	Leica	Germany	Microtome	Sectioning a sample
MVX10	Olympus	Japan	Microscope	To magnify an image
Lumen200PRO	Prior	UK	Fluorescence Illumination	Microscope light
ProScan II	Prior	UK	Shutter Control Unit	To control the timing of shutter
ORCA-HR	HAMAMATSU	Japan	CCD Camera	To send an image to the software
ProgResC14	JENOPTIK	Germany	CCD Camera	
ImagePro Microscope Control	MediaCybernetics	USA	Capturing Software	To capture the image from the camera

2.4.1.6 Sectioning and Capturing Images

Digital images of samples are produced by repeating automatic sectioning and image capturing a sample. Figure 2-6 shows the flowchart of one cycle of the data acquisition process.

Figure 2-6: Flowchart of HREM data acquisition.

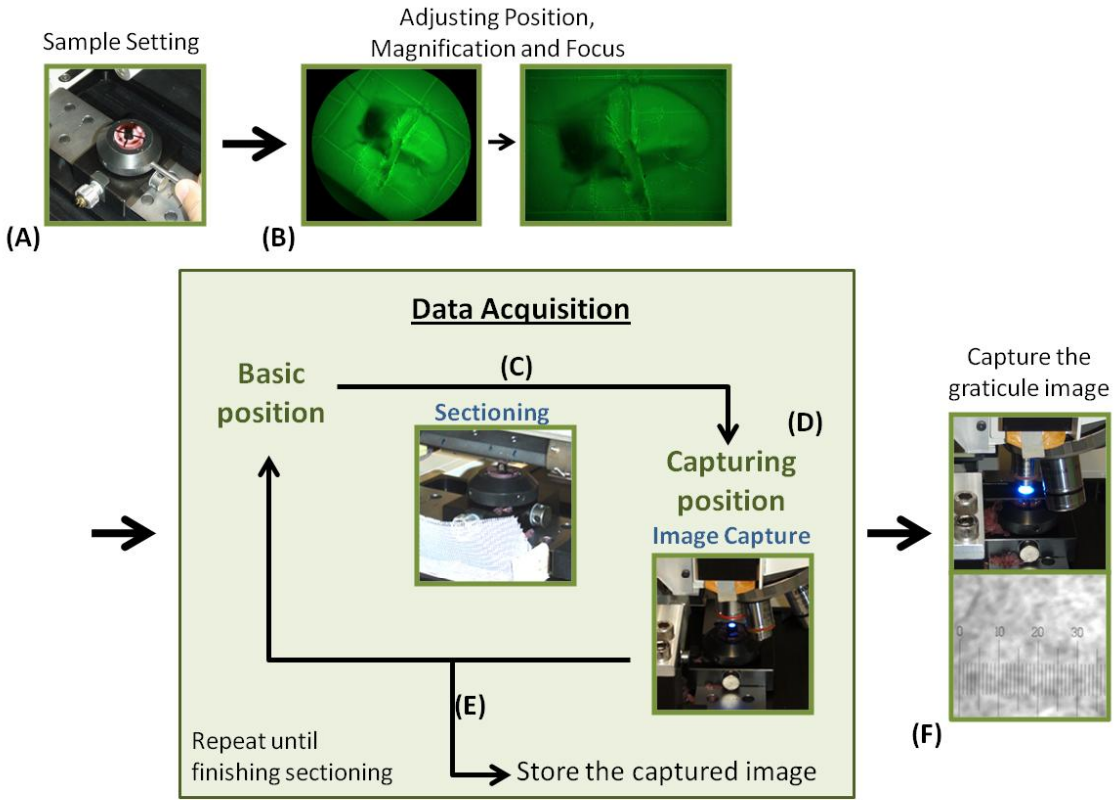

After setting a sample (A), the image needs to be optimized by adjusting position, magnification and focus (B). Then, each sample is automatically sectioned by sliding microtome before imaging the surface of the sectioned block (C). The minimum thickness of the section is 1 micrometre. After sectioning the sample, episcopic illumination lights up the sample followed by digital capture of the surface of the

sectioned block by the CCD camera (D). A captured image is stored in TIFF format and then the same step continues for the next capturing (E). This step is normally repeated more than a thousand times in the human fetal heart until finishing sectioning the sample. The captured images are completely aligned without any distortion of the samples. Sectioned samples are available for further histological investigations. The size of each original image is 4000 x 2624 pixels in HAMAMATSU CCD camera and 1360 x 1024 pixels in Jenoptik CCD camera. In either case, images are captured in 8 bit format (256 greyscales). After sectioning, an image of a graticule is captured for calibration using the same setting as for the sample dataset (F).

Image resolution depends on not only the sensor resolution of the CCD camera ("How many pixels we can capture") but also the optical resolution of the microscope. Optical resolution, the ability of the microscope to resolve detail, is generally determined by the quality and the size of the lens. We use the macro zoom fluorescence microscope (MVX10, Olympus Inc.) which has relatively high numerical aperture (the index contributes to focal length and brightness) and is suitable to obtain clear and bright images for big samples because sample size is relatively large in the human fetal heart (5 - 20 mm in lengths).

2.4.1.7 Data Processing

Manipulation of digital images is necessary to obtain clear 3D images reconstructed from the original raw volume dataset. Table 2-6 shows the list of hardware and software programs for data processing. Each program has a special role to optimize the quality of volume datasets. Figure 2-7 shows an example of an image before and after data processing.

Table 2-6: Hardware and Software for data processing.

Hardware

Product Name	Company	Spec
iMac (20 inch display)	Apple	2.66 GHz model, ATI Radeon HD 2600 PRO Graphic Card, RAM 4 G bite

Program Software

Product Name and version	Company/ Organization	Purpose	Note
Photoshop CS3 ver 10.0.1	Adobe	To optimize the quality of images	Commercial software
ImageJ ver 1.40	National Institute of Health (USA)	Image cropping, background standardization and adjust size of the volume dataset	Public Domain Software
Graphic Converter ver 5.8	Lemke Software	To create a movie file of raw data	Commercial software
OpenLab ver 5.02	Improvison	Re-registration (to adjust image position)	Commercial software
Osirix ver 3.2	Osirix Foundation	Digital dissection, 3D reconstruction, measurement	Freeware (General Public License)

Figure 2-7: Flowchart of optimisation of digital images. First, original images are converted to grey scale (A) and background of all images was standardized to overcome any variations in illumination or fluorescence detection between images (B). Next, registration of all images is adjusted if optics has been realigned during data collection (C), followed by cropping images to remove unnecessary parts of images (D). Then, image brightness and contrast are optimised (E) and the image series sub-sampled for use in 3D modelling (F). Contrast and image quality are clearer after processing compared to the original raw image.

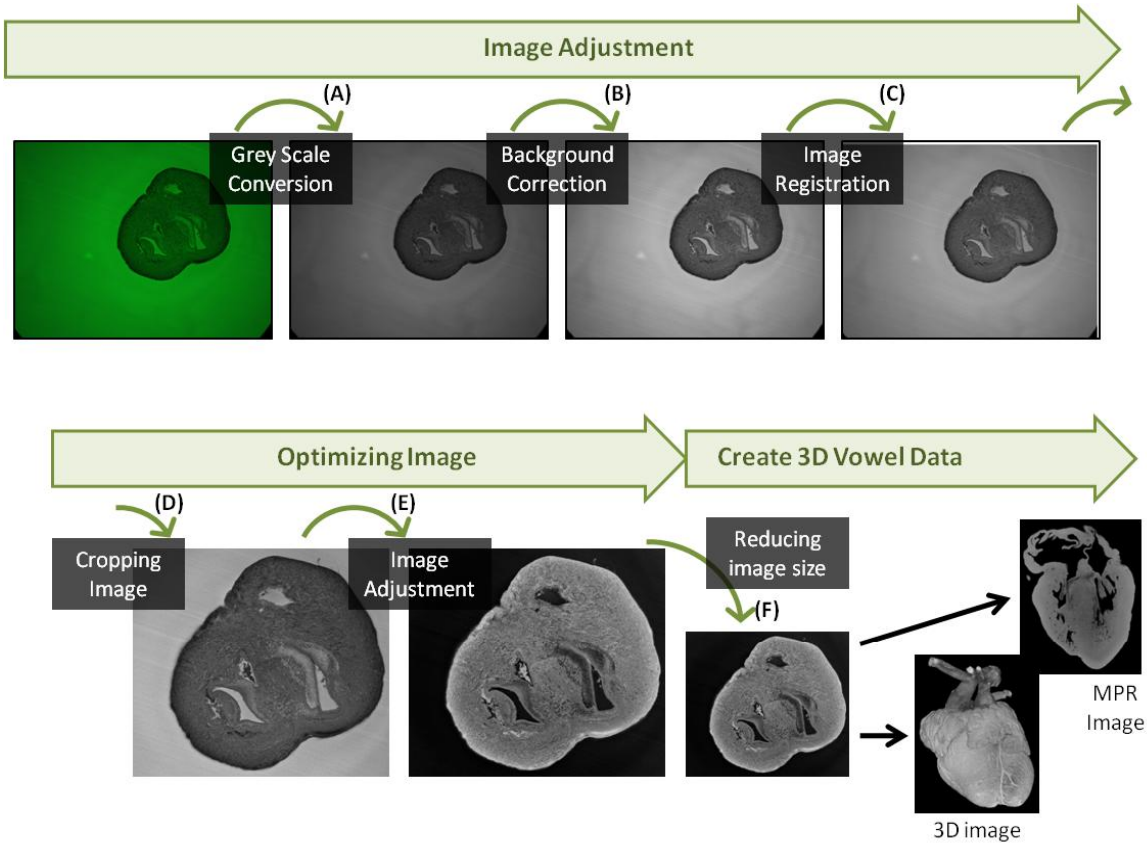

2.4.1.8 Creating 3D Volume Dataset

After adjusting image quality, calibration of digital images needs to be calculated for proportional reconstruction of 3D images. Figure 2-8 demonstrates the calibration of each 3D axis of HREM volume dataset.

Figure 2-8: Calibration of voxel data to create a volume dataset. To create 3D images by Osirix software, each pixel length (□m/pixel) of 3D axes (X, Y and Z) needs to be properly inputted for 3D calibration. Pixel dimension in X and Y-axes can be calculated using the graticule image captured during HREM process (A). Pixel dimension in Z-axis depends on the thickness of HREM sectioning (B). Then, the proportional 3D image is reconstructed by calibrating pixel dimension of 3 axes.

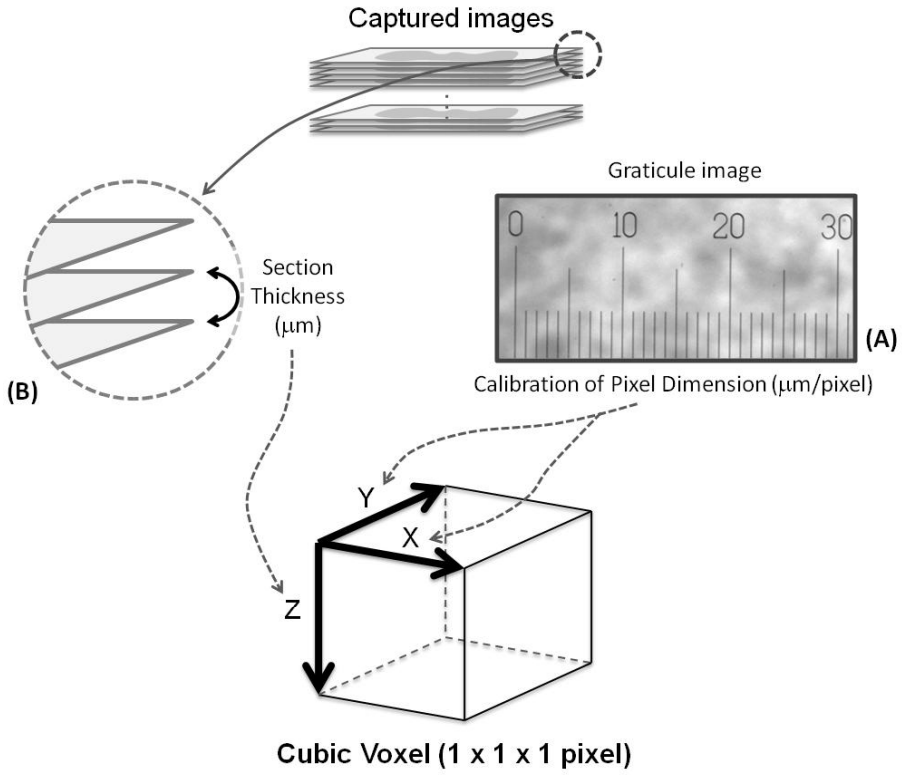

2.4.1.8: Qualitative 3D Data Assessment (Volume Rendering and Multi-planar Reconstruction)

Volume rendering (VR) is a technique used to display a 2D projection of a 3D volume dataset from the volume or rendering the volume directly as a block of data using voxel grey values. The visual appearance of the model will therefore depend on how the individual voxel values are interpreted by the rendering software (opacity, window length, window width and colour lookup tables). Figure 2-9 shows a range of images depending on various image settings. These images provide visually different information in the observation of 3D images.

Figure 2-9: Examples of various image setting of 3D VR image of a human fetal heart (11 post menstrual weeks). (A) Anterior view. The general appearance of the whole heart is easy to recognize in the left picture while the coronary arteries are clear in the centre picture. The yellow picture shows more contrast of the coronary arteries than the others; however, small coronary arteries were masked (arrow). (B) View from the apex. General structures are seen clearly in the left picture. The centre picture shows enhanced coronary arteries, but other structures are fading. Peripheral coronary arteries can be seen in the right picture; atriums and ventricles are less clearly defined than in the left picture. (C) Comparison of coronary arteries from the reverse. Peripheral arteries are recognized clearly in the right picture although the general structure can be seen as in the other images.

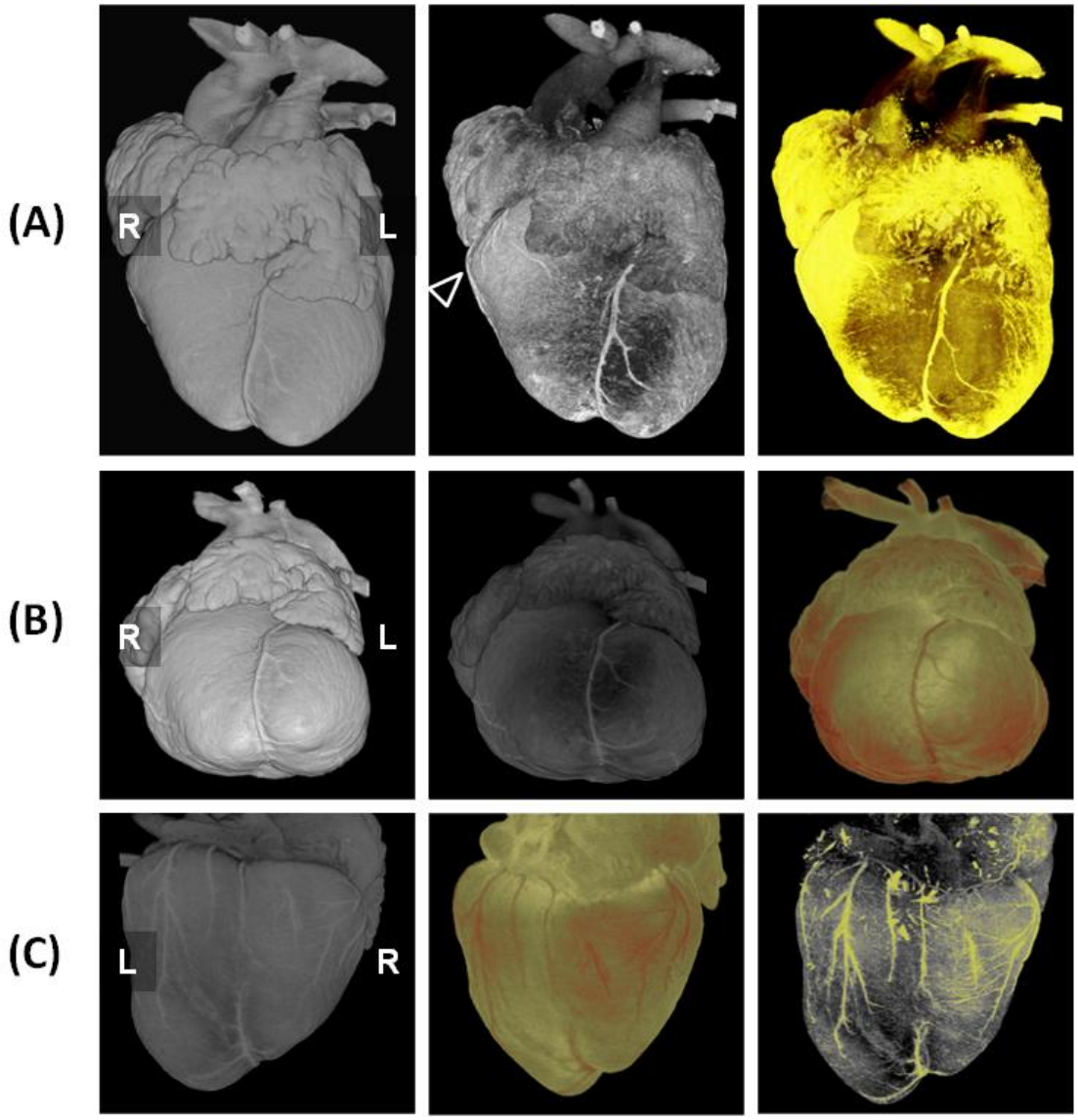

The inside of the heart can be observed qualitatively by eroding VR images or multi-planar reconstruction (MPR) images, which are 2D images reconstructed by cutting virtual slices of the 3D volume. Figure 2-10 shows examples of VR and MPR images.

Figure 2-10: Examples of VR image (A-E) and MPR image (F) of the human fetal heart (11 and 14 post menstrual weeks). (A) Ventricular cavity and septum can be observed. (B) Eroded images in the atrial level. 3D structure of atrial inner cavities is clearly seen. (C) Eroded images from the left caudal view. Tricuspid aortic valve (arrow) and section of left circumflex coronary artery (arrow) are seen. (D) Eroded image from the right caudal view. Structure of the pulmonary valve from the right ventricle can be seen (arrow). The arrow is the left anterior-descending coronary artery. (E and F) 3D structure of semilunar valves in the pulmonary valve is clearly recognized (*). Thickness of the pulmonary valves (*) and PA wall are identified in the MPR images. The black arrow shows the viewpoint of the VR image.

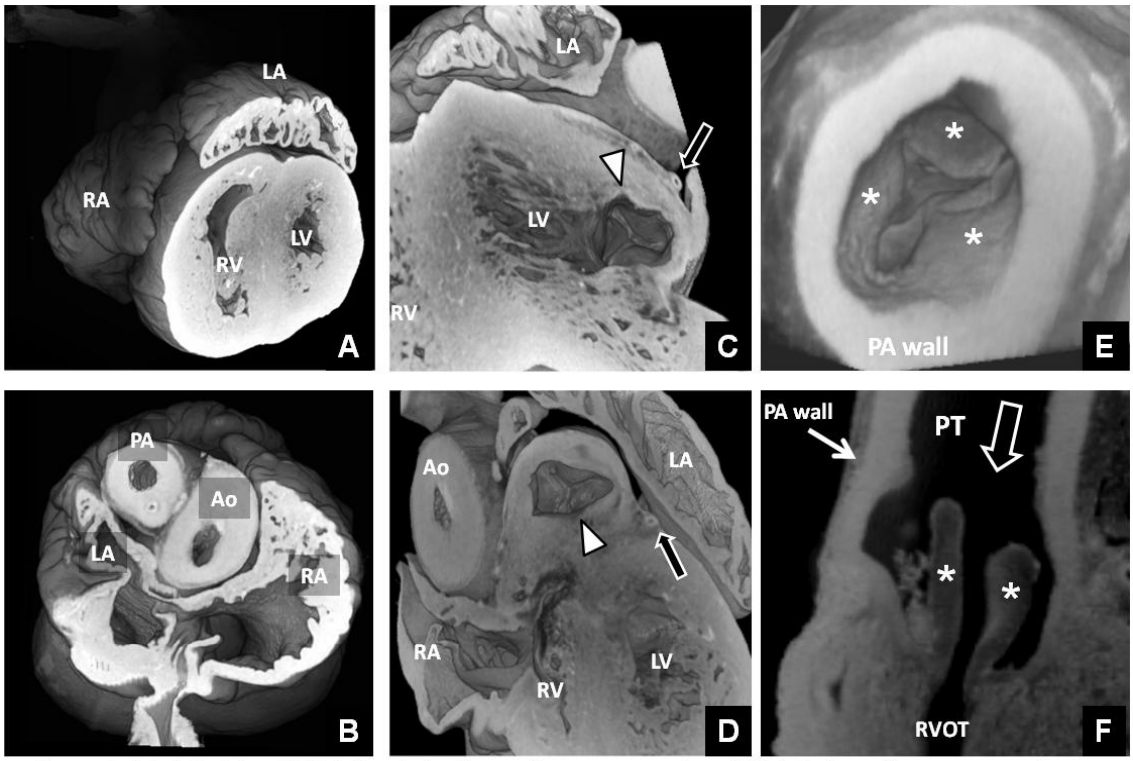

Ao; aorta, LA; left atrium, LAD; left anterior descending coronary artery, LCX; left circumflex coronary artery, LV; left ventricle, RA; right atrium, RV; right atrium, RVOT; right ventricular outflow tract, PA; pulmonary artery, PT; pulmonary trunk

2.4.1.9 Quantitative 3D Data Assessment (Length and Volume)

Geometrical measurement for morphological quantification in the 3D volume dataset consists of length and volume. Length is measurable in the VR or MPR images by the calliper in the software. Volume can be measured in the VR mode by selecting region of interest and calculating automatically. Figure 2-11 shows examples of length and volume measurements in the 3D images.

Figure 2-11: Geometrical measurement of 3D images. (A): Length by MPR image. Length shows cardiac width at the four-chamber view. Measurement is 0.343cm (3.43mm). (B) Length by VR image. The actual measurement is 1.1mm. (C) Volume measurement of ventricle by VR image. Atriums and great arteries are rejected (left). Region of interest of ventricles is selected (centre) and ventricular mass volume is calculated automatically (right). Cardiac mass volume (the volume of ventricular myocardium) is 0.2678 mm^3.

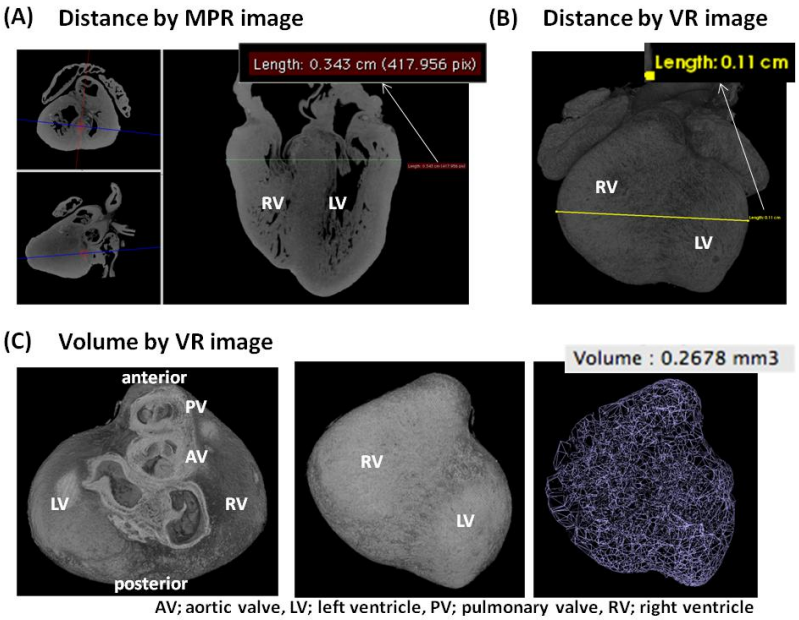

AV; aortic valve, LV; left ventricle, PV; pulmonary valve, RV; right ventricle

2.4.2 Measurement of length of morphological specimens by a microscope

2.4.2.1 Measurement of length by an eyepiece graticule

A micro-scale graticule inside an eyepiece was used to measure the length of samples (Figure2-12). Samples on the stereo-microscope were directly measured by an eyepiece graticule (A). In contrast, a graticule slide by the eyepiece graticule was calibrated with the same magnification (B). Then, we corrected the direct measurement of the sample by the calibration of the graticule slide (C).

Figure 2-12: Flowchart of the microscopic measurement using graticule in the eyepiece.

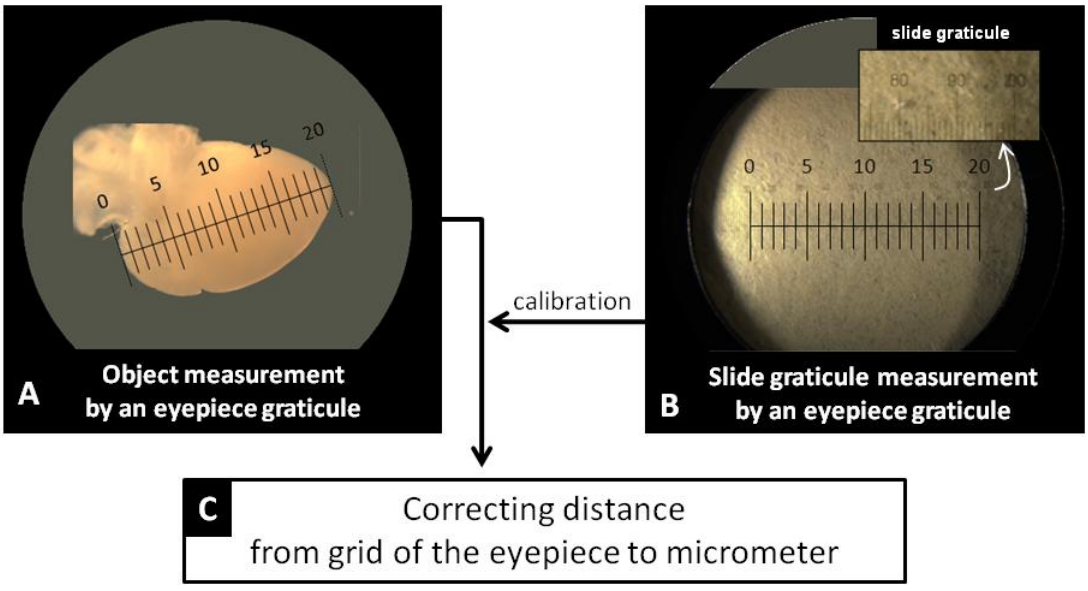

2.4.2.2 Measurement of length by digitally acquired pictures

Another way to measure length of samples was measurement using digitally acquired images of samples (Figure2-13). Samples on the stereo-microscope were digitally captured by a CCD camera (A) and the length of samples in pixels by software (Image J 1.40) was measured (B). The slide graticule was digitally captured with the same magnification (C) followed by calibration of pixel dimension (micrometer/pixel) of the images (D). The measurement of the samples was converted from pixels to micrometer using the calibration data of the slide graticule (E).

Figure 2-13: Example of digital measurement.

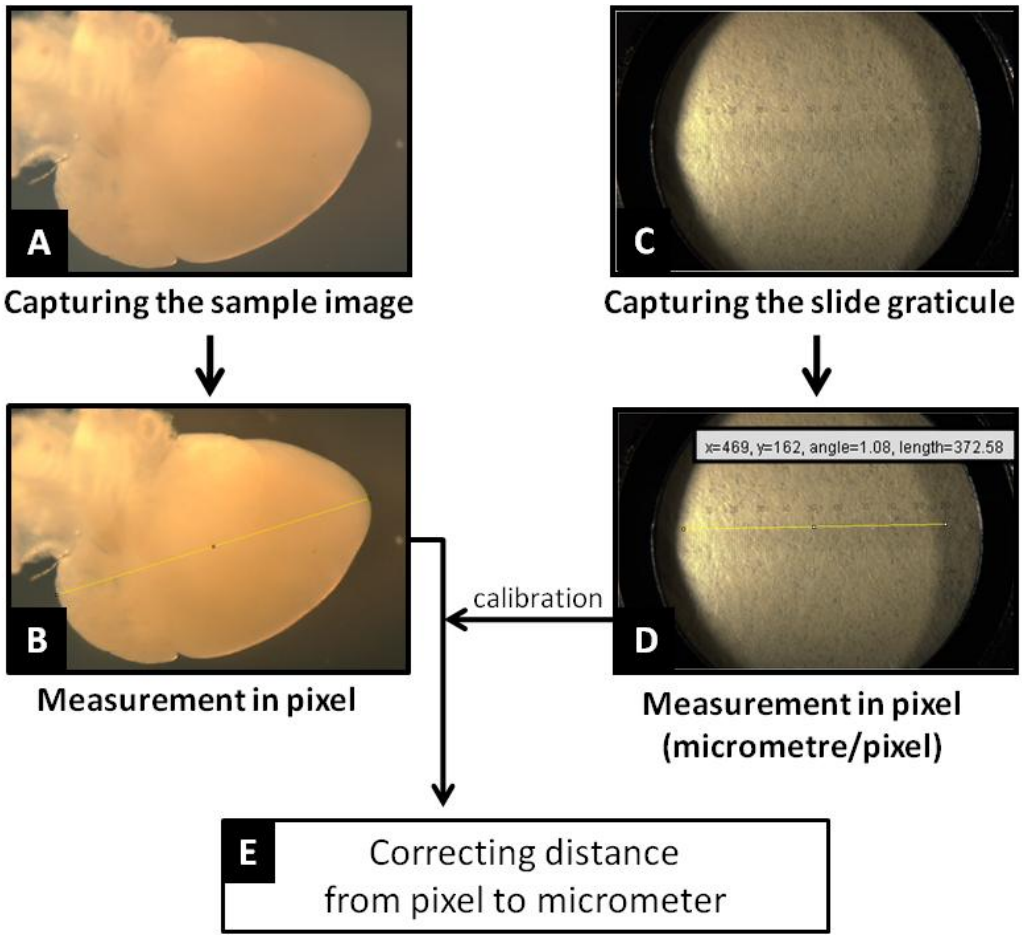

2.4.3 Histological Staining using plastic embedded sections

Histological staining is the standard method for assessing the detailed structure of tissue. However, there are several limitations of histological staining of sections of samples in HREM. Polymer glycol methacrylate (GMA), produced after polymerization of JB4 solution for HREM, cannot be de-plasticised, and plastic resin inhibits impregnation of several dyes into tissue (Rousselle and Wicks 2008). Impregnated resin covers the tissue surface and cellular matrix, resulting in the mechanical blockage of staining tissue by dyes. Thus, less staining is possible for plastic embedded sections.

In this research, the haematoxylin-eosin (HE) stain, which is for identification of the basic structures of cellular matrix, was successful for staining although specific stains, such as Masson trichrome, Elastic van Gieson stains or enzyme labelled antibody method of immune-histochemistry, proved unsuccessful. Table 2-7 shows the protocol of the HE stain for HREM sections.

Table 2-7: Protocol of Haematoxylin-Eosin (HE) stain for HREM sections.

1	Xylene	40 min
2	Delafield's or Harris' haematoxylin	5 min
3	Running tap water	5 min
4	Dip in distilled water	
5	Acid alcohol	15 sec
6	Dip in tap water	
7	Eosin	2 min
8	Dip in tap water	
9	Dry slides in oven at 45oC	10 min
10	Xylene	40 min
11	Mount to slides	

2.4.4 Three Dimensional Fetal Echocardiography

2.4.4.1 Spatio-Temporal Image Correlation

Spatio-Temporal Image Correlation (STIC) is a recent modality which allows us to create 3D images of fetal hearts by digitally captured consecutive 2D images in vivo. Many cardiologists use a transabdominal approach that may result in poorer image resolution when scanning small fetal hearts in the first trimester and we chose to use a transvaginal four dimension (4D) probe. This produces a detailed fetal heart scan using high frequency ultrasound. In this research, we used the volume data captured by STIC with the transvaginal 4D probe to create 3D images of fetal hearts in the first trimester.

Original data for STIC analysis was collected using Voluson E8 system with the transvaginal 4D probe (RIC 6-12 MHz transducer) (General Electric Medical Systems Kretztechnik, Zipf, Austria). Original STIC data was acquired in the transverse axial plane in the four chamber view of grey scale with 25 degree of the volume sweep angle and 7.5 seconds of the acquisition time. Acquisitions were performed during fetal rest and in the absence of fetal movement. The data was stored into the hard drive of the echo machine and transferred for offline analysis.

2.4.4.2 Data Analysis

Volume analysis was performed with 4D View software (GE Healthcare, Kretz Ultrasound). We used MPR mode to investigate cardiac morphology in vivo while volume rendering of the heart was unsuitable for 3D reconstruction because the border of the cardiac surface was unclear and undetectable because of lung tissue surrounding the fetal hearts. Figure 2-14 shows standard planes for morphological analysis in this research. We compared MPR images of cardiac structures in vivo captured by 3D fetal echocardiography with those in vitro reconstructed by HREM.

Figure 2-14: Standard planes of MPR image in 3D echocardiography.

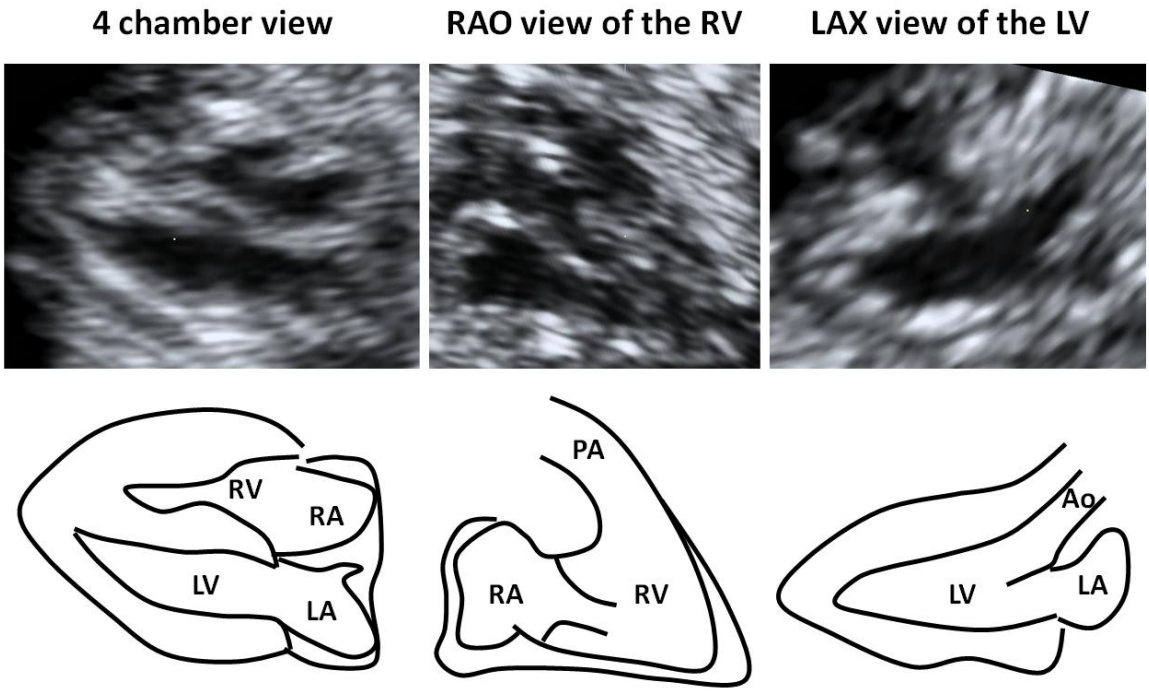

Ao: aorta, LA: left atrium, LAX: long axis, LV: left ventricle, PA: pulmonary artery, RA: right atrium, RAO: right anterior oblique, RV: right ventricle

3.0 Chapter Three:

Morphometric Validation of High Resolution Episcopic Microscopy

3.1 Introduction

No morphological validation of HREM has been published as yet while HREM is novel for qualitative and quantitative investigation of structure of samples. Clarifying morphological effects by HREM is important before assessment of 3D structure of human fetal hearts. Image data in HREM is based on use of fixed samples, embedded in plastic. The preparation of such samples may cause degradation or shrinkage of the specimen. Therefore, this validation study was used to clarify the morphological effect on heart samples by HREM processing.

3.2 Subjects and Methods

Two adult (6-7 weeks old), five neonatal (1day) and ten fetal (E18.5 stage) mouse hearts were used for this validation study. All samples were fixed by 4% paraformaldehyde (PFA) and stored in the refrigerator. To clarify the hypotheses, two comparative studies were performed. One was the comparison of visual appearance between 3D VR images and photographs of samples taken before HREM process. The other was comparison of the measurement of samples before and after the HREM process. Ventricles were retained in the adult and neonatal hearts by dissecting other parts of the cardiovascular system to increase accuracy of the morphological measurement. Fetal hearts included atria, ventricles and great arteries.

Table 3-1: Protocol of Measurement of Mouse Heart Samples.

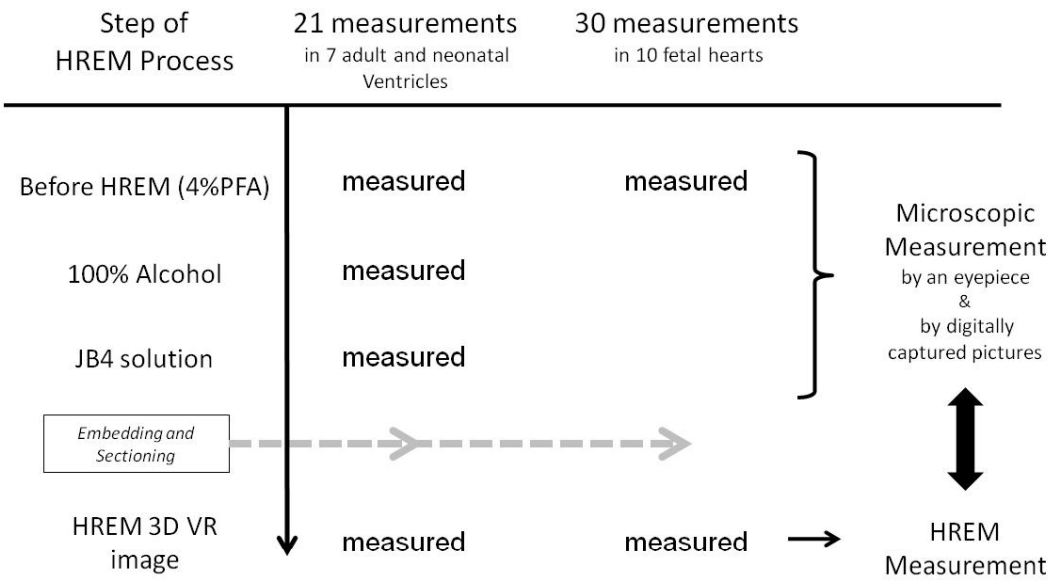

Table 3-1 shows the protocol for measurement of samples. All morphometry was performed using two microscopic measurements (as written in Chapter 2.4.2) and by the measurement of 3D VR image (see Chapter 2.4.1.9). First, the external diameter in three arbitrary parts of each sample was measured by two microscopic measurements before the process of HREM (21 measurements in 7 ventricles and 30 measurements in 10 whole hearts, a total of 51 parts). In seven dissected ventricles, the same part was measured in the steps of the HREM process (100% alcohol and JB4 solution). Figure 3-1 shows an example of external measurement of the same part of the ventricle at each step (picture01 of sample No 04).

Figure 3-1: Microscopic measurement in each step during HREM process. The visually same part of the samples was measured by microscopic measurements and 3D software of the HREM volume dataset (yellow line). Microscopic measurements were performed in two ways: using an eyepiece graticule directly digitally-acquired pictures.

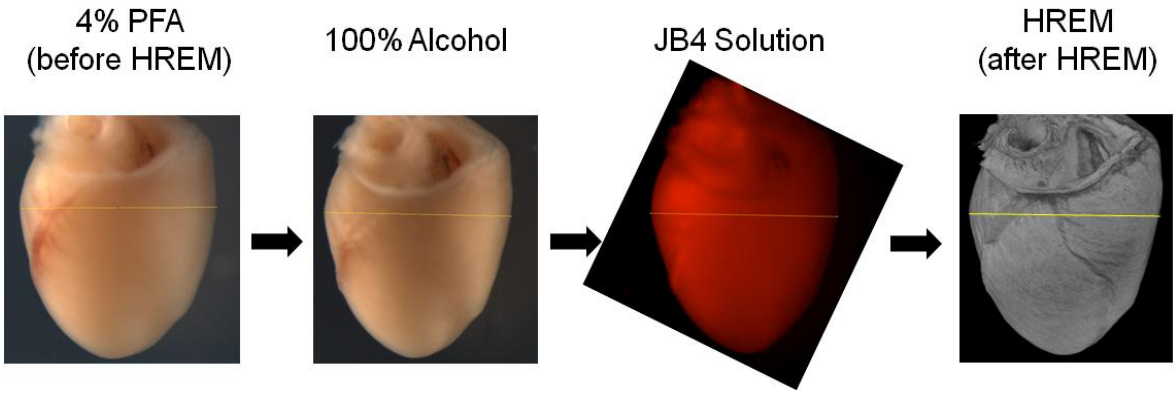

Measurements during the preparation were impossible in the 10 fetal hearts because whole hearts were difficult to put in exactly the same position during measurement on a microscope. After embedding samples, HREM was processed in all 17 samples and 3D volume datasets were created by the method described in Chapter 2.4.1. Then, all measurements in each sample were compared during the HREM process and the percentage of length in each step was calculated against the measurement before HREM. The visual appearance of sample pictures between before and after HREM was also compared.

Data analysis was performed using SPSS software (SPSS Inc., Chicago). A Bland-Altman plot was created for assessment of methodological difference between two morphological microscopic measurements and limits of agreement were calculated. One-way ANOVA was used to test the difference between each step, and paired t-test

was used for comparison of measurement before and after HREM processes. Statistical significance was taken in cases of p value less than 0.05.

3.3 Results

All hearts were successfully processed by HREM to reconstruct 3D VR images. Visual appearances of 3D VR images were similar to the photographs before HREM, and were proportionally balanced from any angle. Visual appearances of samples were identical from any angle (Figure 3-2).

Figure 3-2: Appearance of 10 fetal mice hearts (E18.5) before and after HREM. (A) Sample pictures for qualitative comparison (Sample Code; Val 01 – 10). Three photographs were taken from a different view in each sample (left-sided picture of each position). The right-sided pictures were VR images of each position. Both-sided images were identical and no obvious deformation can be seen. (B) One magnified picture before and after HREM (Val 04, position 2). The surface of the sample is much clearer than the original photograph and detailed structure of atria can be seen.

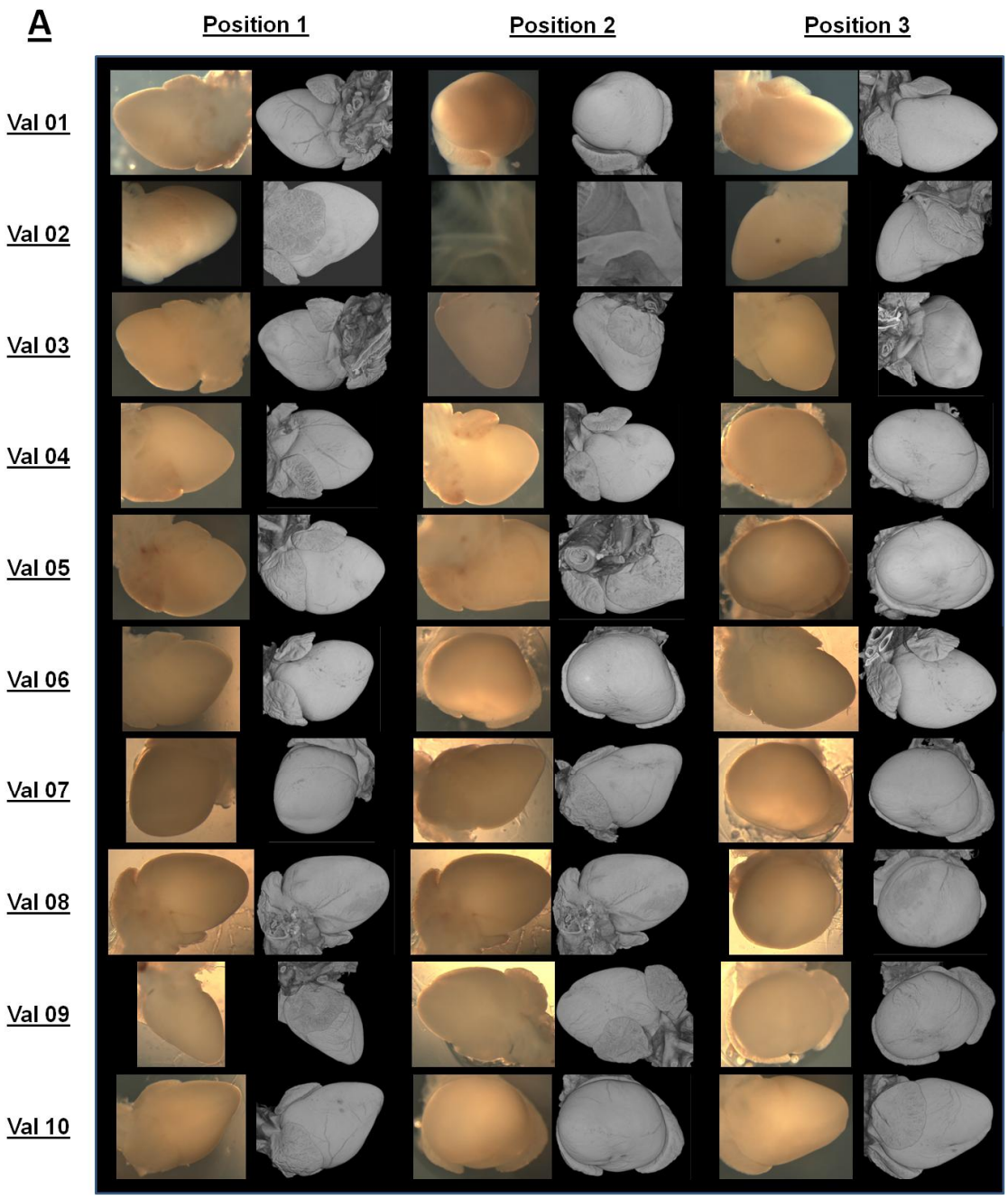
A
Position 1
Position 2
Position 3
Val 01
Val 02
Val 03
Val 04
Val 05
Val 06
Val 07
Val 08
Val 09
Val 10

B

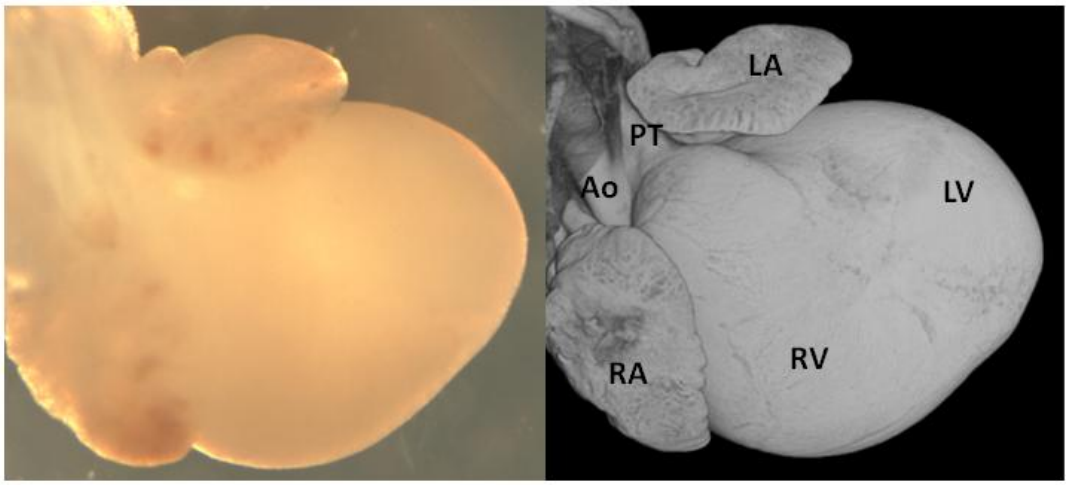

Ao; aorta, LA; left atrium, LV; left ventricle, RA; right atrium, RV; right ventricle, PT; pulmonary trunk

Forty-six of 51 measurements by the microscopic measurements were successful while five measurements in the step of JB4 solution were impossible because of unstable heart position during the measurement. Figure 3-3a demonstrates Bland-Altman plots from two microscopic measurements. There was no biased distribution in the comparison of measurements of the same position by between two ways of microscopic measurements. (mean -0.003 mm, Limits of agreement -0.033 to 0.027 mm) (Figure 3-3A). In the data taken by comparison among measurements of 21 parts in the 7 ventricles in each step, there were significant decreases in size during the processing steps from 4% PFA to 100% alcohol and from JB4 solution to HREM 3D images (from 100 to 93.9% and from 93.6 to 89.5%, respectively) (Figure 3-3B). No difference was found in the step between 100% alcohol and JB4 solution (from 93.9 to

93.6%). There was an overall 12.1 +/- 2.1 % of shrinkage of length after HREM (Figure 3-3C).

Figure 3-3: Results of microscopic measurement and comparison of each step of HREM process.

(A) Bland-Altman Plot of measurement between by an eyepiece graticule and by digitally captured pictures

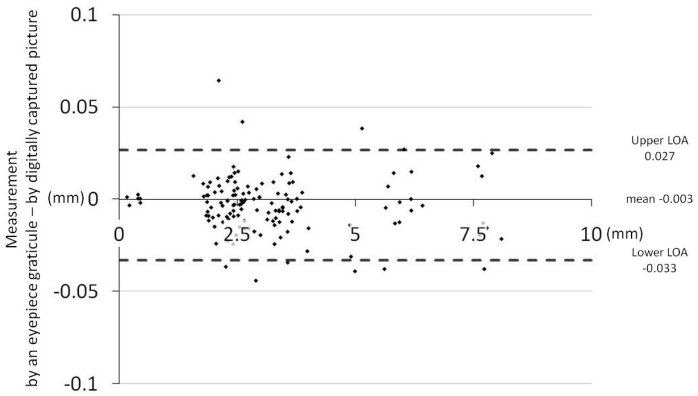

(B) Change of length of samples during preparation in HREM (Measurement at the step of PFA as 100%)

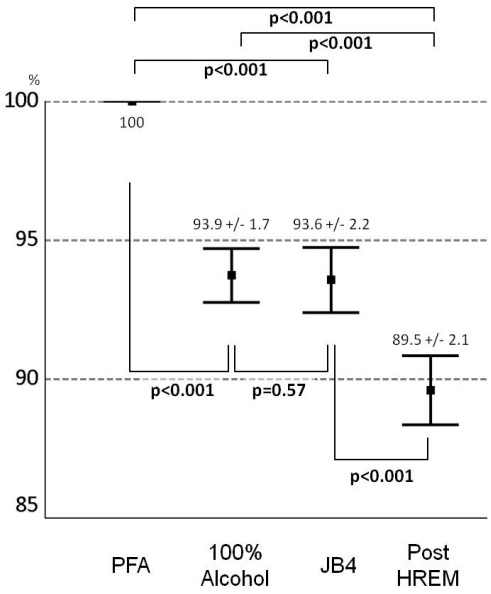

(C) Change of length before and after HREM (Measurement before HREM as 100%)

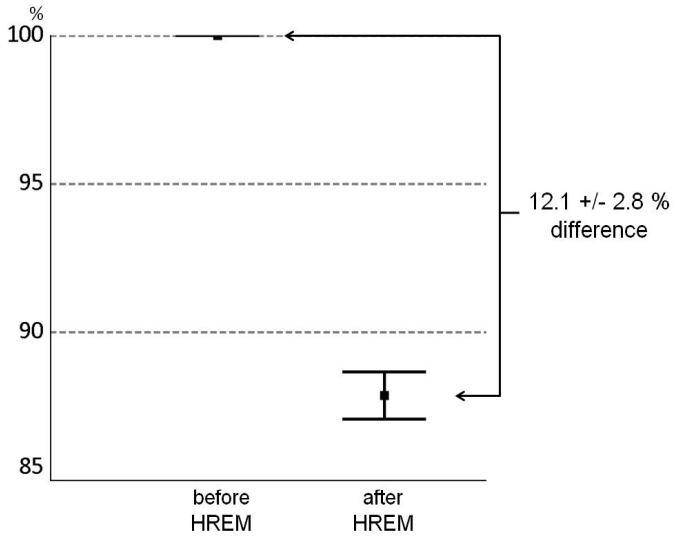

3.4 Discussion

Although HREM has the potential to create clearer 3D images of small specimens than other methods, a basic question under discussion is the effects of the HREM process on samples. Mclean et al emphasized the importance of calibration of dimensional changes occurring during tissue preparation and data processing during 3D reconstruction from serial sections (McLean and Prothero 1991). However, no validation study regarding HREM or EFIC process has been reported to date and deformation of samples may cause misleading morphological or histological results. Therefore, importantly, the primary task of this thesis is to clarify the morphological effects on 3D images by HREM because the process includes many steps (i.e. preparation, embedding, sectioning, data processing).

The heart is one of the soft tissues causing shrinkage or swelling of myocytes by various fixatives which Gerdes et al pointed out had significant effects on

morphometry in the heart tissue (Gerdes, Kriseman et al. 1982). Potentially, every laboratory process treating specimens can cause histological effects, such as swelling or shrinkage, on samples. Many reports described histological effects on samples by the process of each investigative method depending on sample types, solution, chemical reaction or circumstances such as temperature or humidity. Histological deformation or denaturation may result in morphological alteration of samples.

Formalin and PFA are common fixatives and alcohol is a common solution for dehydration of samples as many methods include hydrophobic cascades. Parker et al reported significant shrinkage of tissue by alcohol despite no major shrinkage by 10% formalin (Parker and Warner 1970), followed by Eisenberg et al describing the effect of dehydration by alcohol on myocardial fibre tissue resulting in 10% of shrinkage of samples (Eisenberg and Mobley 1975),Thus, preparation of the dehydration process by alcohol may cause histological and morphological shrinkage of samples.

Monomer glycol methacrylate (GMA), which is the main composition of JB4 solution A and changes into a polymer by an enhancer (JB4 solution B), can cause another influence on tissue in the HREM process. In general, embedding in wax caused shrinkage and in GMA caused swelling because of hydrophilic substance; therefore, one possible effect by GMA on tissue is swelling (Steigman, Weinreb et al. 1984; Rousselle and Wicks 2008). Another influence is by a chemical reaction during the polymerization process of GMA as polymerization shrinkage of plastic material has been described in many reports since the 1950s in the dental medicine (Smith and Schoonover 1953; Vasudeva 2009). In 1983, Hanstede et al reported GMA caused

9.3% of shrinkage by dehydration and 1-2% of further shrinkage by polymerization in liver tissue after trivial swelling (Hanstede and Gerrits 1983). Gerrits et al also reported that GMA resulted in trivial swelling followed by about 2% of shrinkage by polymerization in liver tissue (Gerrits, Horobin et al. 1992). Thus, the embedding process with GMA, including the dehydration process, may cause about 12% of shrinkage overall.

The results show that visual appearances of the surface of the heart are identical to photographs of original samples. Furthermore, detailed structures of the surface of atriums and ventricles are clearly visible and no visual deformation is recognized in HREM. In contrast, the mouse heart showed about 6.1% shrinkage in dehydration and 4.4% in polymerization despite about 10% in dehydration and 2% in polymerization in other tissue in previous reports, suggesting shrinkage in the HREM process may be different because of diversity of histological reaction among various tissues by HREM. In the whole process of HREM, shrinkage has occurred overall about 12%, which is almost equal to the percentage of previous reports. These findings show that the HREM process causes more than 10% shrinkage in the heart tissue, but the whole 3D cardiac structure is maintained and proportional. This may suggest that qualitative assessment for cardiac morphology is suitable in the HREM process, although quantitative assessment need to be interpreted carefully because proportional shrinkage of the heart may underestimate the size of samples.

It is important to recognize the variation of effects in HREM because histological effects in laboratory processes may be different in various tissues, ages

and species. Shrinkage or deformation effects may vary within the heart, e.g. ventricles, atriums, valves, arteries or veins. Our result showed 10.5% of shrinkage in ventricles although there was 12.1% of shrinkage in all measurements including ventricles, atriums, valves and great vessels. This difference suggests us that ventricles may show less shrinkage than other components of the heart and there may be variation of shrinkage or deformation even within the heart. Therefore, further investigation is needed to repeat different stages and looking at different tissue.

Additionally, in terms of morphometry, the two measurements provided acceptable similar values in the Bland-Altman plotting. Morphometry by means of an eyepiece graticule is conventional, and is the standard method for microscopic measurement (Baak 1987). In contrast, measurement using digitally-acquired images can be used by means of a projection of microscope and graticule. Therefore, the results of a similar value of the two different measurements suggest that digital measurement has the same accuracy with an eyepiece graticule and the two methods may be used interchangeably for morphometry of small cardiovascular samples.

Morphometry in small hearts includes some limitations. Morphological measurement is not always equal to histological measurement and there might be other histological alterations by the HREM process. Appearance of the 3D HREM image is identical to the original photographs. However, it is difficult to set 3D images to be in absolutely the same position as the original photograph. Automatic measurement might be more accurate than manual measurement in the software.

In conclusion, the HREM process does not affect qualitative assessment of morphological 3D structure of the heart. However, there is an average of 12% of proportional shrinkage of the samples during the HREM processes because of dehydration and polymerization. Therefore, morphological measurements in HREM may be underestimated and needs to be compensated for when comparing morphological specimens.

4.0 Chapter Four

Qualitative and Quantitative Morphological Investigation of the human fetal heart

4.1 Introduction

Knowledge of the normal variation in the early fetal heart is important to distinguish between normality and malformation. Especially in the field of paediatric cardiology, assessment of cardiac phenotypes in the fetus is vital because most of the diseases are congenital structural malformations which may occur during cardiogenesis or heart maturation. However, it is difficult to discuss normal morphology before establishing the basic components of heart structures. In Chapter 3 of this thesis, we have shown the utility of HREM for morphological assessment of small hearts. Therefore, this morphological study was performed to assess the cardiac phenotype of the normal human fetal heart qualitatively and quantitatively in the late first trimester and early second trimester, after cardiogenesis.

4.2 Subjects and Methods

Thirty six samples (9 to 17 post menstrual weeks) collected from surgical TOP were enrolled in this study as described in Chapter 2.3.1. HREM was processed and 3D volume dataset was created in each sample by the method described in Chapter 2.4.1.

4.2.1 Qualitative 3D data assessment

The visual appearances of each cardiac component including both atriums, atrioventricular junction, both ventricles, great arteries and coronary arteries, were assessed using 3D VR mode or MPR mode by the method described in Chapter 2.4.1.8. Heart diagnosis was based on sequential segmental analysis (Ho, Baker et al. 1995) and

findings of detailed structures in each component were described using 3D reconstructed images or histological slides.

4.2.2 Quantitative 3D data assessment of the heart

Morphometry was performed by the method described in Chapter 2.4.1.9. Table 4-1 and Figure 4-1 shows a list of standard views and each measurement site. Linear distance was measured in standard MPR images, which included the four chamber view, right anterior oblique view of the right ventricle (RAO view) and left ventricular long axis view (LAX view) (Figure 4-1 A-C). Measurement sites were widths of the hearts and lengths from the apex to atrioventricular or semilular valves (Table 4-1 and Figure 4-1; a-j). Measured values were divided by 0.879 which was the shrinkage ratio of HREM so as to compensate for shrinkage of length for comparison with morphological specimens discussed in Chapter 3. Ventricular mass volume was automatically calculated without compensation.

Table 4-1: List of measurement of length.

A: Four Chamber View					
a	maximum ventricular width (Width Vent)	c	Length from the apex to the mitral annulus at the free wall (Ap-MV)	e	Length from the apex to the mitral annulus at the septum (Ap-SepMV)
b	width of the AV groove (Width AVG)	d	Length from the apex to the tricuspid annulus at the free wall (Ap-TV)	f	Length from the apex to the tricuspid annulus at the septum (Ap-SepTV)

B: RAO View of the Right Ventricle	
g	Length from the apex to the tricuspid annulus at the inferior wall (RV inlet)
h	Length from the apex to the pulmonary annulus at the free wall (RV outlet)

C: LAX View	
i	Length from the apex to the mitral annulus at the inferior wall side (LV inlet)
j	Length from the apex to the aortic annulus at the anterior side (LV outlet)

Figure 4-1: Measuring points in each standard image (A - C; MPR images, D; VR image).

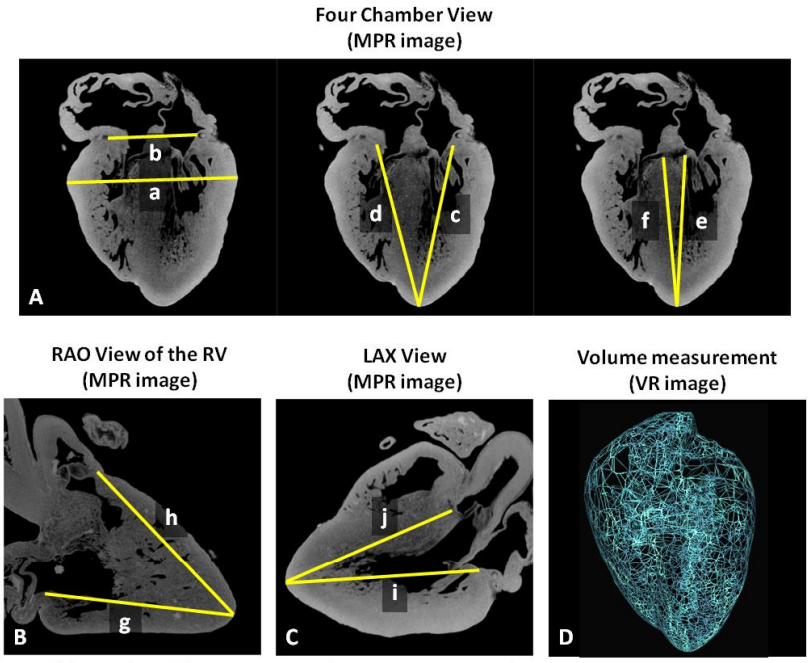

a: Width Vent, b: Width AVG, c: Ap-MV, d: Ap-TV, e: Ap-SepMV, f: Ap-SepTV,
g: RV inlet, h: RV outlet, I: LV inlet, j: LV outlet

4.2.3 Quantitative 3D data assessment of Great Arteries

Morphometry of both great arteries by HREM was also performed by the method described in Chapter 2.4.1.9. Figure 4-2 shows the images of measurement of external diameter and wall thickness of great arteries. External diameter and wall thickness of both great arteries were measured above the Valsalva sinuses, just above the sinotubular junction, using cross-sectional MPR images which are perpendicular to each great artery (Figure 4-2A). Maximum and minimum external diameters of the great arteries were measured and averaged (Figure4-2B). The thickness of great arterial walls was measured at 3 points (maximum, minimum and one random point) and averaged. Measurements in HREM were compensated by dividing by the shrinkage ratio (0.879) to compare with wall thickness in later gestation from postmortem specimens.

External diameter and wall thickness of great arteries were also measured using digitally acquired pictures detailed in Chapter 2.4.2.2 in 23 human fetal hearts of post-mortem specimens archived at the Cardiac Morphology Unit at Royal Brompton Hospital (14 - 32 post menstrual weeks). Arterial walls were cut perpendicularly and photographed three times, and then wall thickness was measured in each image (Figure 4-2C). The external diameter was also measured just above the Valsalva sinuses from three different views (Figure 4-2D). All measured values were averaged and external diameter, wall thickness and ratio of the wall thickness to the external diameter were plotted on graphs against postmenstrual weeks.

Figure 4-2: Images of morphometry of great arteries. (A) Longitudinal MPR section of the pulmonary trunk. The dashed line is the level of measurement in the cross-sectional image of the pulmonary trunk. (B) Measurement sites in the cross-sectional view. Cross-sectional view showed oval, not precise circle, despite digital sectioning was cut perpendicularly. Maximum and minimum diameters were measured for external diameter. Three points, including maximum, minimum and one random width, were measured for wall thickness. (C) A measurement site of the wall thickness of a morphological specimen (arrow). The arterial wall was cut perpendicularly and the width of the cut surface measured (arrow head). (D) The external diameter was measured just above the Valsalva sinuses.

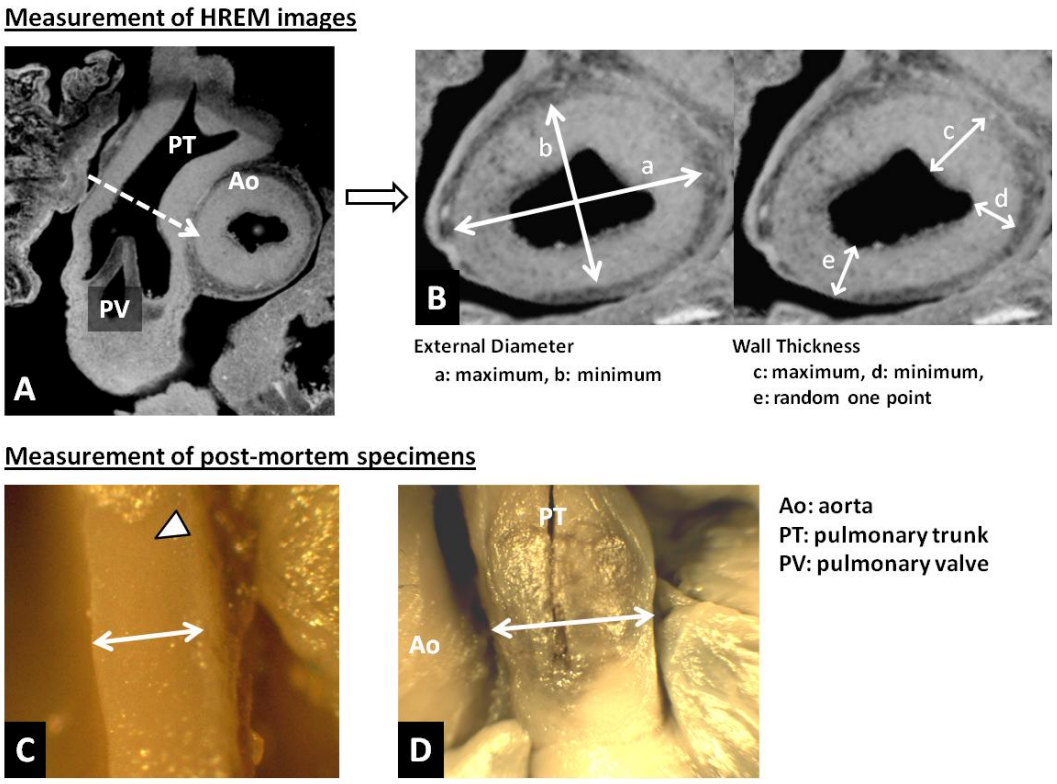

Analysis has been performed by SPSS software (SPSS Inc., Chicago). Linear regression and least squares method were used for regression analysis to assess relationship between postmenstrual weeks and each length. Cubic function was used for regression analysis for ventricular mass volume against postmenstrual weeks. Analysis of covariance (ANCOVA) was used for comparison of slope of linear regression lines. Paired t-test was used for comparison of each value and statistical significance was taken in cases of p value less than 0.05.

4.3 Results

All 36 samples were successfully processed for in HREM although investigations were limited in several cases because of damage incurred during retrieval from surgical TOP. Reconstructed images by HREM showed normal arrangement of atrial appendages and normal atrioventricular and ventriculoarterial connections with no ventricular septal defects, except for artefactual tears, suggesting structurally normal heart in all samples.

4.3.1 Qualitative assessment

Right Atrium, Left Atrium and Atrial Septum

Both atriums comprised four basic components (appendage, venous and septal components and vestibule), however their sizes were unbalanced from 9 to 11 weeks (Figure 4-3). The atrial appendages were noticeably larger than the other three components in the both atria (Figure 4-3A). In the right atrium, the right atrial

appendage was broad and large with a wide junction to the atrial cavity. The inner surface of the right atrial appendage was creased showing thin walls lined with coarse pectinate muscles that extended toward the smooth walled vestibule (Figure 4-3B). The junction between the right atrial appendage and the venous component forms the terminal crest (crista terminalis) vertically located at the posterior wall of the atrial cavity. The venous component was slim and long receiving the superior and inferior caval veins. The terminal crest was a muscle band continuing into the wavy membrane of the venous valves (the Eustachian and Thebesian valves) which were already formed and prominent (Figure 4-3C and D). The size of the vestibule making up the body of the right atrium together with the venous component was small.

The imbalance between the atrial body and the atrial appendage was also evident in the left atrium. The left atrial appendage demonstrated a hooked shape and thin and its size was large (Figure 4-3E). It crossed over the anterior interventricular sulcus and covered the anterior wall of the pulmonary trunk. The junction to the atrial chamber demonstrated a narrow neck of the appendage but there was no evidence of a terminal crest. Wrinkles with ridges of pectinate muscles were limited to within the appendage (Figure 4-3F). The venous component was small receiving four pulmonary veins whose orifices are in close proximity to one another in each side (Figure 4-3G). The vestibule was also small supporting the mitral valves. The foramen ovale opened widely, guarded by a membrane-like valve and occupied large area of the small septal component in both atria (Figure 4-3H).

With growth of the ventricles, the right and left atrial appendages shifted from their anterior positions to lie more laterally after the first trimester. The imbalance of sizes between the appendages and other atrial components improved with gestation. Both atrial appendages became less prominent after first trimester while the other atrial components and atrial cavities grew in size resulting in balanced atria by 17 weeks.

Figure 4-3: Atrial morphology in the first trimester. (A) 11 weeks heart from right-cranial view. Large atrial appendage surrounds the anterior part of the heart. (B) Lateral inside view of the right side of the heart by saggital sectioning. Creases of the atrial appendage (arrow head) extend to the small vestibule of the right atrium. (C) Coronal section of 11 weeks heart. The right atrial appendage has creases and coarse pectinate muscles. The border between the appendage and the venous component forms the membranous terminal crest (black arrow). The venous component is slim connecting both the inferior and the superior caval veins (white line and arrow). (D) 11 weeks heart from right-caudal view. The membranous terminal crest (black arrow) extends to the Eustachian valve which is large and prominent. The orifice of the superior caval vein (arrow head) and the foramen ovale (*) can be observed beyond the Eustachian valve. (E) The left atrial appendage in the 11 weeks heart. The left appendage is large and hooked shape covering the anterior interventricular sulcus (arrow head). (F) Inside of the atria from posterior-cranial view. Pectinate muscles are limited within the appendages (*) and the appendage joins the atrial chamber at the

narrow neck of the orifice of the appendage (arrow head). The venous component is small receiving pulmonary veins in both sides (white arrow). (G) Orifices of the pulmonary veins (upper: right pulmonary veins from left anterior view, lower: left pulmonary veins from right anterior view). The orifice of the upper and the lower pulmonary veins is in close proximity forming the joined orifice in either side (arrow heard). (H) Septal component from each atrial view. The left-sided picture is from right atrial view and the left picture is from the left atrial view. Foramen ovale (arrow) covered with foramen flap (*) is large and occupying most part of the septal component.

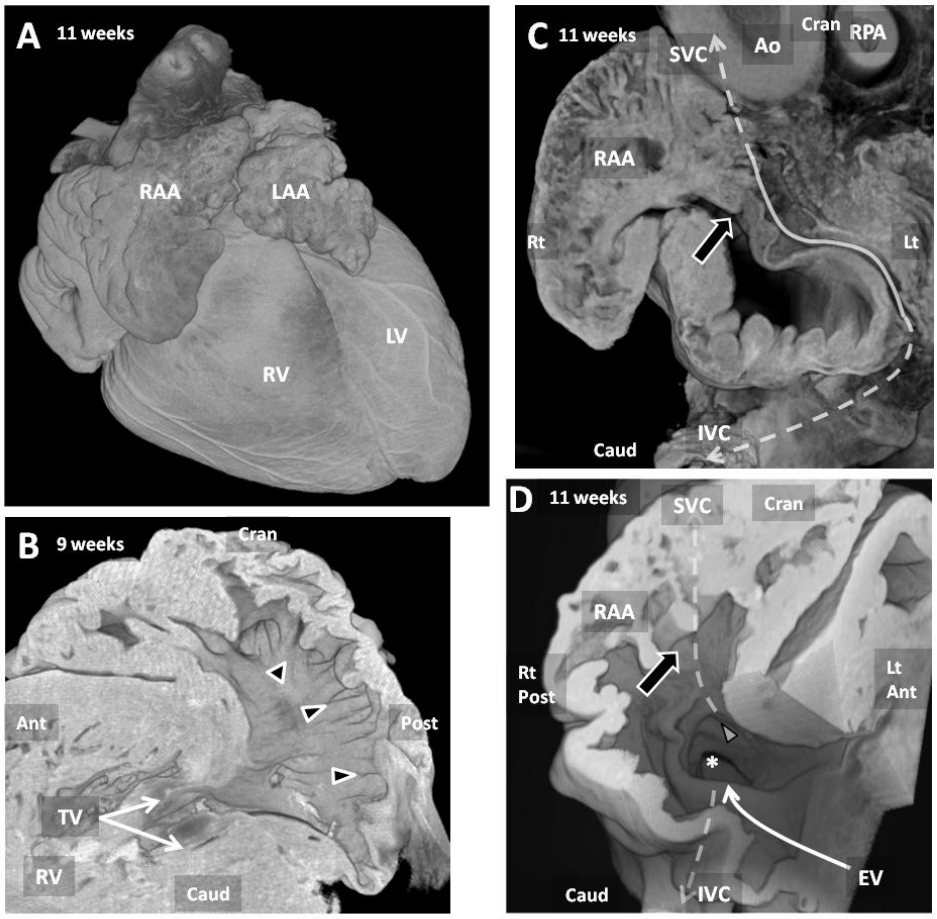

Ao: aorta, EV: Eustachian valve, IVC: inferior vena cava, LAA: left atrial appendage, LV: left ventricle, RA right atrium, RAA: right atrial appendage, RPA: right pulmonary artery, RV: right ventricle, SVC: superior vena cava, TV: tricuspid valve,

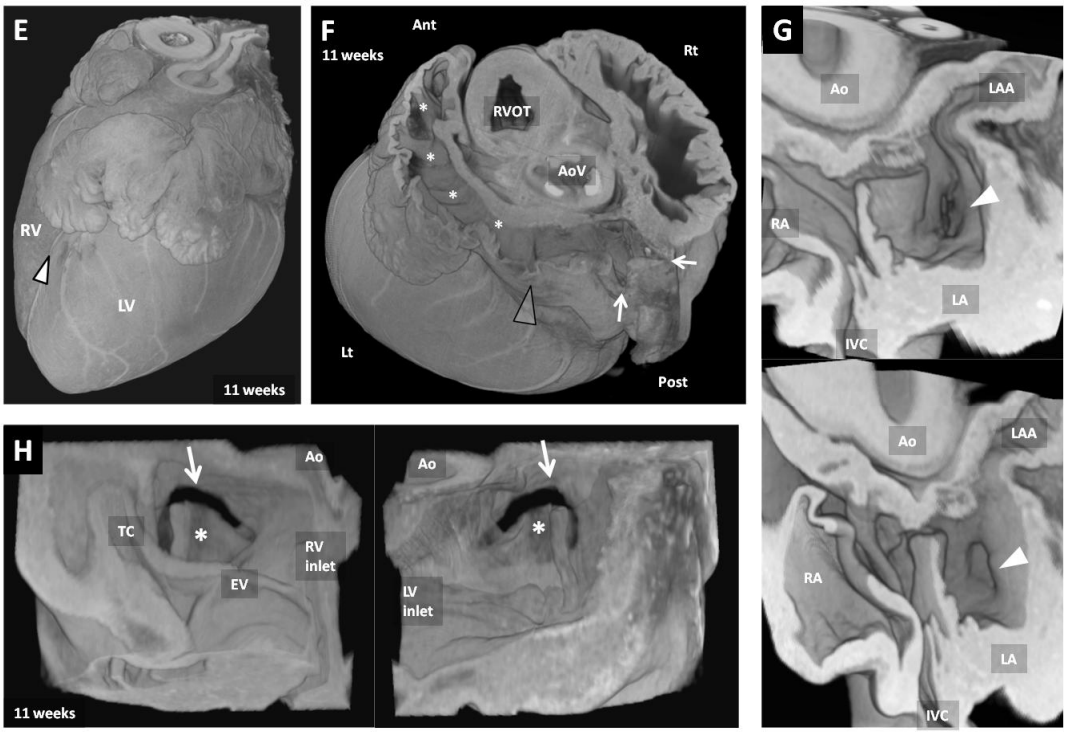

Ao: aorta, AoV: aortic valve, EV: Eustachian valve, IVC: inferior vena cava, LAA: left atrial appendage, LV: left ventricle, RA right atrium, RAA: right atrial appendage, RPA: right pulmonary artery, RV: right ventricle, RVOT: right ventricular outflow tract, SVC: superior vena cava, TC: terminal crest, TV: tricuspid valve,

Atrioventricular Junction

A noticeable finding at the atrioventricular junction is the difference in levels of attachments of the mitral and tricuspid valves at the cardiac septum, a feature termed 'offsetting of the atrioventricular valves'. Table 4-2 shows the number of cases with visually recognizable offsetting of the atrioventricular valves. From 9 to 10 weeks, no offsetting could be recognized and the membranous portion of the ventricular septum was unclear. Differences in levels of the atrioventricular valves gradually appeared from about eleven weeks and obvious offsetting was seen from 16 weeks onward. Figure 4-4 illustrates the levels of the atrioventricular valves in the four chamber view of the MPR images.

Table 4-2: Cases of Offsetting of Atrioventricular valves.

Gestational Weeks (number of cases)	No offsetting	borderline	Clear offsetting
9-10 (7)	7 (100%)	0	0
11-12 (11)	4 (36%)	7 (64%)	0
13-14 (6)	0	1 (17%)	5 (83%)
16-17 (4)	0	0	4 (100%)

Figure 4-4: Offsetting of Atrioventricular valves. (A) 9 weeks heart. The atrioventricular valves are at the same level in the four chamber view (left) and continuity between the mitral and the tricuspid valve can be clearly seen (right). (B) 14 weeks heart. Clear offsetting of the atrioventricular valves is recognized.

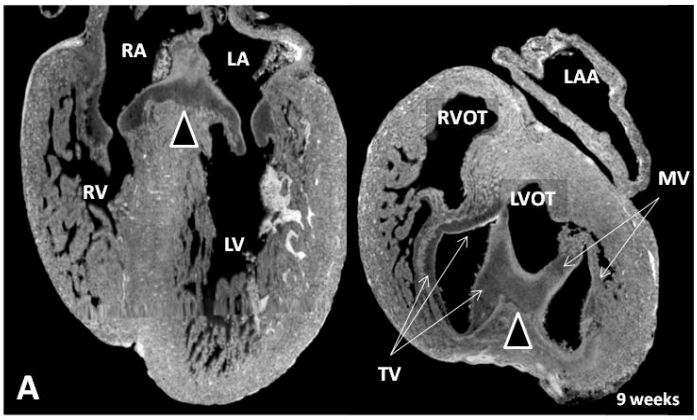

LA: left atrium, LAA: left atrial appendage, LV: left ventricle, LVOT: left ventricular outflow tract, MV: mitral valve, RA: right atrium, RV: right ventricle, RVOT: right ventricular outflow tract, TV: tricuspid valve

Another noticeable finding was prominence of the atrioventricular sulci (Figure 4-5). The four chamber view showed narrow atrioventricular junction compared to the ventricular width in the MPR images. VR images from the atrial view demonstrate

visually narrow atrioventricular junction compared to the ventricular mass and ventricles appear prominent in this view.

Figure 4-5: Images of Atrioventricular Junction. (A) MPR images show atrioventricular groove in each gestation (arrows). Sulci are deeper in later gestation. (B) 3D images of hearts viewing the atrioventricular junction from the atrial aspect show relatively small atrioventricular orifice compared to the ventricles.

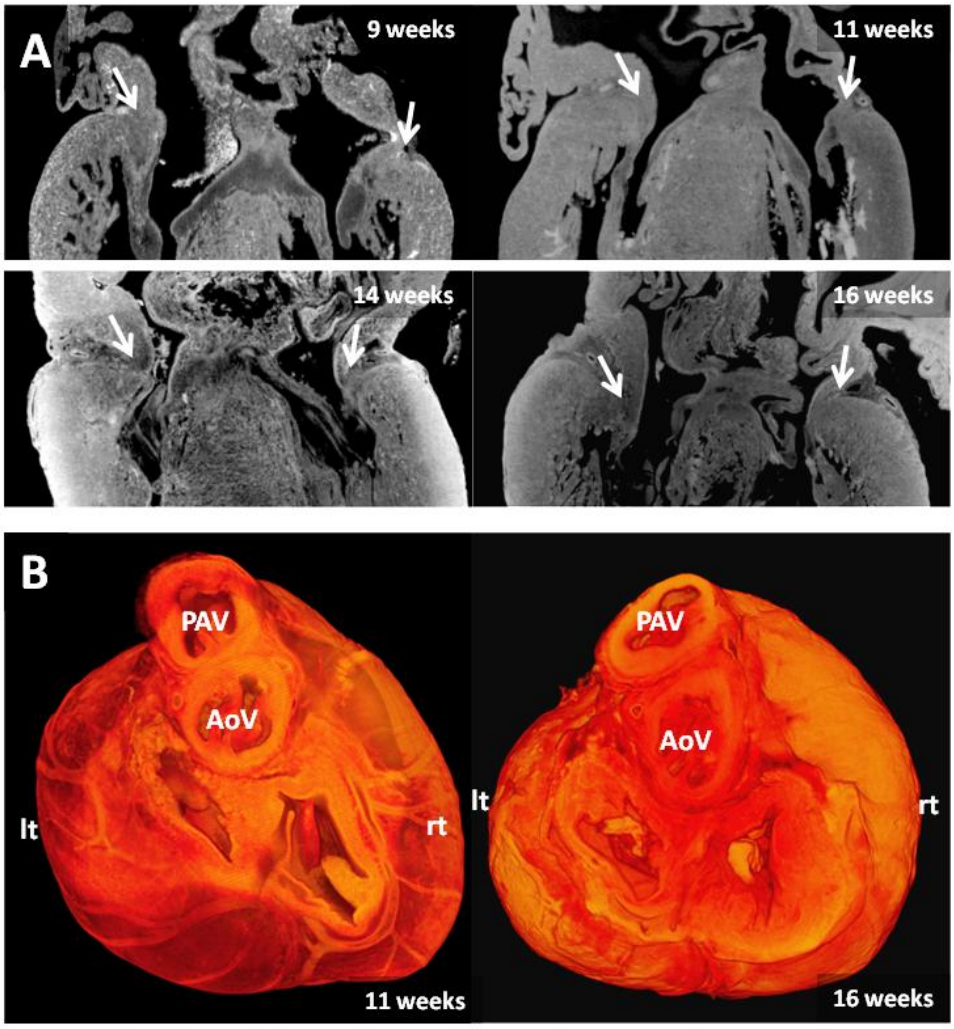

AoV: aortic valve, LV: left ventricle, RV: right ventricle, PAV: pulmonary valve

Right Ventricle, Left Ventricles and Ventricular Septum

Both ventricles have already formed tripartite components (inlet, apical and outlet) and the myocardium was compacted in the left ventricle at 9 weeks. Myocardial trabeculations were coarse in the right ventricle and fine in the left ventricle and this finding was more obvious in later gestation (Figure 4-6A).

The inlet component of the right ventricle supported the tricuspid valve whose leaflets were round and thick at around 10 weeks. The anterior leaflet was supported by the large anterior papillary muscle attaching to the free wall of the apical trabecular component (Figure 4-6B and C). The posterior leaflet was small supported by thin branches of the anterior papillary muscle. The septal leaflet was attached to the ventricular septum by immature tendinous chords which were short and fuzzy. The characteristic musculature in the right ventricle including septomarginal trabeculation and moderator band, were already formed (Figure 4-6D). The septomarginal trabeculation was identifiable as a Y-shaped band cradling the supraventricular crest which formed the infolded roof of the right ventricle. The moderator band appeared as a short and broad extension from the body of the septomarginal trabeculation and the anterior papillary muscle arose immediately from the moderator band. Although the moderator band continued across the ventricular cavity to insert into the parietal wall of the right ventricle, it was not an isolated band at 10 weeks. Its inferior aspect remained attached to the apical trabeculations, appearing like a shelf-like structure rather than a band (Figure 4-6B). The apical component of the right ventricle showed characteristically coarse trabeculations compared to the left ventricle [Figure 4.6G].

The left ventricular inlet surrounded the mitral valve and its apparatus including the two groups of papillary muscles. The mitral valve has no chordal attachment to the ventricular septum (Figure 4-6C and E). Fine criss-crossing trabeculations were observed not only in the apical part but also in the lower two-thirds of the septal surface of the left ventricle before 11 weeks (Figure 4-6F).

In the end of the first trimester (around 14 weeks), trabeculations in the both ventricles matured and became clear (Figure 4-6G). In the right ventricle, trabeculations including septomomarginal trabeculation and moderator band were clearly recognized and the septal surface was irregular and coarse. The tendinous chords of the septal leaflet of the tricuspid valve became fine and the base of the anterior papillary muscle extended into muscle bundles that joined the coarse trabeculations in the apical part. In the left ventricle, fine trabeculations on the upper part of the septal surface was less prominent and smooth area remained immediately beneath the aortic valve.

Figure 4-6: Fetal ventricular morphology in the first trimester. (A) Trabeculations in each ventricle. The upper picture illustrates fine trabeculations in the left ventricle and coarse trabeculations in the right ventricle at 11 weeks. The middle and lower pictures demonstrate more prominent trabeculations at 14 weeks in each ventricle. (B) Structure of the tricuspid valve by axial sectioning from base to the apex. The anterior leaflet is supported by the large anterior papillary muscle attaching to the apical trabecular free wall (black arrow). The posterior leaflet is small connecting to small branches of the anterior papillary muscle. The septal leaflet is supported by short and fuzzy tendinous chords (white arrow heads) at 10 weeks. (C) Attachment of papillary muscles in each ventricle. Two papillary muscles attach to the free wall in the left ventricle while the septal leaflet demonstrates septal attachment in the right ventricle in each gestation. (D) Right ventricular structure in the 10 weeks heart. Basic structures of trabeculations have already formed. The moderator band is short and thick bridging between the Y-shaped septomarginal trabecularion and the anterior papillary muscle. The anterior papillary muscle is thick and mainly supports the anterior leaflet of the tricuspid valve. (E) Short axis view at the level of papillary muscle. Two papillary muscles (antero-lateral and postero-medial) are clearly observed at 9 weeks. (F) Longitudinal section of the left ventricle. Myocardium has compacted with fine trabeculations locating on the septal surface (arrow head). (G) Ventricular structure at 13 weeks. In the left-hand image of the right ventricle, coarse trabeculations are more prominent than 10 weeks heart with clear muscle bands including septomoginal trabeculation and moderator band. The septal surface is rough. In the right-hand

image of the left ventricle, fine trabeculations have shifted toward the apex (arrow head) and smooth area has spread (arrow).

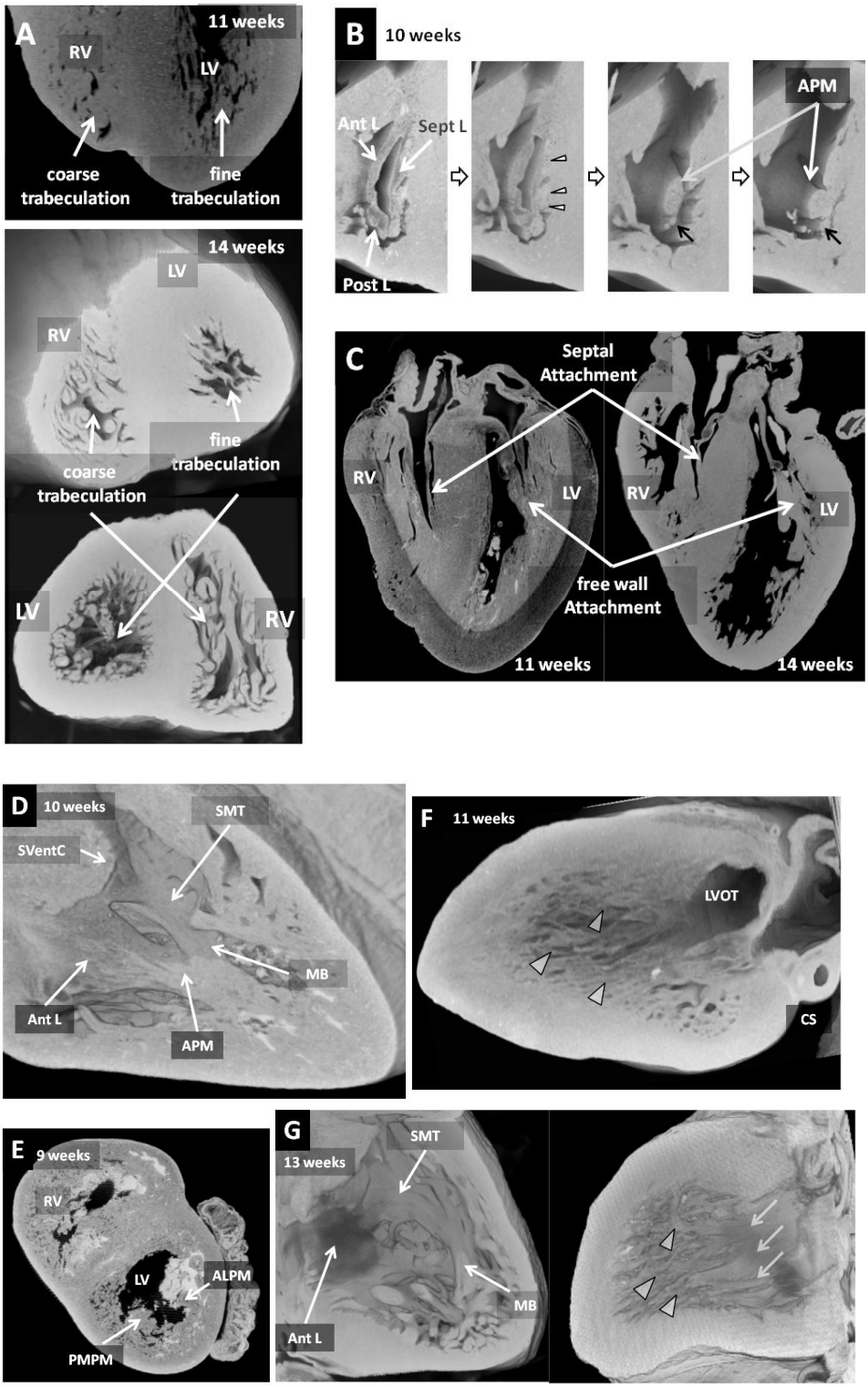

AntL: anterior leaflet, ALPM: anterolateral papillary muscle, APM: anterior papillary muscle, CS: coronary sinus, LV: left ventricle, LVOT: left ventricular outflow tract, MB: moderator band, PMPM: postromedial papillary muscle, PostL: posterior leaflet, RV: right ventricle, SeptL: septal leaflet, SMT: septomarginal trabeculation, SVentC: supraventricular crest

Pulmonary Valve and Aortic Valve

The pulmonary and aortic valves have developed into their typical three leaflet formation at 9 weeks, however the leaflets were globular in longitudinal sections and thick and wavy (redundant looking) on cross-sections (Figure 4-7). No obvious difference of the level of both semilunar valves was seen in HREM images and the annular border between leaflets and arterial walls was unclear at 9 weeks in the histological sections. The semilunar leaflets became fine and borders between the valves and the walls became clearer at around 14 weeks.

Figure 4-7: Images of Semilunar Valves. (A) Pulmonary valve at 9 gestational weeks. The leaflets are thick and round in longitudinal view (left) and wavy in the VR images (middle). Histology illustrates unclear border between the valve and the arterial wall (right). (B) Aortic valve at 13 weeks. Leaflets are much sharper than in the first trimester (left). The closure lines are well defined (middle). Arrow shows a clearer border suggesting a more developed valve structure.

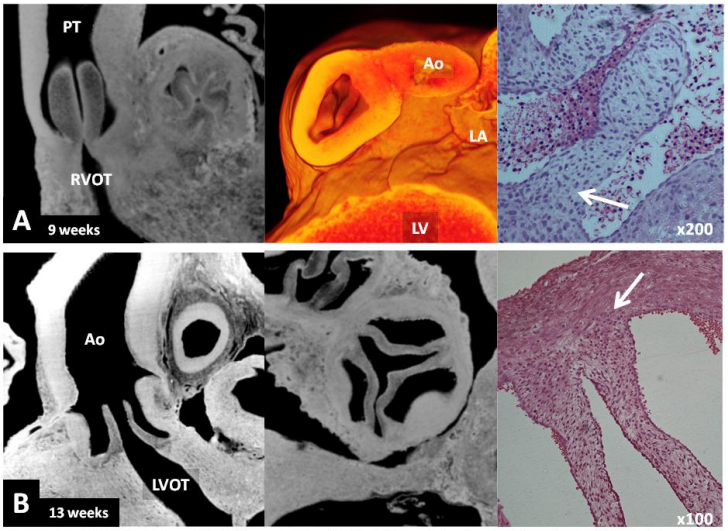

Ao: aorta, LA: left atrium, LV: left ventricle, LVOT: left ventricular outflow tract, RA: right atrium, RVOT: right ventricular outflow tract, PT: pulmonary trunk, SID: sample ID

Pulmonary Trunk, Aorta and Ductal and Aortic Arch

The great arteries formed a normal spiral relationship and the pulmonary trunk normally bifurcated before connecting to the arterial duct which forms the ductal arch. The aorta branched into three neck vessels at the aortic arch. In the histological sections, the aorta and the pulmonary trunk were still fused together at the root of great arteries and clear separation was seen only from around 16 weeks.

An important finding of the great arteries was the remarkably thick arterial walls in the first trimester (Figure 4-8). Thick arterial walls were present in both great arteries with narrow lumen at around 9 to 10 weeks. From around 16 to 17 weeks, the arterial walls were noticeably thinner while the lumens were larger. Histological sections demonstrated dense cells in the arterial walls in the first trimester.

Figure 4-8: Thickened Great Arterial Wall. (A) Aorta and aortic valve of 9 post menstrual weeks. The wall is remarkably thick and the valve leaflets are nodular. (B) Great arteries at 11 weeks of gestation. The aorta shows thick wall in the cross-sectional plane. Thick walls are also noted in the pulmonary trunk, the arterial duct and descending aorta. The orifices of the branch pulmonary arteries are small (arrows). (C) Pulmonary trunk at 16 weeks. The arterial wall is thinner and the lumen becomes wider than in the first trimester.

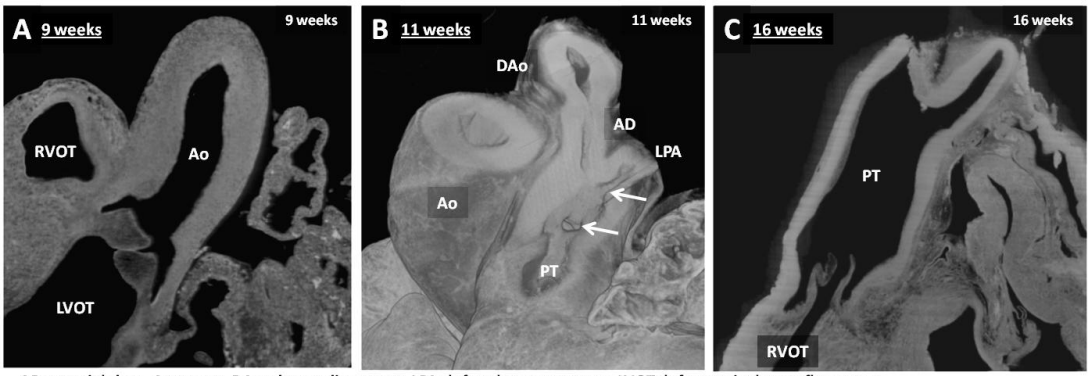

AD: arterial duct, Ao: aorta, DAo: descending aorta, LPA: left pulmonary artery, LVOT: left ventricular outflow tract, RVOT: right ventricular outflow tract, PT: pulmonary trunk

Coronary Arteries

Coronary arteries were visualized in 15 of 19 hearts from 9 to 11 weeks (79%) and all cases had two coronary systems; one the right coronary artery (RCA) arising from the right facing sinus and the other the left coronary artery (LCA) arising from left facing sinus. The LCA bifurcated into the anterior descending branch (LAD) and the left circumflex branch (LCX). A high lateral branch, the third branch at the bifurcation of LAD and LCX, was recognized in 5 of 15 cases (33%).

Interestingly, the coronary arteries were visually prominent in the first trimester, especially the right coronary artery (RCA) and the LCX (Figure 4-9). The RCA and its peripheral branches were clearly seen. Nine of fifteen cases (60%) demonstrated the posterior descending branch (PD) supplied by RCA forming a right dominant system. A left dominant system where the LCX supplied the PD was recognized in only one case. A dual supply of the PD by RCA and LCX, the so-called balanced system, was observed in 5 of 15 cases (33%).

Figure 4-9: Coronary Arteries in the late first trimester. (A) Prominent coronary arteries in the 11 week gestation heart. Normal coronary branching is recognized in each view. (B) Coronary branches from the posterior view in the 9 week gestation heart. Branches from LCX and RCA are well developed forming radial appearances of branches. (C) Dominancy of the coronary system. From the top, images demonstrate a right-dominant, left-dominant and a balanced coronary system, respectively.

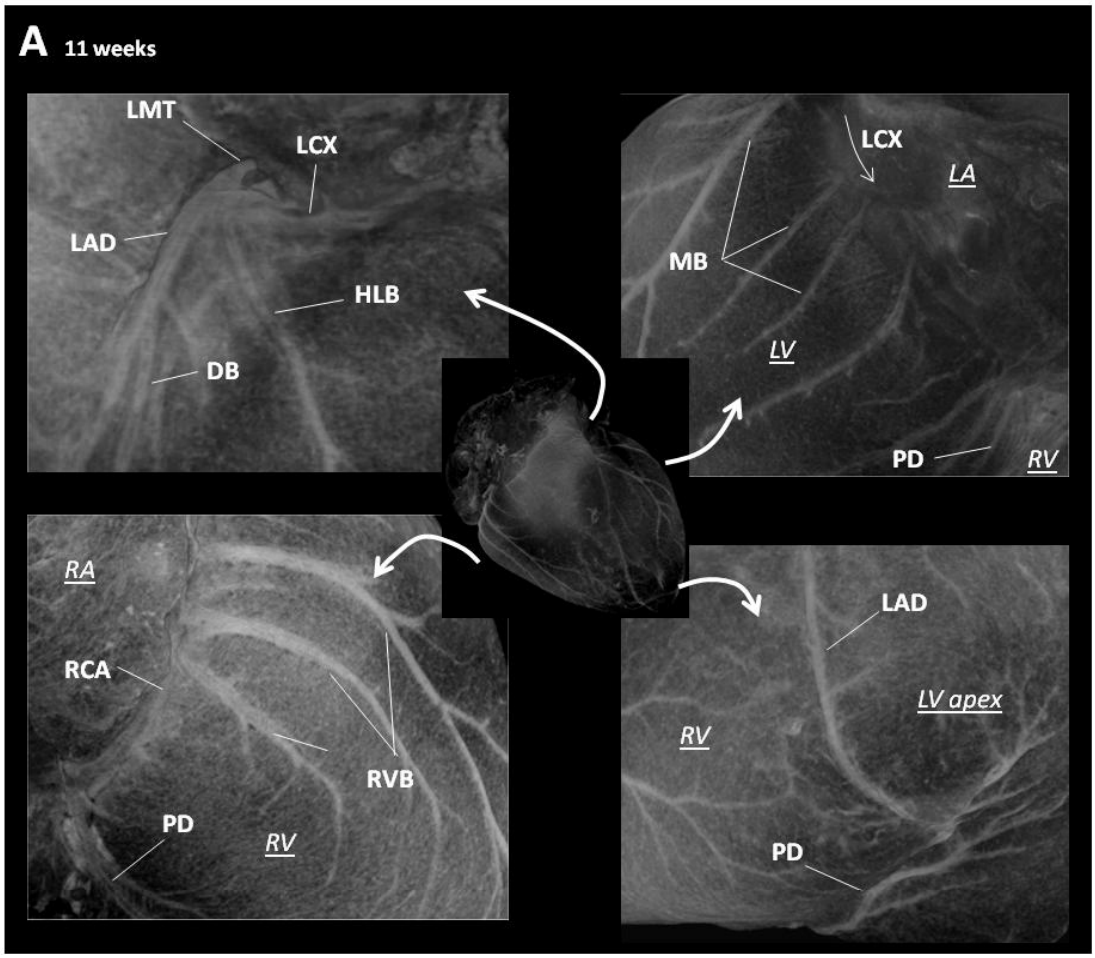

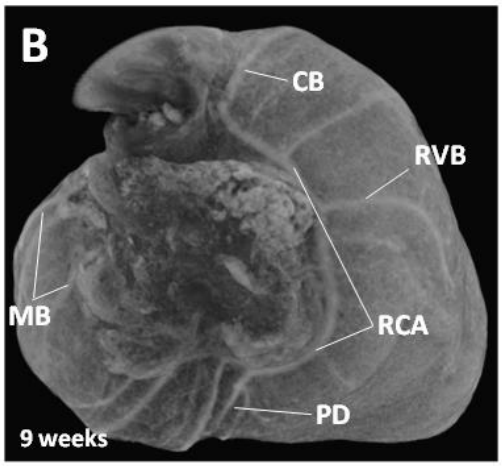

AMB: acute marginal branch, CB: conus branch, DB: diagonal branch, HLT: high lateral branch, LAD: left anterior descending branch, LCA: left coronary artery, LCX: left circumflex branch, LMT: left main coronary trunk, MB: marginal branch, PD: posterior descending branch, RCA: right coronary artery, RVB: right ventricular branch

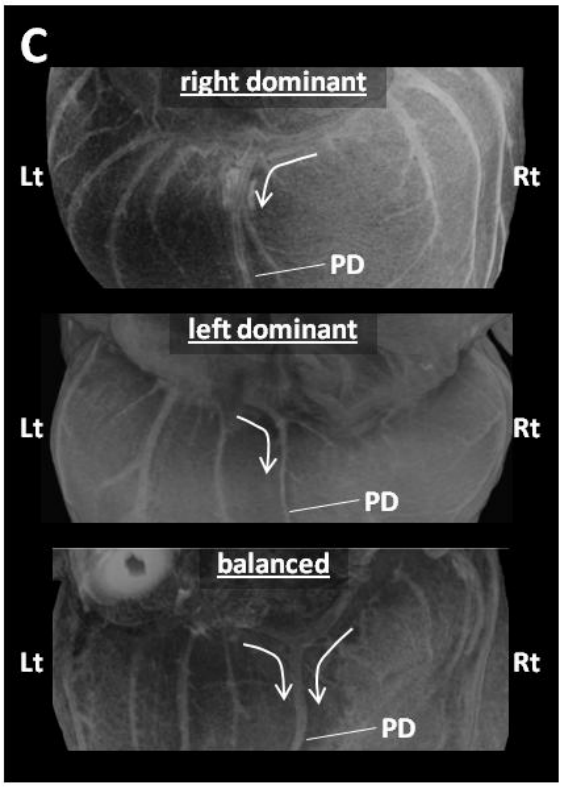

4.3.2 Quantitative assessment

Cardiac length increases linearly with gestation in each parameter (Table 4-3). The slope of the regression line is higher in maximum ventricular width than in width of the atrioventricular groove (0.94 vs 0.64, $p<0.001$) (Figure 4-10A). No important difference of growth is shown in the lengths from the apex to the each atrioventricular valve (0.88 in Ap-TV vs 0.79 in Ap-MV, $p=0.07$) (Figure 4-10B). There is no significant difference between Ap-SepTV and Ap-SeptMV, however, the ratio (Ap-SepTV / Ap-SepMV) significantly decreases with gestation (slope -0.0065, intercept 1.05, $R=0.50$, $p=0.02$) (Figure 4-10C and D). The slope of the regression line is higher in the outlet than in the inlet in the right ventricle (0.69 in the outlet vs 0.56 in the inlet; $p=0.04$)

although no significant difference was seen in the left ventricle (0.78 in the outlet vs 0.76 in the inlet; p=0.04) (Figure 4-11A and B). Volumetry of ventricular mass was available in 13 samples and it shows rapid growth with gestation (regression of cubic function, R=0.98, p<0.001) (Figure 4-12). External diameter and wall thickness of both great arteries increase linearly through gestation (Table 4-4), however, the ratio of wall thickness to external diameter dramatically decreases at around 16 weeks remains constant until term in both great arteries (Figure 4-13).

Table 4-3: Linear regression of parameters of the fetal heart by HREM.

Parameter	slope	Intercept	R	p-value	Paired t	ANCOVA
Width vent	**0.94**	**-6.52**	**0.95**	**<0.001***	**p<0.001***	**p<0.001***
Width AVG	**0.64**	**-4.61**	**0.89**	**<0.001***		
AP-TV	**0.88**	**-5.22**	**0.95**	**<0.001***	**p<0.001***	**p=0.07**
AP-MV	**0.79**	**-4.54**	**0.95**	**<0.001***		
AP-SeptMV	**0.87**	**-6.35**	**0.95**	**<0.001***	**p=0.01***	**p=0.51**
AP-SeptTV	**0.82**	**-5.80**	**0.94**	**<0.001***		
RV inlet	**0.56**	**-2.45**	**0.91**	**<0.001***	**p=0.01***	**p=0.04***
RV outlet	**0.69**	**-3.54**	**0.92**	**<0.001***		
LV inlet	**0.76**	**-4.04**	**0.94**	**<0.001***	**p=0.04***	**p=0.42**
LV outlet	**0.78**	**-4.37**	**0.91**	**<0.001***		

AP: apex, AVG: atrioventricular groove, LV: left ventricle, MV: mitral valve, RV: right ventricle, Sept: septum, TV: tricuspid valve, vent: ventricle

Figure 4-10: Graphs of morphometry of length parameters in four chamber view. (A) Maximum ventricular width (Width Vent) and width of atrioventricular groove (Width AVG). The slopes were significantly different although both value increase linearly. Maximum ventricular width was lower than the reported data by Martinez (the green line). (B) Length of the apex to the atrioventricular valve annulus at the free wall in each ventricle (Ap-MV and ApTV). (C) Length of the apex to the mitral and tricuspid annulus at the septal wall (Ap-SepMV and Ap-SepTV). (D) The ratio of Ap-SepTV to Ap-SepMV. The ratio significantly decreased with gestation.

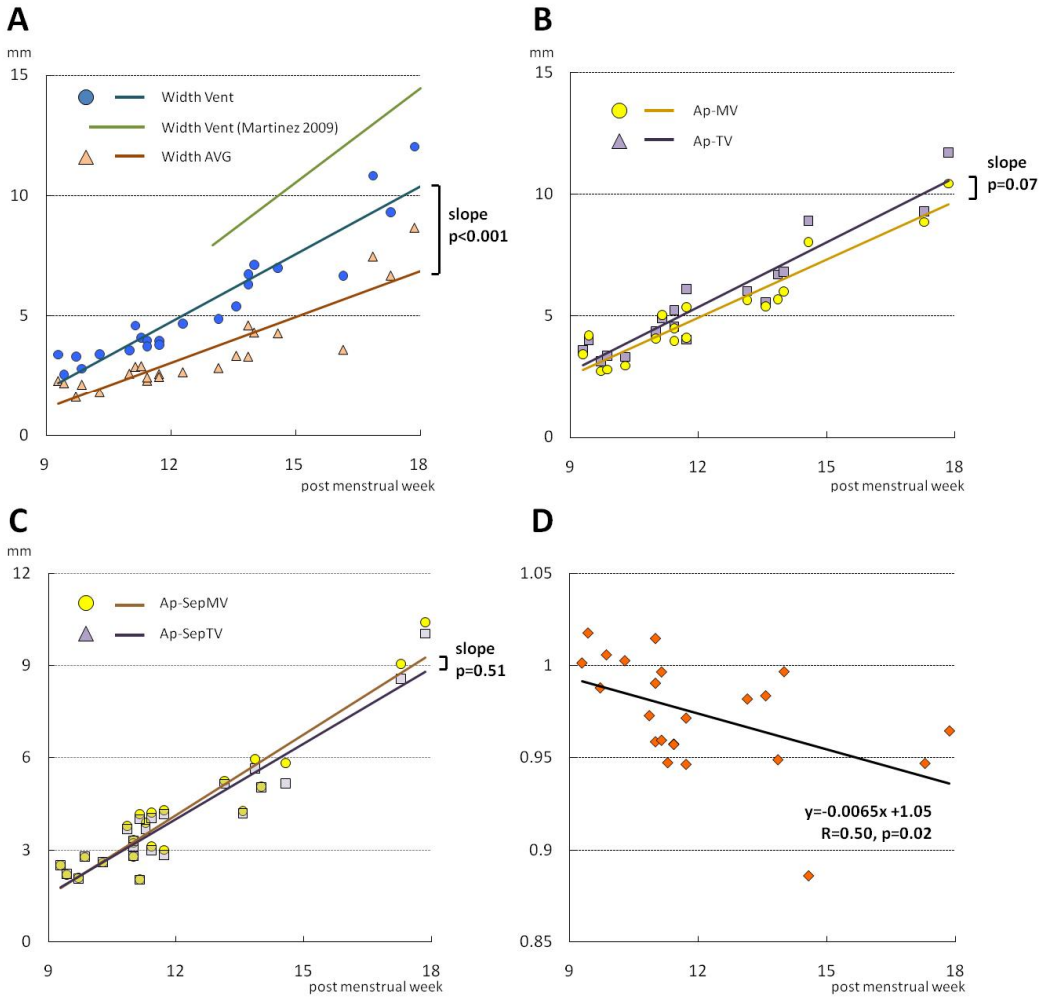

Figure 4-11: Morphometry of the inlet and the outlet components in the right and the left ventricles (A and B). The length and the slope of linear regression were longer in the outlet than in the inlet of the right ventricle. In the left ventricle, the slopes showed no significant difference while the length was longer in the inlet than in the outlet.

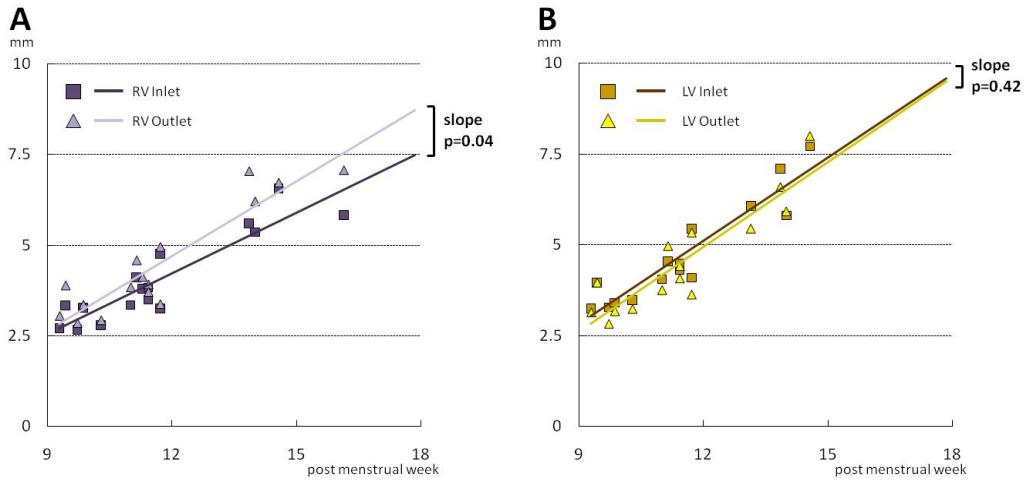

Figure 4-12: Ventricular mass volume. Regression analysis by cubic function highly fitted to the data (R=0.98, p<0.001) Ventricular mass volume increased rapidly with gestation.

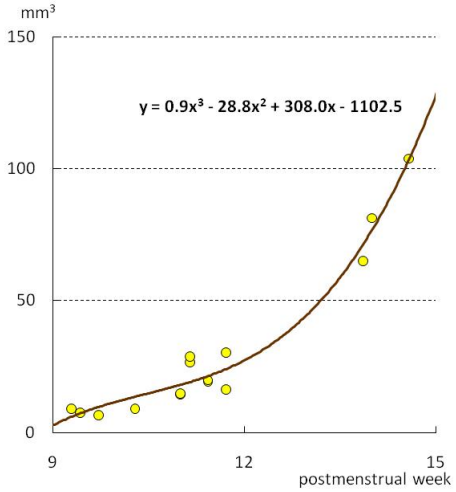

Table 4-4: Linear regression of external diameter and wall thickness of great arteries.

Parameter		slope	Intercept	R	P value
Pulmonary Trunk	External diameter	0.29	-2.22	0.97	p<0.001*
	Wall thickness	0.033	-0.163	0.92	p<0.001*
Aorta	External diameter	0.28	-2.16	0.97	p<0.001*
	Wall thickness	0.030	-0.111	0.94	p<0.001*

Figure 4-13: Graphs of external diameter and wall thickness in the pulmonary trunk (PT) and the aorta (Ao). Upper row shows the external diameter of both great arteries. They increase linearly with gestation and are similar to the reported data (green and blue lines). Middle row illustrates the wall thickness of the both great arteries. Wall thickness also increases linearly in PT and Ao. The ratio of wall thickness to the external diameter demonstrates more than 0.2 at around 10 weeks and rapidly decreases in both great arteries. The ratio remains constant after about 16 weeks until term.

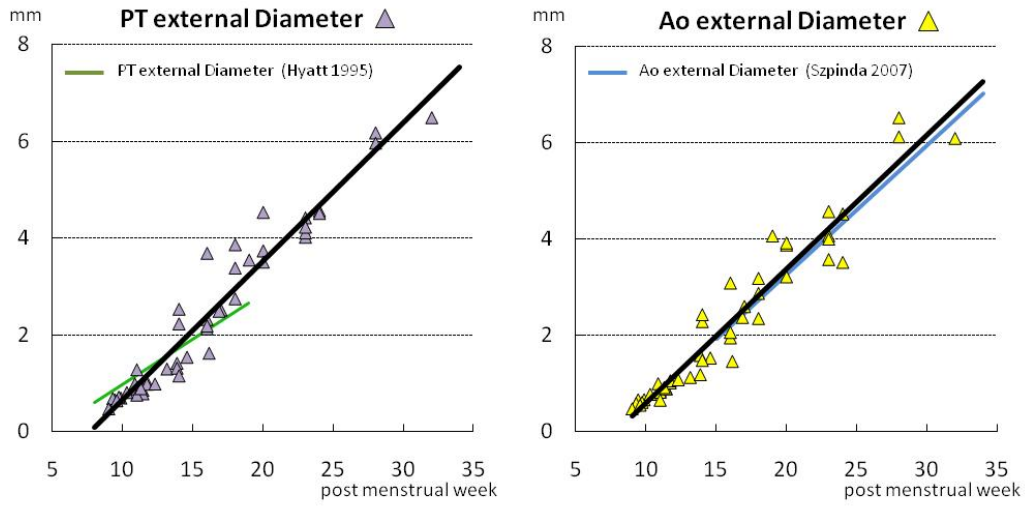

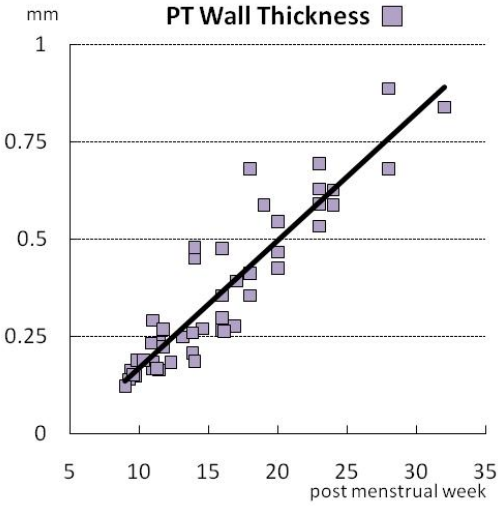
mm
PT Wall Thickness
1
0.75
0.5
0.25
0
5
10
15
20
25
30
35
post menstrual week

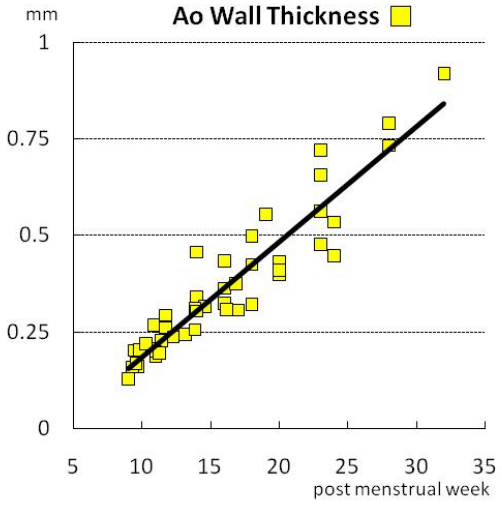
mm
Ao Wall Thickness
1
0.75
0.5
0.25
0
5
10
15
20
25
30
35
post menstrual week

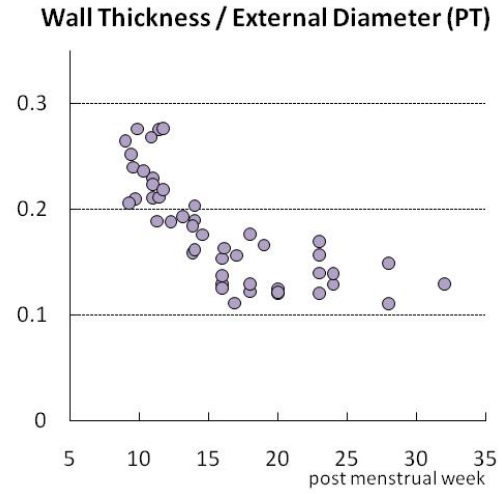
Wall Thickness / External Diameter (PT)
0.3
0.2
0.1
0
5
10
15
20
25
30
35
post menstrual week

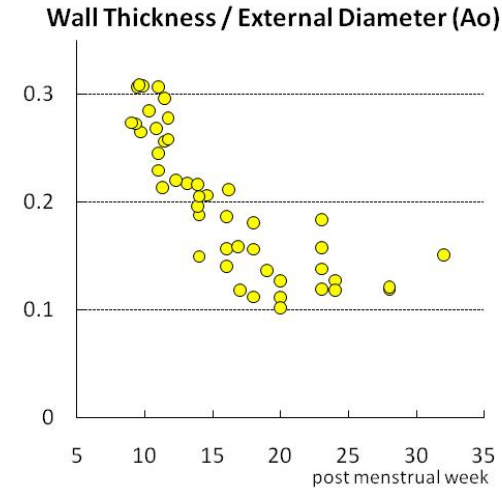
Wall Thickness / External Diameter (Ao)
0.3
0.2
0.1
0
5
10
15
20
25
30
35
post menstrual week

4.4 Discussion

Morphological appearance of the heart during fetal life changes even in normal hearts. Cellular maturation and differentiation programmed by molecular factors and hemodynamic effects to the heart result in geometric growth and acquirement of pump function suggesting dramatic morphological development of fetal heart. However, as Pexieder et al described, little is known concerning the phase of heart maturation although they emphasized the importance of morphological description during and after cardiogenesis (Pexieder, Wenink et al. 1989). Cook et al described increase in size and change of cardiac axis in the 8 to 10 weeks human fetal heart, but no description of the morphology of each component of the heart (Cook, Yates et al. 2004). Thus, detailed 3D information on changes in cardiac morphology of the heart after cardiogenesis remains lacking. Using HREM, we have been able to illustrate some of these changes in the developing human fetal heart in the early stage of heart maturation.

In this chapter, we have presented several specific findings. The first is the dominance of the atrial appendages relative to the rest of the atrial components. In the late first trimester the right atrium has all the components parts of a normal postnatal heart although the huge appendage accounts for much of volume of the atrial cavity. Since the cavity enclosed by the venous, septal and vestibular components (the atrial body) is relatively small, the internal structures such as the venous valves and terminal crest appear relatively large. The left atrial cavity is also relatively small while its basic components are similar to the normal post natal heart.

By the early part of the second trimester of gestation, imbalance between the appendage and the atrial body becomes less prominent. Blom et al reported atrial structures in the human fetal heart during their research of the developing conduction system and they pointed out prominent venous valves and a membranous terminal crest originated from venous-related structures resulting in normal structure of the inside of the right atrium (Blom, Gittenberger-de Groot et al. 1999). The heart dramatically increases in size and matures after cardiogenesis suggesting a significant increase of total cardiac output in the developing heart (Cook 2001). Smrcek et al reported high detection ratio of pulmonary veins by fetal echocardiography at 15 weeks suggesting increase of pulmonary circulation during this period (Smrcek, Berg et al. 2006). These findings suggest that enlargement of atrial cavity caused by increased blood flow may significantly contribute to the formation of balance between appendage and atrial body. Certainly, the atrial appendage is less prominent in later gestation. This finding suggests more rapid growth of the atrial body with less growth of the appendage. Perhaps the left atrial appendage grows least on account of its narrow junction with the atrial body rendering it a cul-de-sac.

The atrioventricular junction showed characteristic development. In the qualitative assessment, visual appearances of the orifices of atrioventricular valves from the atrial aspect, at the annulus, are small compared to ventricular widths suggesting larger parietal growth of the ventricles. In the morphometry of four chamber view, the slope of regression line is significantly higher in the ventricular width than in the width of the atrioventricular groove. These findings suggest that

ventricular growth in the lateral direction is greater in the ventricles than at the atrioventricular junction resulting in prominent atrioventricular sulcus from the late first trimester to the early second trimester. Maximum ventricular width is apparently lower than the value of Martinez's group while we obtained optimal 2D plane for measurement of length and compensated shrinkage in HREM (Martinez, Prajapati et al. 2009). This may imply that measurement of length of 3D objects by manual handling includes the risk of overestimation because of difficulty to obtain an optimal plane.

The offsetting of atrioventricular valves was different between the late first trimester and the early second trimester. Allwork et al reported only one in 5 fetal hearts from 15 to 26 postmenstrual weeks showed a membranous septum (Allwork and Anderson 1979), however, their work was performed using histological sections including significant limitation of optimal views for observation. In our study, the atrioventricular valves are visually at similar levels at 9 postmenstrual weeks in the four chamber view followed by clear offsetting after 16 weeks and our morphometric assessment showed the slope of the regression line is higher in the outlet than the inlet of the right ventricle while no difference was found in between the inlet and the outlet of the left ventricle. This suggests relatively low growth of the inlet component of the right ventricle and that the difference in longitudinal growth of the inlet direction between ventricles may contribute to formation of the offsetting of atrioventricular valves and membranous septum occurring from 9 to 16 weeks.

The characteristic feature of the ventricle after cardiogenesis is development of trabeculations, tendinous chords and papillary muscles. In the first trimester after

cardiogenesis, structures of basic features of trabeculations in the right ventricle have already formed. However, their appearance is still immature compared to the postnatal heart. After 13 weeks of gestation, right ventricular trabeculations become more coarse and prominent with the branched anterior papillary muscle and thin tendinous chords. In the left ventricle, fine trabeculations still exist on the surface of the ventricular septum at around 10 weeks and is diminished with widening of the smooth area of the septal surface after around 13 weeks. The leaflets of the atrioventricular valves are thick and rounded in the first trimester evolving to become slim, thin leaflets after about 13 weeks. Our finding suggests that significant and rapid morphological maturation of the ventricle can be recognized within a few weeks after cardiogenesis.

In our morphometry, ventricular mass volume increases rapidly with gestation and fitted well with the cubic curve although ventricular length showed linear proportion with gestational weeks. Ventricular length may be affected by cardiac cycle more than ventricular mass volume as cavity size changes and cardiac myocytes, in general, may cause minimum change in size during a cardiac cycle. Arraez-Aybar et al also measured myocardial mass volume in the human fetus using 2D histological sections and reported dramatic increase of the volume (Arraez-Aybar, Turrero-Nogues et al. 2008). Myocardial mass volume may be more suitable to assess of ventricular size or hypertrophy in the early stage of human fetal heart despite there may be myocardial shrinkage by the process in HREM. Nevertheless, volumes need to be interpreted carefully using HREM techniques.

The visual appearance of great arteries showed thick arterial walls in the early stages of heart maturation while both great arteries showed linear growth. Thick arterial walls and cellular density in histological sections are prominent at 9 weeks in both great arteries and became less obvious after 16 weeks. In morphometry, there was a dramatic decrease in ratio of the wall thickness to the external diameter by around 16 weeks remaining constant until late gestation although the external diameters of the pulmonary trunk and the aorta demonstrated similar values to a previous report carried out using a microscope (Hyett, Moscoso et al. 1995; Szpinda 2007). These findings suggest to us interpretation of morphometry of vascular systems needs to be performed carefully in the fetal heart because the internal diameters of both great arteries are relatively small compared to their external diameters in the early stage of heart maturation.

The leaflets of the semilunar valves in the first trimester were thick, showed globular appearance in longitudinal section, and had high cellular density suggesting immature cellular structure. In this study, the morphological shape of the semilunar leaflets became finer at around 17 weeks than around 9 weeks. Aikawa et al pointed out decrease of cellular density and structural alteration of elastin and collagen of the aortic valve from the fetus to adult in the human suggesting that dynamic histological change occur by cellular remodelling (Aikawa, Whittaker et al. 2006). Combs et al pointed out that hemodynamic stimulation by unidirectional pulsatile blood flow to the surface of semilunar valves results in gene expression of VEGF/NFATc1 in the valves. (Combs and Yutzey 2009) Thus, morphological maturation of semilunar valves

after cardiogenesis is normally effected by cellular differentiation and hemodynamic influence resulting in maturation of valvular shape.

Visually prominent coronary arteries are recognized in the first trimester after cardiogenesis. The basic structure of the coronary system, which includes the right and the left coronary systems or branching pattern of the arteries, has already established at around 10 weeks. Nowak et al reported coronary vasculature in 199 human fetuses ranging from 4 to 7 months postmenstrual gestation. They found right-sided dominance in more than 80% of coronary systems at 4-months (Nowak, Gielecki et al. 2008). In our study, 60% of hearts from 9 to 11 weeks had a right dominant system. These findings suggest that a right-sided coronary system is dominant in the human fetal heart.

Linear distance was measured in MPR or VR images and volume was calculated from voxel data in VR images. Linear measurement is simple, but includes a fundamental limitation which is minimum length between two arbitrarily-chosen points and cannot be applied to measurement of curved lengths. We chose linear distance to evaluate geometrical cardiac growth because it is basic. Furthermore, we measured using the optimal plane by digital dissection in MPR images and this method will be more suitable than manual morphometry by a calliper. Weninger et al proposed a new method of 3D morphometry of inner cavity of great arteries in the mouse using area data in HREM (Weninger, Maurer et al. 2009). Their method may include potentially more accurate quantification of the arteries than 2D measurement. However, it may be difficult to apply measurement of vascular external diameter or

wall thickness. Further 3D measurement may be optimal for assessment of the developing human heart.

The timing of processing during the cardiac cycle affects ventricular appearances. Cardiac samples fixed at end-diastole are ideal for morphological observation whereas ventricular walls look thick and cavities diminish in systole. Perfusion fixation is an effective method to standardize ventricular appearances for morphological study. However, the cardiac cycle cannot be controlled in fetal cardiac specimens and perfusion fixation is not possible because of the retrieval process and small size of the samples. This may cause over- or under-measurements in morphometry because it is hard to know at what time during the cardiac the measurements were performed. Furthermore, it is impossible to evaluate ventricular wall thickness in this study despite some samples demonstrating significantly thickened ventricular walls suggesting fixation in systole when many artefacts could be included.

There are normal variations in the developing human fetal heart. We have recognized immature structures and dense cellular matrix in myocardium, valves and arterial wall resulting in variation of morphological structure during heart maturation in the normal human fetal heart. Although no molecular factor is found to explain this dynamic structural alteration, cellular remodelling and histological apoptosis may play important roles in the first stage of the developing fetal heart. Further molecular investigations including transcriptional factors causing these dynamic histo-

morphological changes are needed to elucidate developmental steps in the normal human fetal heart.

Morphological assessment of the heart by HREM may include other limitations. Ideally, many more fresh specimens should be obtained to create a normal reference range of the developing fetal heart. However, as discussed in Chapter 2 sample collection is difficult, with retrieval rate of 41% (21/51) for the youngest ages (from 9 to 11 weeks). It is difficult to know the exact date from the conception and true gestational weeks because the postmenstrual gestation is estimated by crown-rump length in an early echo scan. Haematoxylin-eosin stain is the only stain showing technical success yet while specific structures like electrical pathway or conduction system will require special staining procedures to visualize. This may prove to be a fundamental limitation in establishing normal reference ranges in the human fetal heart. Damage of one part of a sample by surgical TOP may affect on morphological alteration to the other intact parts of the same sample. Furthermore, an important factor underlying our 3D models by HREM is fact that the hearts are in-vitro sample and not filled by blood. Thus, our quantitative findings may deviate considerably from in-vivo samples although the qualitative morphologic findings should remain pertinent. Further investigation will be needed to overcome some of these limitations.

In conclusion, human fetal hearts demonstrate specific morphological structures in the late first and the early second trimester. Some specific findings, such as large atrial appendages, the atrioventricular junction, ventricular trabeculations or great arterial walls, alter their appearance dramatically in the early stage of heart

maturation. Length and volumetry of the fetal heart by HREM may show geometrical growth providing normal reference of cardiac morphometry in the human fetal heart. HREM provide significant potential for investigation not only in the animal samples but also in the human fetal heart.

5.0 Chapter Five

Morphological difference of the heart between the human and the mouse

5.1 Introduction

Knowledge of differences in detailed morphology of the normal heart between the human and the experimental models, is valuable because the first step to understand the mechanism of heart maturation is to characterise phenotype after cardiogenesis in experimental models, e.g. transgenic manipulation of the mouse. Detailed morphological assessment by longitudinal observation in the developing embryonic heart in mammalian species remains lacking while some major differences in cardiac morphology between species have been reported to date. In Chapter 4 of this thesis, we have characterized the detailed cardiac structures in the human using both qualitative and quantitative assessment by HREM. Therefore, this morphological comparison was performed to characterize difference of the cardiac phenotype by HREM between the human and the mouse after cardiogenesis.

5.2 Subjects and Methods

Twenty fetal hearts of wild-type mice (10 hearts by stage E14.5 and 10 hearts by stage E18.5 were enrolled in this study as described in Chapter 2.3.3. HREM was processed and 3D volume dataset was created in each sample by the method described in Chapter 2.4.1. Qualitative 3D data assessment was performed by the same method described in Chapter 4.2.1. Quantitative 3D data assessment was performed by the same method described in Chapter 4.2.2 and 4.2.3. Additional measurements of the angle between the inlet and the outlet in each ventricle were performed (Figure 5-1).

Figure 5-1: Additional measuring points for morphometry.

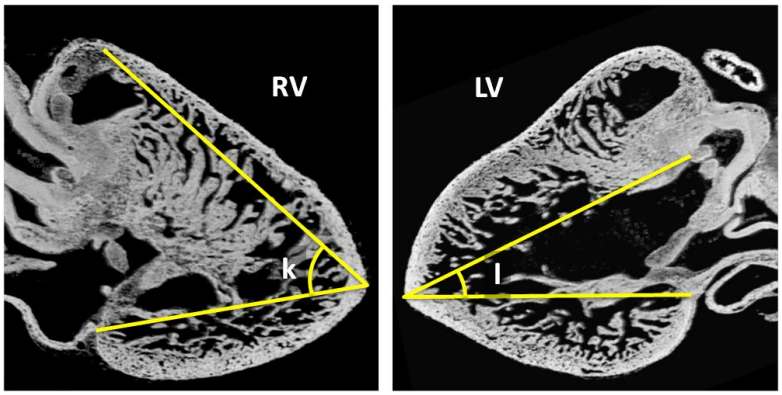

B: RAO View of the Right Ventricle	
k	Angle between the inlet and the outlet in the right ventricle (RV angle)

C: LAX View	
l	Angle between the inlet and the outlet in the left ventricle (LV angle)

LAX: long axis, LV: left ventricle, RAO: right anterior oblique, RV: right ventricle

Analysis has been performed by SPSS software (SPSS Inc., Chicago). Analysis of covariance (ANCOVA) was used for comparison of slope of linear regression lines. Paired and unpaired t-test was used for comparison of each value. Statistical significance was taken in cases of p value less than 0.05.

5.3 Results

3D images were successfully reconstructed using HREM in all 20 hearts . Reconstructed images by HREM showed normal arrangement of atrial appendages and normal atrioventricular and ventriculoarterial connections with no ventricular septal defects suggesting structurally normal heart in all samples.

General appearance

External appearances of the general structure of the heart by stage E14.5 was different from that at stage E18.5 even though both hearts were thought normal (Figure 5-2A). The E14.5 hearts were wide in the lateral direction and demonstrated round-shape ventricles with two ventricular apices and large atria. The E18.5 hearts showed oval-shape and ventricles were more conical rather than round. The edge of the atria was sharp by stage E18.5 and the anterior interventricular sulcus was less prominent. The angle between the inlet and outlet direction was significantly higher by stage E14.5 than by stage E18.5 in both ventricles of the mouse (Figure 5-2B) (54.2 +/- 4.2 degree by E14.5 and 39.8 +/- 5.3 by E18.5 in the right ventricle, 28.7 +/- 1.4 by E14.5 and 17.4 +/- 2.6 by E18.5 in the left ventricle, respectively) In contrast, in the human, the angle between the inlet and outlet direction remained similar in both ventricles during gestation (45.2 +/- 4.9 in the right ventricle and 27.1 +/- 2.4 in the left ventricle, respectively) (Figure 5-3C).

Figure 5-2: External feature of the mouse fetal heart. A: the left-sided picture is 3D VR reconstruction of the mouse fetal heart by stage E14.5 showing round shape appearance. Two small peaks of the apex are recognized in each ventricle (arrow). The right-sided picture demonstrates the 3D image of the mouse fetal heart by stage E18.5 and its general appearance is more oval than by stage E14.5. The anterior interventricular sulcus is not clear. B and C: The angle between the inlet and outlet direction in the mouse (B) and the human (C). In the both ventricles, the angle is importantly larger by stage E14.5 than by E18.5 while there is no significant age-related difference in the angle of both ventricles in the human.

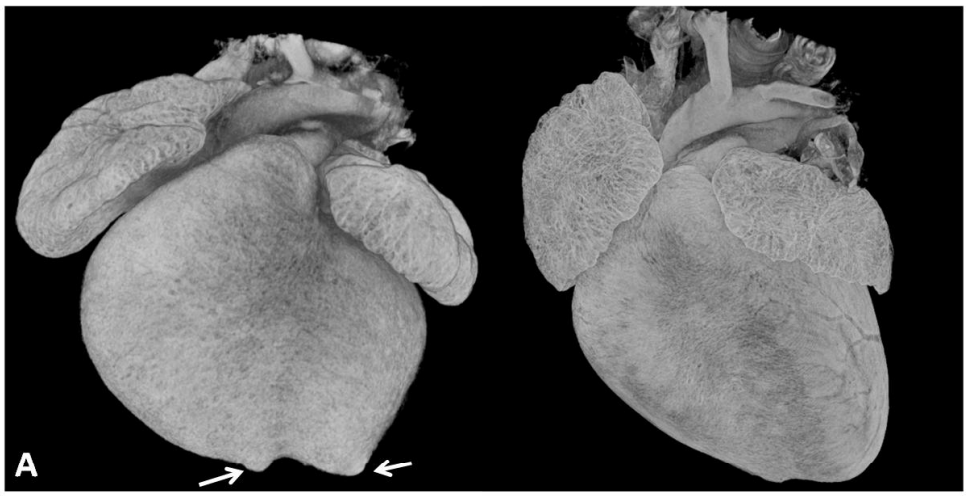

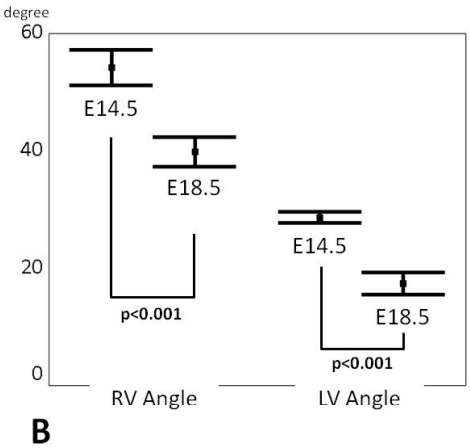

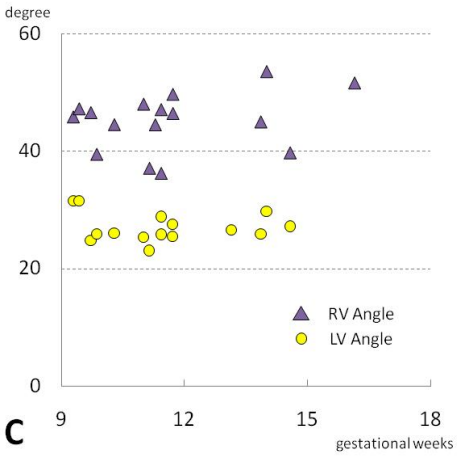

Atria

Like human hearts, the most characteristic finding in both atria was large appendages, however, external difference between appendages in the mouse was much less marked than in the human (Figure 5-3A). By stage E14.5 both appendages were round and broad and the angle of the edge of the appendages was blunted. The junction of the atrial cavities was wide in the right atrium and slightly narrow in the left atrium, but not like the narrow neck of the left appendage in the human. The appendages were in the anterolateral position and did not cover the right ventricular outflow tract or the anterior interventricular sulcus. The external appearance of both atrial appendages demonstrated less difference in the mouse.

The venous component of the right atrium received bilateral superior caval and one right inferior caval veins (Figure 5-3B). The right superior caval vein formed prominent right and left venous valves running in the vertical direction and these valves joined together and connected to a large pectinate muscle attaching to the right atrial wall. The left superior caval vein connected to the large coronary sinus forming a large orifice with a venous flap into the right atrium. The pectinate muscles in the right atrium were cancellous and did not extend to the vestibule which is smooth and supports the tricuspid valve (Figure 5-3C). In the left atrium, pectinate muscles showed pole-like structures and were also limited within the appendages. The vestibule was smooth and supported the mitral valve. Left and right pulmonary veins joined together to form a single orifice in the left atrium. There was no venous valve formation in the left atrium. By stage E18.5, both appendages became more planular and shifted to a

more lateral position. The pectinate muscles became finer in the right atrium and coarser in the left atrium by the stage E18.5 (Figure 5-3D).

Figure 5-3: Atrial structure in the mouse fetal heart (A-C at stage E14.5, D at stage E18.5). A: External appearance of appendages at stage E14.5. Both appendages are round and broad. The junction of appendage to the venous component is wide in the right atrium (*) while slightly narrow in the left atrium (arrow). B: Inside of both atria from the caudal view. Two prominent venous valves (white arrow) are attaching to a large pectinate muscle (black arrow) bridging inside of the right atrial cavity. Back surface showed small-fine pectinate muscles (white arrow head) in the right atrium and rough-coarse pectinate muscles (black arrow head) in the left atrium. C: Atrial structure from the cranial view. Many pole-like pectinate muscles are supporting between anterior and posterior walls of the left appendage (white arrow) while pectinate muscles are small in the right appendage (black arrow head). The vestibules are smooth without extension of pectinate muscles in both atria (*). D: Atrial structures from cranial view at stage E18.5. Both appendages are still round and broad. Pectinate muscles are coarse in the left atrium and fine in the right atrium. A large venous flap originating from the coronary sinus can be seen (arrow).

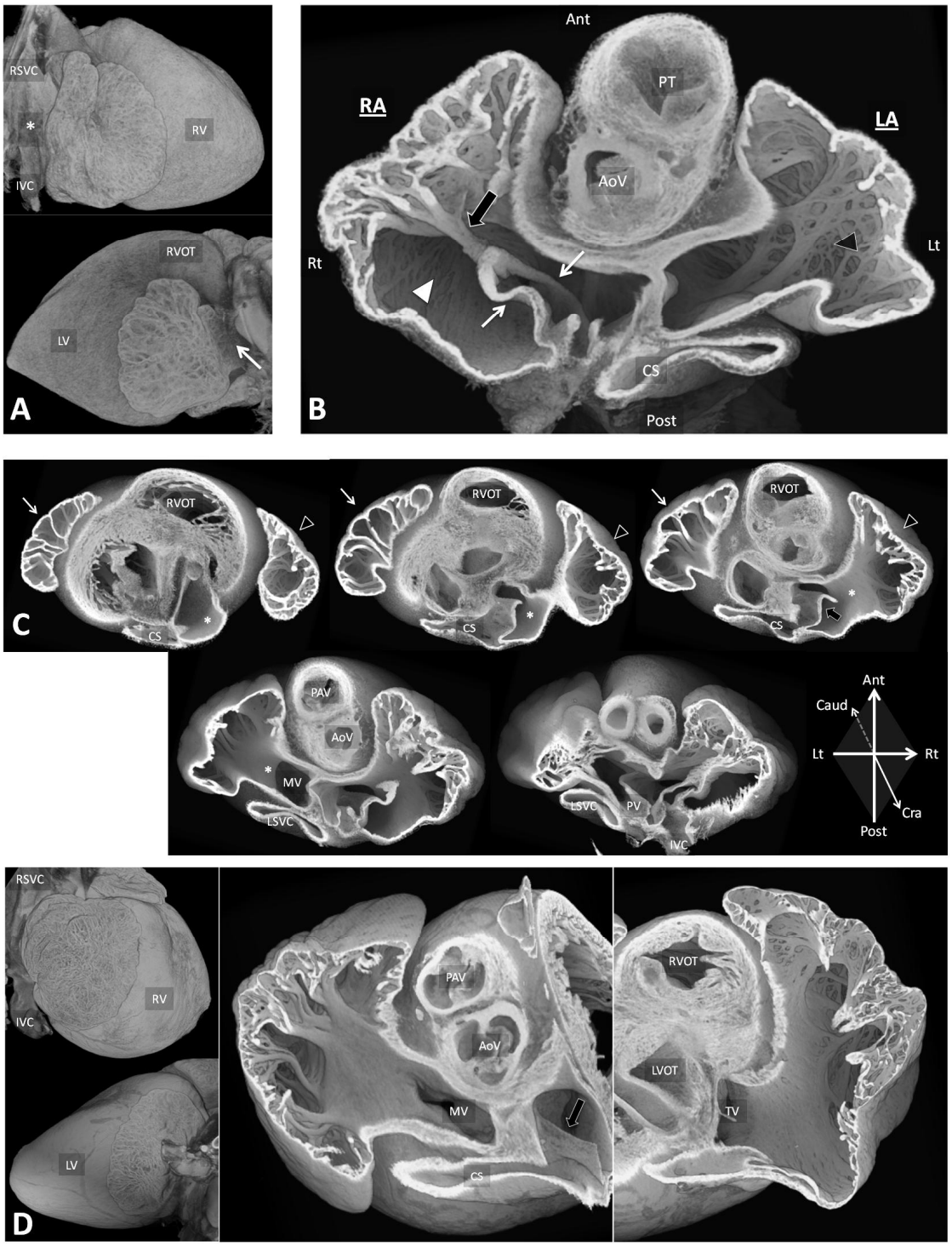
RSVC
RV
IVC
RVOT
LV
A
Ant
PT
RA
LA
AoV
Rt
Lt
CS
Post
B
RVOT
CS
C
PAV
AoV
MV
LSVC
PV
IVC
Ant
Caud
Lt
Rt
Cra
Post
RSVC
RV
IVC
LV
D
PAV
AoV
MV
CS
RVOT
LVOT
TV

Atrioventricular Junction

The most remarkable feature of the atrioventricular junction is that there is no difference in the levels of attachment of the mitral and the tricuspid valve at the cardiac septum (Figure 5-4A). At stage E14.5, the atrioventricular septum demonstrated valvular continuity of the thickened mitral and tricuspid valves and no offsetting of the atrioventricular valves was recognized. By stage E18.5, both valves had become thin and matured, but remained in continuity and the annuli of both valves were at the same level. The septal leaflet of the tricuspid valve attached to the ventricular septum by short fuzzy chordae. The ventricular septum was thick with no formation of the membranous portion of the ventricular septum and no offsetting of the atrioventricular valves. The inlet and outlet lengths showed a parallel increase from E14.5 to E18.5 in each ventricle with no differential growth between the inlet and the outlet portions (Figure 5-4B).

Figure 5-4: Atrioventricular junction in the mouse fetal heart. A: Digitally sectioned 3D image at the inlet level of four chamber view. Both atrioventricular valves are thick and showed continuity at stage E14.5 (arrow). By stage E18.5 both valves had become thinner and the septal leaflet of the tricuspid valve is still attaching to the ventricular septum with short immature tendinous chords (arrow in B panel), however, the continuity is still recognized and the ventricular septum has no membranous portion. C: Morphometry of the inlet and the outlet components in each ventricle. The slopes of the inlet and the outlet lengths demonstrate parallel growth in both ventricles

suggesting no differential growth between the right and left ventricles in the mouse fetal heart.

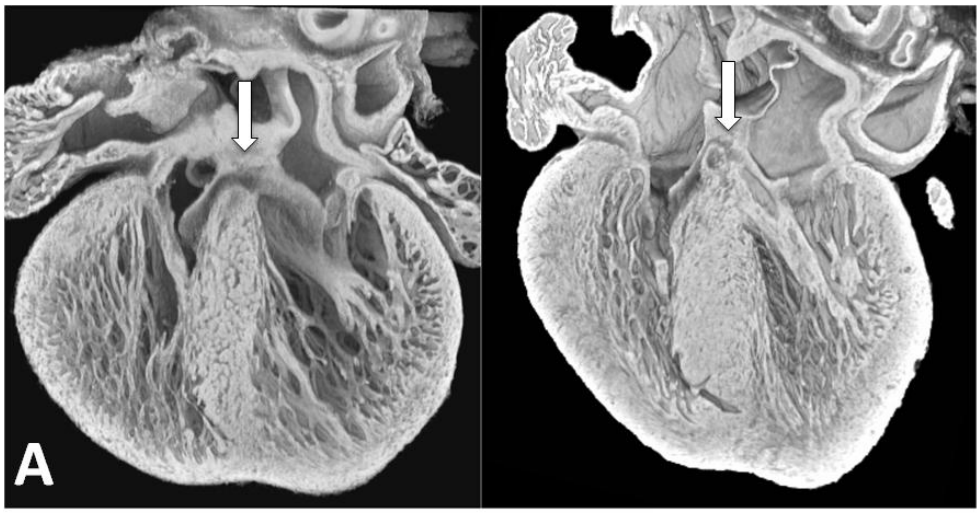

Stage E14.5 Stage E18.5

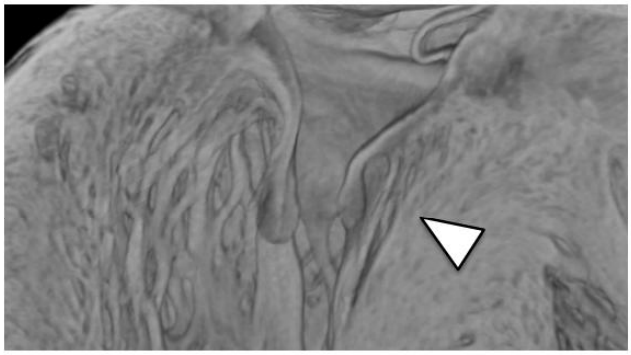

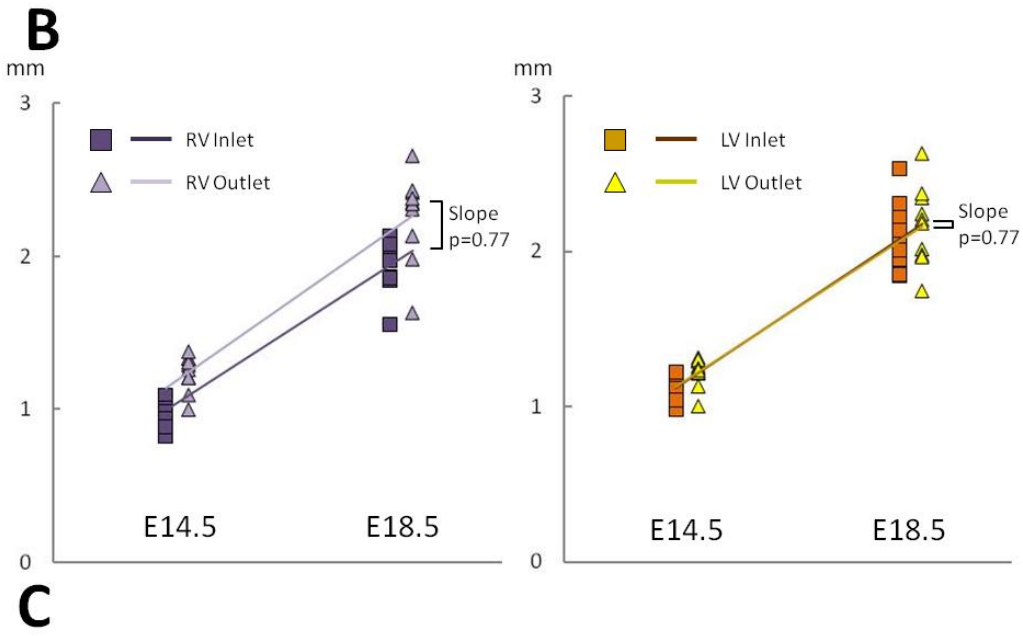

Right and Left Ventricles and Ventricular Septum

It is important to stress that maturation of myocardium including myocardial compaction and formation of trabeculations and muscular band occurred during the observation period (Figure 5-5). The myocardium was immature and non-compacted in both ventricles by stage E14.5 (Figure 5-5A and B). Cancellous musculature bridged the ventricular cavity, especially in the apical part and ventricular free wall was thin in both ventricles. By stage E18.5, the cancellous musculature had disappeared and the myocardium had become dense. The free wall was thick and compacted and clear trabeculations and papillary muscles were recognized.

In the right ventricle, the septal surface had a rough and random structure and trabeculations were immature by stage E14.5 (Figure 5-5C). No muscular band, including the septomarginal trabeculation, could be recognized at this stage. In the apical part, the trabeculations were irregular and minute connecting to very thin right ventricular free wall. Two papillary muscles supporting the anterior and posterior leaflets of the tricuspid valve were short and wide joining to the musculature of the surface of the ventricular septum. The myocardium at the outflow tract showed a honey-comb appearance. By stage E18.5, trabeculations were much more prominent in the right ventricle, muscle bands including the septomarginal trabeculation or septoparietal band running from the septal surface to the parietal part of the free wall, were recognized, however, the moderator band was not formed. The two anterior papillary muscles had matured and extended into muscle bundles joining the septomaginal trabeculation along the septal surface.

The left ventricle demonstrated immature myocardium by stage E14.5 (Figure 5-5D); cancellous trabeculations were prominent in the cavity and myocardium was non-compacted. The septal surface was filled by irregular and small trabeculations. Two papillary muscles supporting the mitral valve were formed, attaching to the free wall of the left ventricle. By stage E18.5, the cancellous trabeculations had disappeared and myocardium was compacted with fine trabeculations in the apical area.

Figure 5-5: Ventricular structure of the mouse fetal heart (left-sided pictures at stage E14.5 and right-sided pictures at stage E18.5). A and B: Digitally sectioned 3D images of the ventricles. Both ventricles show cancellous myocardium suggesting an immature ventricular structure by stage E14.5 (white arrow). Myocardium demonstrates clear trabeculations and dense structure by stage E18.5 (black arrow). Papillary muscles are compact (black arrow head). C: Right ventricular structures. The septal surface has random and immature musculature and no clear muscle band can be recognized at stage E14.5. Two anterior papillary muscles attaching to the septal wall (white arrow) are short and thick. The outflow tract demonstrates honey-comb structure of the free wall. By stage E18.5, the septomarginal trabeculation can be recognized (*) and coarse trabeculations in the right ventricle become clear including septoparietal trabeculation (star mark). The papillary muscles show fine structure attaching to the base of the septomarginal trabeculation (black arrow). The outflow tract shows dense myocardium (black arrow head). D: Left ventricular structure. Myocardium is non-compacted by stage E14.5 while it is compacted at stage 18.5 (white arrow head).

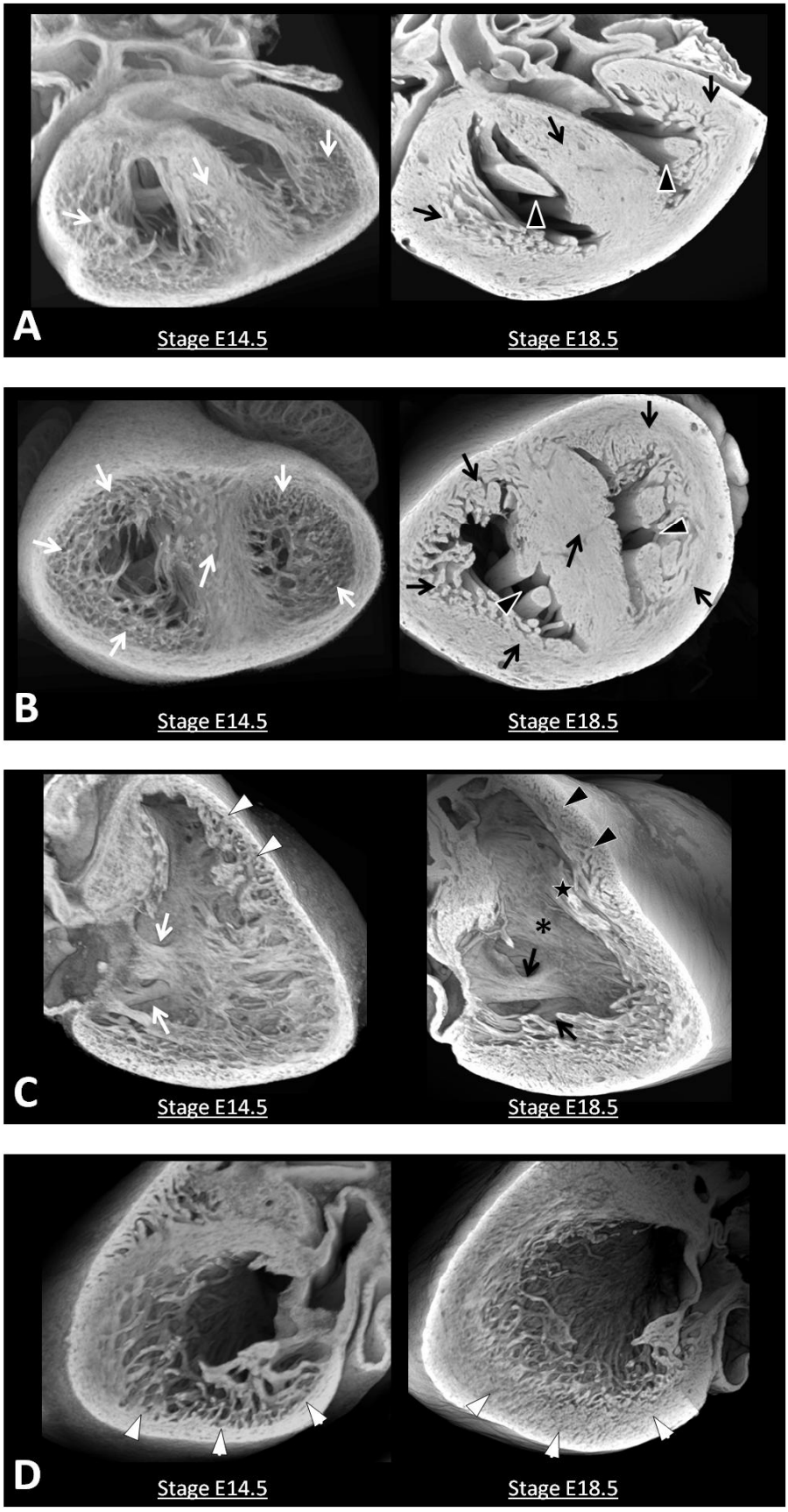
A
Stage E14.5
Stage E18.5
B
Stage E14.5
Stage E18.5
C
Stage E14.5
Stage E18.5
D
Stage E14.5
Stage E18.5

Pulmonary and Aortic Valves, Pulmonary Trunk and Aorta

Similar to the human, the pulmonary and aortic valves have developed into their typical three leaflet formation by stage E14.5 and leaflets were globular in longitudinal sections and thick and wavy (redundant looking) on cross-section (Figure 5-6). The leaflets became thin and fine by stage E18.5.

The wall thickness of the great arteries was less prominent than in the human, although thick arterial walls were present in the aorta and pulmonary arteries at stage E14.5 in the mouse. The ratio of wall thickness to the external diameter was significantly higher at E14.5 than at E18.5 in both great arteries (0.23 at E14.5 vs 0.14 at E18.5 in the aorta and 0.21 at E14.5 vs 0.12 at E18.5 in the pulmonary artery, respectively).

Figure 5-6: Structure of the semilunar valves and great arteries. A: The aortic valve and aorta at each gestation. The aortic valve is thick and round on cross -section at stage E14.5 while the aortic valve is thinner and finer at stage E18.5 (white arrow). The aortic wall is relatively thicker at stage E14.5 than at stage E18.5 (white arrow). B: Ratio of wall thickness to the external diameter in the mouse great arteries. The ratio is significantly higher at stage E14.5 than at stage E18.5 in both great arteries.

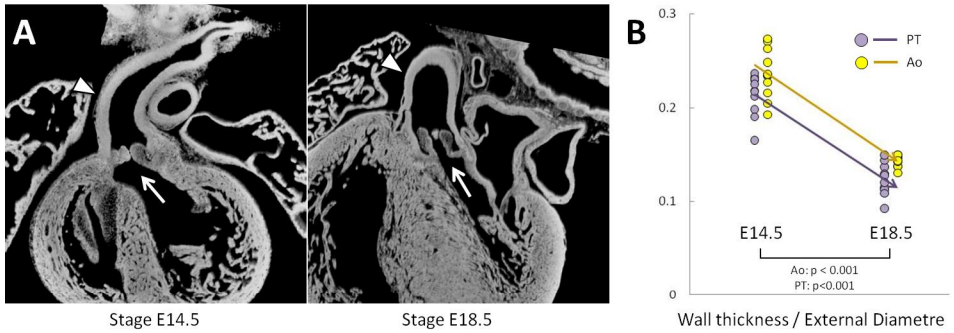

5.4 Discussion

Morphological appearance of the heart in the mouse fetus changes even in the short duration of heart maturation. Maturation and remodelling of cellular matrix controlled by molecular factors may result in specific morphological alteration during the embryonic life in the mouse. Seo et al emphasized utility of morphological investigation of atrial appendages to decide laterality using 275 mutant mice (Seo, Brown et al. 1992). Webb et al described detailed structures of the mouse fetal heart in the late stage (stage E17 or 18) using scanning electron microscope and stressed the importance of cardiac morphology in experimental models (Webb, Brown et al. 1996). However, manual manipulation limits 3D assessment for tiny embryonic hearts and detailed information on changes in cardiac morphology of the developing mouse hearts remains lacking. Using HREM, we have been able to characterize some changes in the developing mouse fetal heart during heart maturation and compare them with the human fetal heart in the early stages.

In this chapter, we have presented several specific findings in the developing mouse heart compared with the human fetal heart. The first is that the mouse fetal heart changes its general appearance during heart maturation. Even atria look large in the mouse heart, the general appearance of the heart at stage E18.5 is significantly different from that at stage E14.5 and ventricles transform from round to oval shapes after ventricular septation in the mouse fetal heart.

Morphometry shows that the inlet to outlet angles in both ventricles are more acute at stage E18.5 than at stage E14.5 in the mouse although they remain similar at

both stages in either left and right ventricle in the human. Petit et al demonstrated a 3D reconstructed model of the mouse heart using micro-MRI that showed similar round appearance of the mouse fetal heart at stage 14.5 (Petiet, Kaufman et al. 2008). Webb et al illustrated oval shapes of the ventricles at stage E17 or E18 in the fetal mouse by scanning electron microscopy and serial histological sections (Webb, Brown et al. 1996). These findings suggest a more dramatic geometrical change in the mouse fetal heart than in the human fetal heart.

The external appearance and internal structures of the atria in the mouse is different from those in the human. Although both atrial appendages are large in the mouse, they showed similar round and planar appearance and less marked difference compared to the human fetal heart. Internal structures show several differences between the right and the left atria, eg formation of venous valves and pattern of pectinate muscles. Interestingly, the pectinate muscles in the mouse demonstrated opposite findings to the human. In the mouse, finer pectinate muscles are in the right atrium and coarser pectinate muscles are in the left atrium while finer pectinate muscles are in the left atrium and the coarser pectinate muscles are in the right atrium in human. Webb et al described detailed intra-atrial structures of the mouse heart using scanning electron microscopy and pointed out formation of the prominent venous valves at about stage E18 (Webb, Brown et al. 1996). They also reported bilateral superior caval veins with the large coronary sinus, single orifice of the pulmonary veins or no venous valve formation in the left atrium, similar to our results in this chapter.

However we have shown several differences from the observations of Webb. They reported that pectinate muscles extend to the vestibule in the right atrium, however, all our samples at stage E14.5 and E18.5 demonstrated a smooth vestibule, without extension of pectinate muscles in both atria. Furthermore, we have found a clear difference in the patterns of pectinate muscles in the appendages from various observation-angles between both atria. Coarse pectinate muscles bridge the inside of the left appendage and cancellous pectinate muscles are seen in the right atrium, suggesting the potential to distinguish atrial morphology in the mouse. We have shown in detail clear continuity between pectinate muscles and bilateral venous valves sandwiching the orifice of the superior caval vein in the right atrium. Observation for detailed morphological structure by digital manipulation using 3D reconstructed images by HREM has less limitation than other methods by manual manipulation.

The geometrical differences in ventricular development may contribute to the formation of the offsetting of the atrioventricular valves and the membranous septum although others described that delamination of the tricuspid valve contributes to establishment of offsetting of the atrioventricular valves. In the human heart at around 11 gestational weeks, both atrioventricular valves are at the same level and there is no membranous septum. By about 16 gestational weeks the membranous septum has formed and there is clear offsetting of the valves. In contrast, the mouse heart does not show offsetting of the atrioventricular valves, even in the later embryonic stage and the ventricular septum has only a muscular portion with no formation of the membranous septum. Our morphometry shows proportional growth of the inlet

portion of both ventricles compared to the outlet portion in the mouse, while the inlet growth is less than the outlet in the human and is responsible for the formation of the membranous septum and the offsetting of the atrioventricular valves. Webb et al described incomplete delamination of the septal leaflet of the tricuspid valve represents the developmental formation of the membranous septum (Webb, Brown et al. 1996; Webb, Brown et al. 1998). De Lange et al demonstrated that the septal leaflet of the tricuspid valve delaminates from the muscular ventricular septum late in development in the mouse (de Lange, Moorman et al. 2004), however, we found no evidence in the fetal mouse to support the theory of delamination of the tricuspid valve contributing to establishment of offsetting of the atrioventricular valves. Atrioventricular fibrous continuity of both valves still clearly existed by around stage E17.5 and the ventricular septum had only muscular but no membranous portion in the mouse, even though detachment of the septal leaflet had occurred. These findings suggest that the delamination of the tricuspid valve has little relationship in the formation of the offsetting of the atrioventricular valves while there is a clear relationship between offsetting of atrioventricular valves and formation of the membranous septum in the human (Chapter 4, Figure 4-4). The early and late stages of heart maturation in the mouse are characterised by atrioventricular valvular continuity without offsetting and no membranous septum as shown clearly by Wessels et al (Wessels and Sedmera 2003). Thus, from a morphological point of view, our results suggest that the geometrical differences in ventricular development may contribute to the formation of the offsetting of the atrioventricular valves and the

membranous septum. Manual manipulation of small samples may result in misleading information, particularly in the observation of the offsetting of the atrioventricular valves in the mouse heart resulting from a lack of optimal planes for morphological investigation.

The mouse ventricular trabeculations show remarkable changes during heart maturation although trabecular remodelling occurs before heart maturation and hearts grow proportionally in the human. Myocardium has not compacted and trabeculations demonstrate rough and random structure at stage E14.5 and trabeculations, papillary muscles and muscular bands are fine and clear at stage E18.5 while basic trabeculations can be recognized at 9 weeks in the human. Wennik et al reported that the earlier trabeculations in primitive right and left ventricles are similar to each other and ventricular trabeculations are formed by the completion of the ventricular septation in the human embryo (Wenink and Gittenberger-de Groot 1982). Sedmera et al reported that trabecular remodelling occurs at around stage E14.5 in the mouse and at around 8 weeks in the human (Sedmera, Pexieder et al. 2000). Wessels described that compaction of the myocardium occurs from stage E11.0 to E16.0 in the mouse (Wessels and Sedmera 2003). Our human samples demonstrated compacted myocardium in the left ventricle after 9 weeks and basic trabeculations, including muscular bands in the right ventricle, at the beginning of heart maturation. Thus, myocardial maturation in the mouse goes beyond the period of ventricular septation and continues during heart maturation suggesting that significant changes of general cardiac appearance may result from dynamic trabeculations in the mouse.

There are several morphological characteristics that differ between the mouse and human ventricle, particularly in the right ventricle of the mouse where the papillary muscle supporting the anterior and the posterior leaflets of the tricuspid valve, attach directly to the root of the Y-shape septomarginal trabeculation and there is no moderator band bridging the ventricular septum and free wall. Apical trabeculations are similar in both ventricles in the mouse unlike in the human. There are fewer differences between the mouse and the human left ventricle.

The semilunar valves demonstrate similar findings in the mouse and human. The aortic and pulmonary valves have developed into tri-leaflet structures by stage E14.5 and each leaflet is thick and wavy, suggesting redundancy. By stage E18.5 both valves become fine suggesting valvular maturation has occurred during this period. Hinton et al reported a change of extracellular matrix in the developing semilunar valves in the mouse. Cusp remodelling as shown by collagen and elastic fibre fragments lying in close proximity to proteoglycan, occurs in the semilunar valves by stage E18.5 (Hinton, Lincoln et al. 2006). Aikawa et al described a structural alteration of elastin and collagen of the aortic valve in the human fetus suggesting that the dynamic histological change occurs by cellular remodelling (Aikawa, Whittaker et al. 2006). Kruithof et al reported that extracellular remodelling continues after birth in the mouse as part of the postnatal maturation of the atrioventricular valves (Kruithof, Krawitz et al. 2007). These reports have demonstrated that valvular remodelling continues and extends into adult life, suggesting that there is a similar process of valvular maturation in mammals. Further similarities include the thickened arterial

walls in the early stage of heart maturation in both species that becomes less prominent after a short period of heart maturation suggesting a similar process of vascular maturation in the mouse and human.

There are some limitations of morphological observation in the mouse fetal heart. There is no standard mophometry, despite the new method proposed for morphometry of great arteries by measuring circumference and area by HREM (Weninger, Maurer et al. 2009), developmental staging in the mouse is not exactly same as in the human which may make it more complex to understand the mechanism of heart development and there may be different effects of shrinkage by the HREM process between the mouse and the human. Furthermore, a fundamental problem is that specific inter-species differences may result in an entirely different mechanism of cardiac development, even though the mouse is genetically similar to the human.

In conclusion, the mouse fetal heart demonstrates major changes in cardiac structure during heart maturation that differ both in morphology and timing of compared to the human fetal heart. 3D observation of morphological differences and specific development during heart maturation contribute to more detailed observation of heart structure including trabeculations in the atria and ventricles in normal and mutant mice. 3D morphometry by HREM may have further potential for detailed quantification of developmental heart in the human fetal heart. Morphological assessment by HREM provides vital information on phenotypic development in experimental animal models.

6.0 Chapter Six

Comparing in-Vitro and in-Vivo “state of the art” imaging of the Human Fetal Heart

6.1 Introduction

The technical limitations of clinical examination of fetal hearts in the early stage of maturation pose significant problems, owing to the tiny size of fetal hearts; precise information on cardiac anatomy and function is vital for fetal or perinatal management in children with congenital heart disease (CHD). The resolution of current imaging modalities for prenatal cardiac diagnosis is still low, and remains less than optimal in diagnosing fetal CHD in the first and early second trimesters. Post-mortem examination is the gold standard for morphological analysis of the heart, when performed by an experienced morphologist, but this provides no functional information and is of course only carried out on terminated or dead subjects. In Chapter 4 of this thesis, the detailed structures of the human fetal heart (using HREM) were characterised. This comparison was performed to examine the suitability of HREM and trans-vaginal 4D fetal echocardiography to define the morphological features of the human fetal heart after cardiogenesis.

6.2 Subjects and Methods

19 of the 36 samples processed by HREM (and described in Chapter 4) were compared with 36 fetuses examined by 4-dimensional trans-vaginal fetal echocardiography (4DTV) at 9 to 12 post-menstrual weeks. Echocardiographic methods are described in Chapter 2.4.4.1, and analysed as described in Chapter 2.4.4.2. Firstly, the visual quality of the four-chamber image, captured by 4DTV echocardiography, was evaluated visually into three groups (‘poor’, ‘acceptable’ or

'good'). 'Poor' images were defined as those where it was difficult to recognise the four chambers or atrioventricular valves; 'acceptable' quality images were defined as those with a good four chamber view but poor contrast; 'good' images were defined as those with a clear four chamber view and acceptable contrast (Figure 6-1 A-C). Multi-planar reconstruction (MPR) images of the human fetal heart were compared for ventricular length, width in end-systole, and width in end-diastole, in the standard four chamber view (Figure 6-1D) using both HREM measurements. Compensation was made for shrinkage by the method described in Chapter 3.5.

Figure 6-1: Visual quality of original images of 3D volume data by echocardiography. (A: poor, B: normal, C: good; 11, 11 and 12 weeks of gestation, respectively). A: The apex of the right ventricle is not clear. B: The ventricles in the normal image are clearer but the atrio-ventricular junction is still unclear. C: General shapes of the four chambers are clearly seen. D: The length of the ventricle was measured from the apex to the atrio-ventricular junction of the ventricular septum. The width was the maximal distance of the ventricles perpendicular to the ventricular length. (LA: left atrium, LV: left ventricle, RA: right atrium, RV: right ventricle, SP: spine)

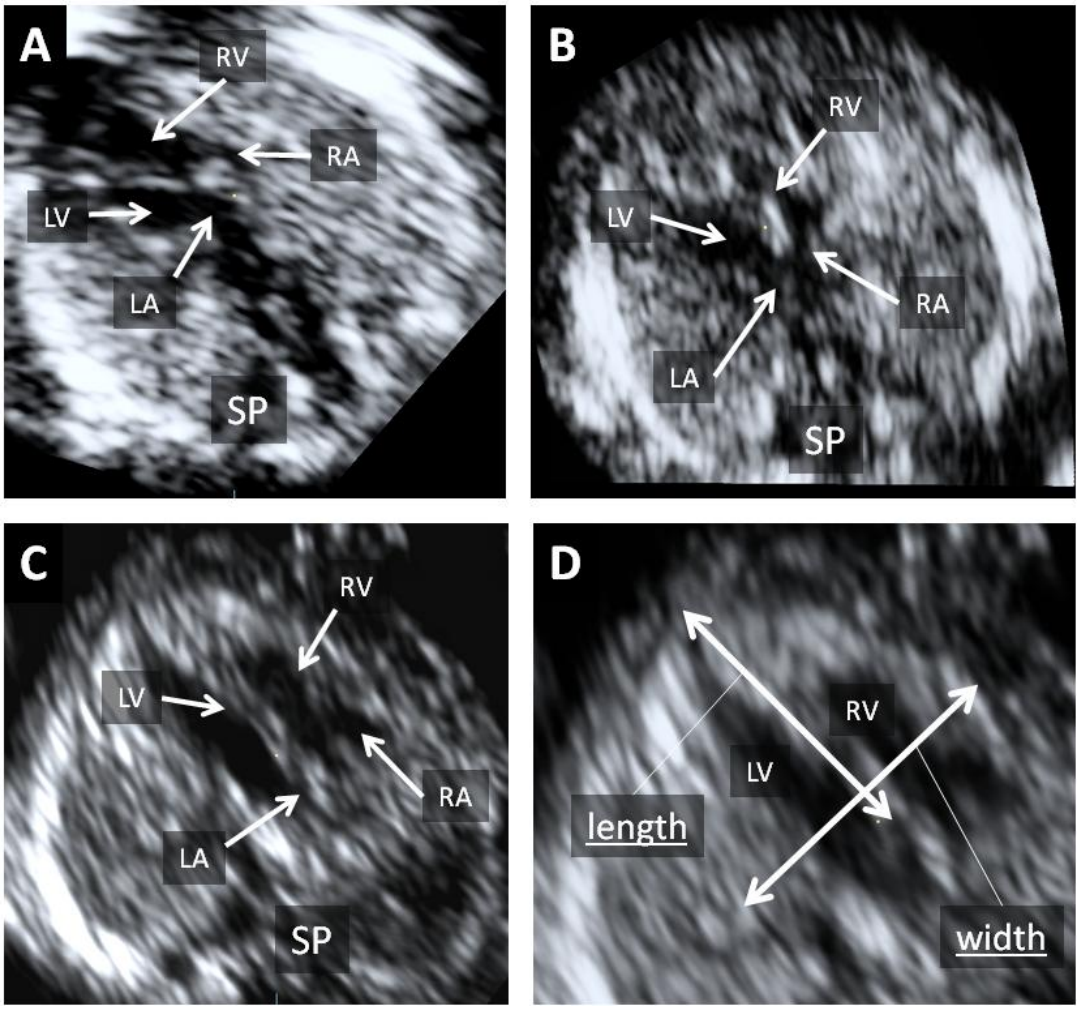

6.3 Results

Image quality was generally poor in the earliest gestational ages studied. Table 6-1 shows the numbers of cases in each post-menstrual gestation and image quality of the four-chamber view. At 9 and 10 weeks of gestation, none of the images were of 'good' quality.

Good quality was seen in 2 of 12 (17%) at 11 weeks, and 6 of 20 (30%) at 12 weeks.

Table 6-1: Quality of four-chamber view by post-menstrual gestational weeks.

	9 weeks	10 weeks	11 weeks	12 weeks	total
good	0	0	2	6	8
acceptable	0	2	3	6	11
poor	1	1	7	8	17
	1	3	12	20	36

Only 2 of 36 cases demonstrated good MPR image quality. In the other 34 cases, it is difficult to discern cardiac structures. Figure 6-2 illustrates the image quality and MPR images in the 36 cases.

Figure 6-2: Quality of images. Even when the quality of the four-chamber view is good or acceptable, almost all of the cases show poor MPR imaging, suggesting poor alignment of 3D volume images.

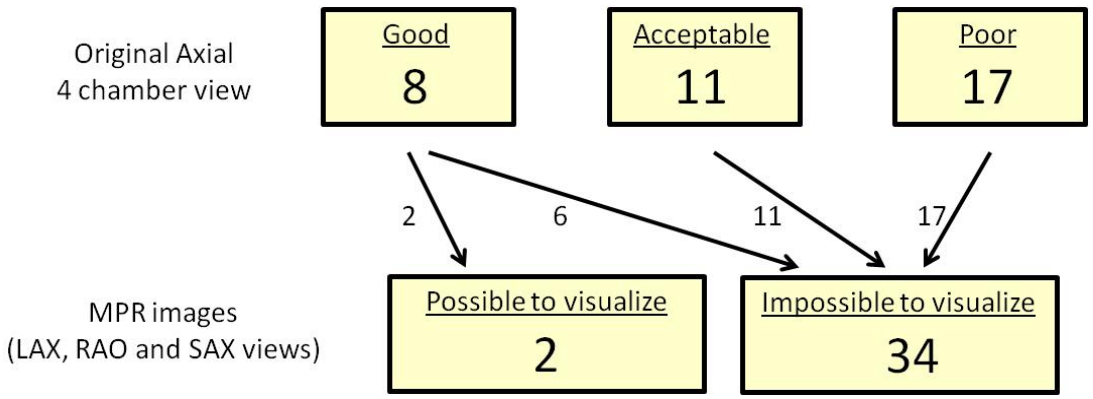

Figure 6-3 shows a comparison of MPR images (four-chamber view, right anterior oblique (RAO) view of the RV, and long axis (LAX) view of the LV) in HREM and 4DTV echocardiography in the two cases. It was impossible to recognize the thickened great arterial walls, prominent coronary arteries, or thickened valvular structures in the MPR images from 4DTV echocardiography.

Figure 6-3: Comparison of MPR images acquired by HREM and 4DTV (A: four-chamber view, B: RAO view, C: LAO view). The images on the left used 4DTV echocardiography, those on the right HREM. A: Human fetal hearts at 12 weeks (left) and 11 weeks (right). The structure of the atrio-ventricular valves is difficult to discern, while myocardia and inter-ventricular septum are clearly seen. B: Human fetal hearts at 12 weeks (left) and 10 weeks (right). Right ventricular structure can be seen in 4DTV echocardiography. However, it is hard to recognize the structures of free walls. C: Human fetal hearts at 12 weeks (left) and 11 weeks (right). The left ventricle demonstrates similar shape to the post-mortem sample. Valvular structure is not clearly seen, while the myocardium is clear. (Ao: aorta, LA: left atrium, LV: left ventricle, RA: right atrium, RV: right ventricle, RVOT: right ventricular outflow tract)

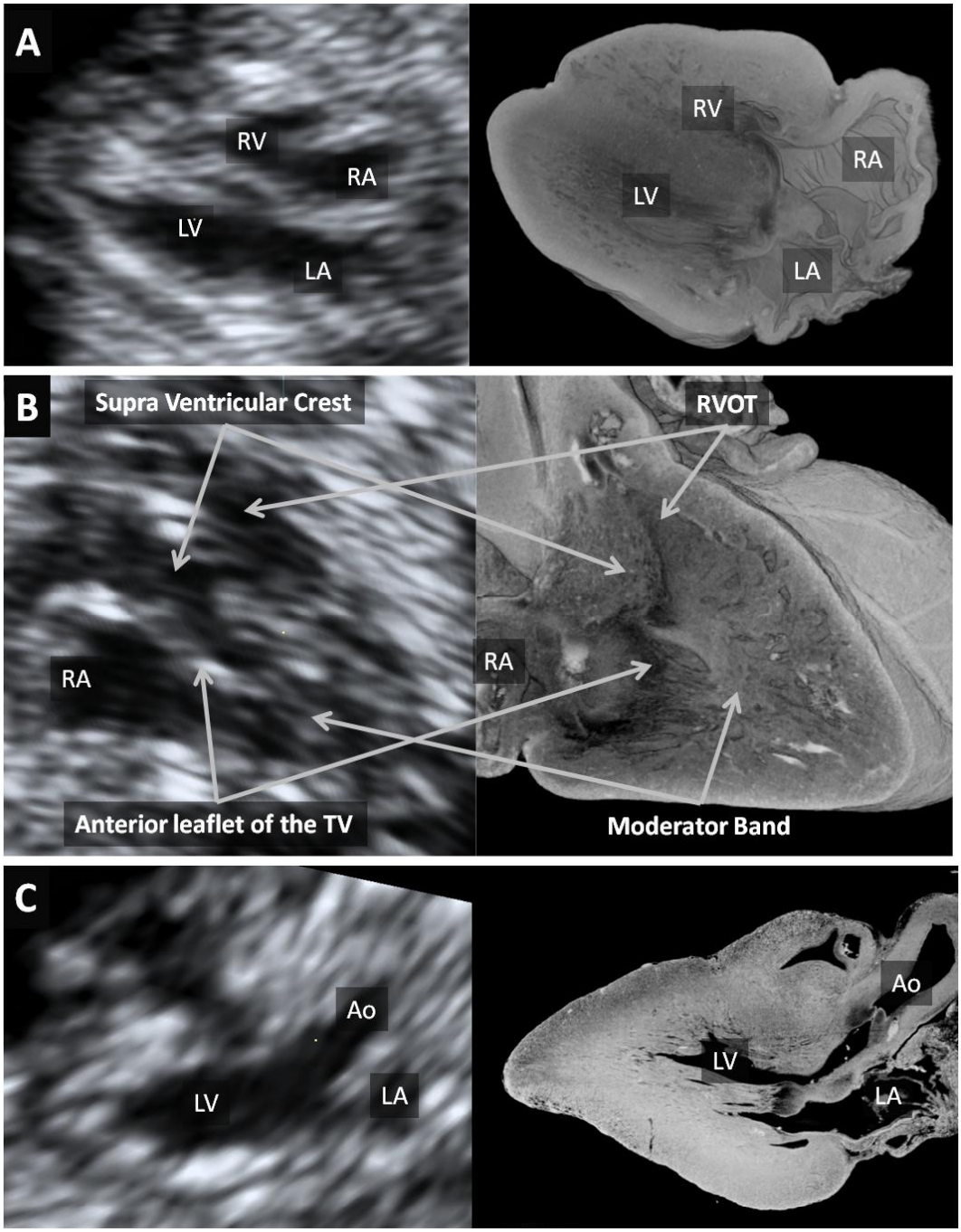

No offsetting of atrio-ventricular valves was recognized in the four-chamber view by 4DTV. The attachments of both atrio-ventricular valves in the four-chamber view are unclear in 25 of 36 cases, but recognisable in the remaining 11 cases (10w3d – 12w6d of postmenstrual gestation). The levels of the mitral and the tricuspid annulus

are the same in all 11 cases, resulting in no offsetting of the atrio-ventricular valves in these gestations. Figure 6-4 shows the number of offset cases of the atrioventricular valves and four-chamber images in each gestation.

Figure 6-4: The level of the atrio-ventricular valves by 4DTV. A: The attachment of atrioventricular valves can be seen in all 11 of the 36 cases which show no offsetting of the mitral and the tricuspid valves. B: The attachment sites of the atrioventricular valves. The yellow triangle identifies the level of the mitral valve, the blue arrow identifies the tricuspid valve, in each postmenstrual gestation. No difference is seen in the level of either valve, Thus there was no offsetting of the atrioventricular valves in any case.

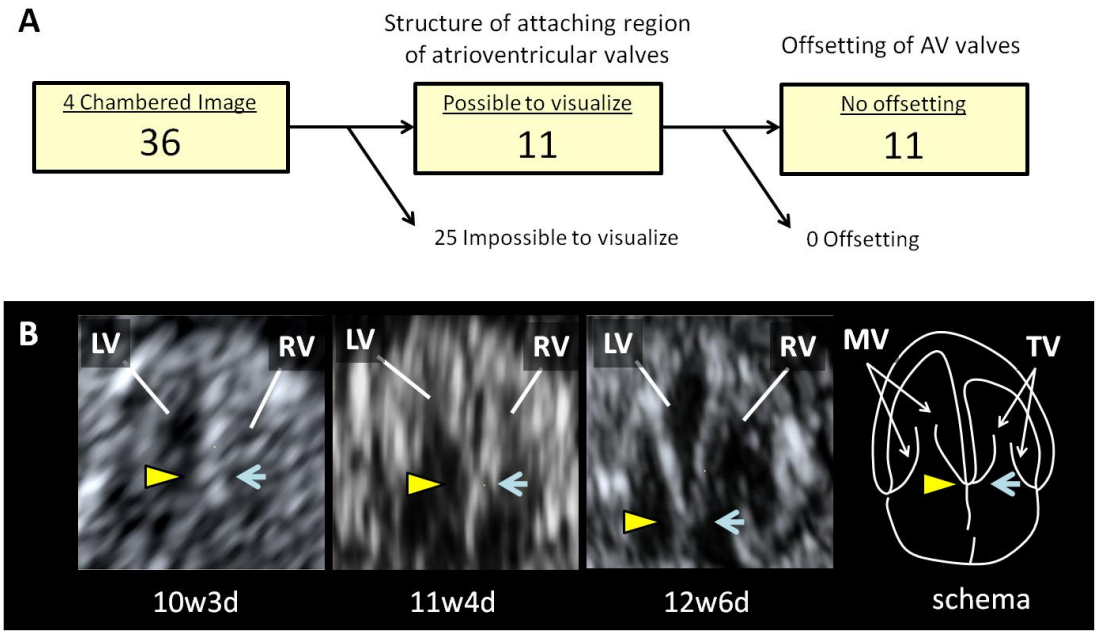

Measurements of ventricular length and width were possible in 34 of 36 cases. Figure 6-5 shows comparison of measurements of ventricular width and length by

gestational week in 4DTV echocardiography, in end-systole, end-diastole, and HREM. Ventricular length is seen to increase linearly with gestational week in both methods, but ventricular width appeared larger when measured in 4DTV echocardiography against HREM.

Figure 6-5: Comparison of measurement of ventricular length and width using 4DTV echocardiography and HREM.

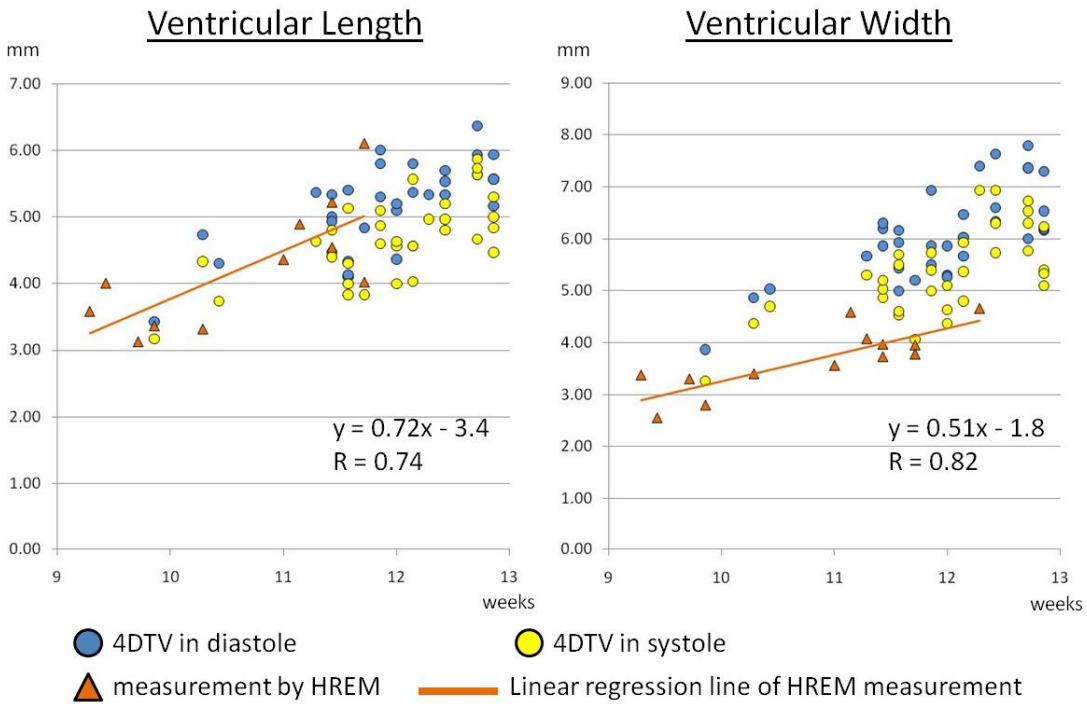

6.4 Discussion

Fetal echocardiography at the first trimester can be done technically, but knowledge of normal cardiac structure at the early stage is vital for clinical assessment. With technological improvement our anatomical and physiological knowledge should be reassessed. Knowledge of cardiac development came from pathological 2-dimensional slices and theories. This is the first time to use 3-dimention high resolution modalities to demonstrate the fetal cardiac development. Nevertheless, this is the first time to combine knowledge from ex-vivo and in-vivo 3D methods.

Fetal 3D echocardiography in early gestation faces several fundamental limitations. The first is a significant limitation in the accurate positioning of a high-frequency trans-vaginal probe - capturing details of small structures in the fetal heart requires said probe to be positioned close to the fetus. The second limitation is that fetuses are very mobile and the difficulty of capturing a static image. The third limitation is the amount of space around the fetus in the uterus, allowing various fetal positions which limit echo windows. Therefore, fetal 3D echocardiography is still technically challenging.

In our results, most 3D echo data did not produce acceptable MPR images. Even when the high frequency probe was used, echo image resolution was not high enough for detailed morphological observation: The fetal heart is less than 4 mm before 12 weeks. At this age, the minimum axial resolution (spatial resolution in the direction of the ultrasound beam), and lateral resolution (ability to discern two separate objects perpendicular to the direction of the ultrasound beam) is

approximately 100 micrometres; the minimum depth of resolution (spatial distance of consecutive 2D echo images) is about 200 micrometres. The quality of original 2D images is vital for 3D echocardiography; current STIC require more than seven seconds to capture enough original data. Clearly, it is very difficult to expect the fetus to remain immobile during capture. Our data shows 22% (8 of 36 cases) showed good 2D images, while acceptable MPR images were gained in only 6% (2 of 36 cases). This suggests that current 3D echocardiography is still technically of limited value for morphological investigation during the first trimester in vivo.

MPR images of 4DTV demonstrated similar structures to those of HREM. In the RAO view, the right ventricle was triangular and there were no obvious visualisations of trabeculations or myocardial bands. In the LAX view, inlet and outlet components were identical to the normal heart structure. In contrast, it was impossible to clearly visualize structures such as atrial appendages, ventricular trabeculations, myocardia, structures of the semilunar valves, or the thickness of the great arterial walls. Thus, image resolution is still not satisfactory for detailed morphological observation in 4DTV, and the large gap of image quality between current ultrasound modality with HREM. General cardiac structures can be observed by 3D reconstructed images taken by 4DTV.

Only the four-chamber view enabled us to make detailed morphological investigations. Eleven four-chamber images demonstrated no offsetting of atrioventricular valves, though it was hard to visualise the attachment structures of valves in about two-thirds of these views. In Chapter 4, we illustrated similar findings for aligned levels of the atrio-ventricular valves from 10 to 12 weeks of post menstrual

gestation, using post-mortem specimens by HREM. In our clinical practice offsetting of the atrio-ventricular valves was recognisable at around 14 weeks of post-menstrual gestation by 2D fetal echocardiography (Figure 6-6) similar to HREM described in Chapter 4. Thus, 4DTV images in vivo and HREM ex-vivo show similar findings, suggesting that echocardiography has the potential for detailed morphological investigation of early human fetal hearts as long as the image quality improves.

Figure 6-6: Four chamber view of 14 weeks' of human fetal heart from clinical practice. Position of attachment of the mitral valve (yellow triangle) is more distant from the apex than that of the tricuspid valve in end-systole and end-diastole.

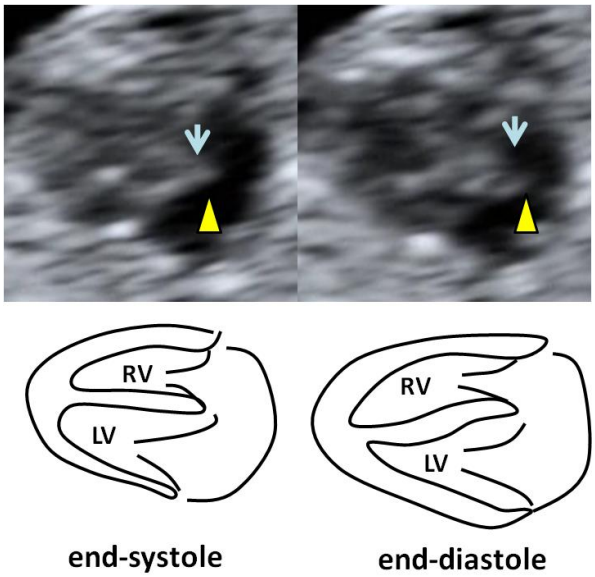

Geometrical measurements showed different 4DTV and HREM values. In the four-chamber view, ventricular width was longer in 4DTV in systole than in HREM. Ventricular length though, increased with gestation in both measurements. Chamber shapes in in-vivo samples are always affected by cardiac cycle, physiological blood

pressure, flow, and haemodynamic load. Ex-vivo samples are exsanguinated and the cardiac cycle is undetectable. Discrepancies in the measurement of ventricular width may suggest in-vivo haemodynamic influences on morphometry in developing fetal hearts. Further investigation is needed on morphometry in both in- and ex-vivo samples.

It is always difficult to obtain clearly rendered images of the heart surface by clinical modalities, such as CT, MRI or echocardiography. The general appearance of cardiac 3D images is reconstructed by volume or surface rendering algorithms, which depict the surface of the heart. However, the heart in-vivo is surrounded by, and attached to, several organs, such as the pericardium, thymus, diaphragm and lungs which are of similar density to the heart, making and it hard to distinguish the heart and poor rendition of its surface. Therefore, the general appearance of cardiac 3D images is technically unsatisfactory. Multi-planar reconstruction is the only valuable technique allowing morphological evaluation of cardiac 3D images in early fetuses.

In conclusion, we have compared in-vivo echo images, acquired by the latest 4DTV technology and using trans-vaginal high frequency probes, with images reconstructed by HREM in early post-cardiogenesis fetal hearts. Current 3D ultrasound modalities are still unsatisfactory for evaluating detailed cardiac structure in the first trimester, suggesting further technological progress is required before morphological investigation of small fetal hearts in vivo is viable.

7.0 Chapter Seven:

Conclusions

I have investigated the 3D structures of human fetal hearts during the first stage of heart maturation,. Newly developed modalities, HREM for 3D morphological analysis in post-mortem samples, and 4DTV for clinical examination in vivo, were used to provide detailed analysis of normal human fetal hearts in early gestation. Knowledge of normal cardiac phenotype during heart maturation will be vital for further investigations into the origin of congenital heart disease or mutations. Therefore, detailed and precise description of the development of human fetal hearts is vital.

HREM - computer-based 3D reconstruction - enables us to visualize detailed spatial structures of small specimens. This includes the many steps in the process which may affect the histological or morphological structures of samples. The general appearance of 3D reconstructed images by HREM looks identical to pictures of original heart samples. However, heart samples demonstrate 12% overall shrinkage due to dehydration and polymerization by HREM. Assessment of hearts by HREM may require allowance for this shrinkage (See Chapter 3).

Post-mortem samples analysed by HREM demonstrated unique morphological findings in the first step of heart maturation. Myocardium, ventricular trabeculations, valves and great arterial walls illustrated thick and immature structures, followed by histological maturation a few weeks after cardiogenesis. Morphologically, several characteristics were recognized during this period, such as large atrial appendages, developmental process of formation of the membranous ventricular septum and prominent coronary arteries, and heart size increased linearly with gestation. Thus,

normal human fetal hearts demonstrate not only geometrical, but also histological and morphological development post-cardiogenesis. (See Chapter 4)

Mouse hearts demonstrate dramatic morphological alterations during their short period of heart maturation. In comparison to human hearts, many differences of morphological findings are to be seen in the first stage of mouse heart maturation, such as general ventricular arrangement, venous valves and trabeculations in atria or myocardial architecture in ventricles. There are some similar morphological findings to the human fetal heart, however, such as large atrial appendages, lack of formation of the membranous septum or thickened great arterial walls. Similar findings regarding detailed morphological structures in the first stage after cardiogenesis suggest the same mechanisms are at work in the maturation in developing fetal hearts in mammals. (See Chapter 5)

Detailed information regarding cardiac morphology is vital for prenatal heart diagnosis in the first trimester. Fetal echocardiography tends to be performed earlier in clinical practice, however, technical limitations of image acquisition and picture resolution make it difficult to visualize clear 3D images for fetal cardiac diagnosis. Current modalities for clinical investigation by 4DTV do not have high enough resolution for detailed morphological investigation from 10 to 12 weeks of post-menstrual gestation, while only original data of the four-chamber view demonstrated identical findings of no offsetting of atrio-ventricular valves. Further development of 3D echocardiography will be required for more precise cardiac diagnosis in the first trimester. (See Chapter 6)

In this thesis, I have described morphological development in normal human fetal hearts for the few weeks post-cardiogenesis detail, contributing to basic and clinical diagnosis of human fetal hearts in the first trimester after cardiogenesis.

Publications related to this thesis

- **Matsui H**, Mohun T, Gardiner HM. Three-dimensional reconstruction imaging of the human fetal heart in the first trimester. Eur Heart J. 2010;31:415
- Gindes L, **Matsui H**, Achiron R, Mohun T, Yen Ho S, Gardiner H. Comparison between ex-vivo HREM imaging and in-vivo 4DHRTV ultrasound of the first trimester fetal heart. Ultrasound Obstet Gynecol. 2011 in print

References

AbortionAct. (1967). "The UK Statute Law Database." from http://www.statutelaw.gov.uk.

Achiron, R., L. Gindes, et al. (2008). "Three- and four-dimensional ultrasound: new methods for evaluating fetal thoracic anomalies." Ultrasound Obstet Gynecol **32**(1): 36-43.

Aikawa, E., P. Whittaker, et al. (2006). "Human semilunar cardiac valve remodeling by activated cells from fetus to adult: implications for postnatal adaptation, pathology, and tissue engineering." Circulation **113**(10): 1344-52.

Allan, L. D. (1995). Normal views of the great arteries. In: Fetal heart scanning. New York, Churchill Livingstone.

Allan, L. D., S. K. Chita, et al. (1989). "The accuracy of fetal echocardiography in the diagnosis of congenital heart disease." Int J Cardiol **25**(3): 279-88.

Allan, L. D., R. Santos, et al. (1997). "Anatomical and echocardiographic correlates of normal cardiac morphology in the late first trimester fetus." Heart **77**(1): 68-72.

Allan, L. D., M. J. Tynan, et al. (1980). "Echocardiographic and anatomical correlates in the fetus." Br Heart J **44**(4): 444-51.

Allwork, S. P. and R. H. Anderson (1979). "Developmental anatomy of the membranous part of the ventricular septum in the human heart." Br Heart J **41**(3): 275-80.

Alvarez, L., A. Aranega, et al. (1987). "The quantitative anatomy of the normal human heart in fetal and perinatal life." Int J Cardiol **17**(1): 57-72.

Anderson, R. H. and S. Y. Ho (1997). "Sequential segmental analysis: description and categorization for the millennium." Cardiol Young **7**: 98.

Anderson, R. H. and I. M. Taylor (1972). "Development of atrioventricular specialized tissue in human heart." Br Heart J **34**(12): 1205-14.

Anderson, R. H., J. L. Wilkinson, et al. (1974). "Morphogenesis of bulboventricular malformations. I. Consideration of embryogenesis in the normal heart." Br Heart J **36**(3): 242-55.

Arnolds, W. J. (1978). "Oriented embedding of small objects in agar-paraffin, with reference marks for serial section reconstruction." Stain Technol **53**(5): 287-8.

Arraez-Aybar, L. A., A. Turrero-Nogues, et al. (2008). "Embryonic cardiac morphometry in Carnegie stages 15-23, from the Complutense University of Madrid Institute of Embryology Human Embryo Collection." Cells Tissues Organs **187**(3): 211-20.

Arteaga-Martinez, M., E. Halley-Castillo, et al. (2009). "Morphometric study of the ventricular segment of the human fetal heart between 13 and 20 weeks' gestation." Fetal Pediatr Pathol **28**(2): 78-94.

Baak, J. P. (1987). "Quantitative pathology today--a technical view." Pathol Res Pract **182**(3): 396-400.

Bartelings, M. M. and A. C. Gittenberger-de Groot (1989). "The outflow tract of the heart--embryologic and morphologic correlations." Int J Cardiol **22**(3): 289-300.

Becker, A. E. and R. H. Anderson (1983). Cardiac pathology. An integrated text and colour atlas. London, Churchill Livingstone.

Bennasar, M., J. M. Martinez, et al. (2009). "Feasibility and accuracy of fetal echocardiography using four-dimensional spatiotemporal image correlation technology before 16 weeks' gestation." Ultrasound Obstet Gynecol **33**(6): 645-51.

Blausen, B. E., R. S. Johannes, et al. (1990). "Computer-based reconstructions of the cardiac ventricles of human embryos." Am J Cardiovasc Pathol **3**(1): 37-43.

Blom, N. A., A. C. Gittenberger-de Groot, et al. (1999). "Development of the cardiac conduction tissue in human embryos using HNK-1 antigen expression: possible relevance for understanding of abnormal atrial automaticity." Circulation **99**(6): 800-6.

Born, G. (1883). "Die Plattenmodelliermethode." Arch Mikr Anat **22**: 584-99.

Brandle, K. (1989). "A new method for aligning histological serial sections for three-dimensional reconstruction." Comput Biomed Res **22**(1): 52-62.

Braverman, I. M. and A. Ken-Yen (1983). "Ultrastructure and three-dimensional reconstruction of several macular and papular telangiectases." J Invest Dermatol **81**(6): 489-497.

Braverman, M. S. and I. M. Braverman (1986). "Three-dimensional reconstructions of objects from serial sections using a microcomputer graphics system." J Invest Dermatol **86**(3): 290-4.

Bullen, P. J., S. C. Robson, et al. (1998). "Human post-implantation embryo collection: medical and surgical techniques." Early Hum Dev **51**(3): 213-21.

Butcher, J. T., D. Sedmera, et al. (2007). "Quantitative volumetric analysis of cardiac morphogenesis assessed through micro-computed tomography." Dev Dyn **236**(3): 802-9.

Castillo, E. H., M. Arteaga-Martinez, et al. (2005). "Morphometric study of the human fetal heart. I. Arterial segment." Clin Anat **18**(4): 260-8.

Combs, M. D. and K. E. Yutzey (2009). "Heart valve development: regulatory networks in development and disease." Circ Res **105**(5): 408-21.

Conte, G. and A. Pellegrini (1984). "On the development of the coronary arteries in human embryos, stages 14-19." Anat Embryol (Berl) **169**(2): 209-18.

Cook, A. C. (2001). "The spectrum of fetal cardiac malformations." Cardiol Young **11**(1): 97-110.

Cook, A. C., R. W. Yates, et al. (2004). "Normal and abnormal fetal cardiac anatomy." Prenat Diagn **24**(13): 1032-48.

Cooper, M. H. and R. O'Rahilly (1971). "The human heart at seven postovulatory weeks." Acta Anat (Basel) **79**(2): 280-99.

de Lange, F. J., A. F. Moorman, et al. (2004). "Lineage and morphogenetic analysis of the cardiac valves." Circ Res **95**(6): 645-54.

De Vries, P. A. and J. M. Saunders (1962). "Development of the ventricles and spiral out¯ow tract in the human heart. A contribution to the development of the human heart from age group IX to age group XV." Carnegie Contributions to Embryology **256**: 89-114.

deAlmeida, A., T. McQuinn, et al. (2007). "Increased ventricular preload is compensated by myocyte proliferation in normal and hypoplastic fetal chick left ventricle." Circ Res **100**(9): 1363-70.

Dhanantwari, P., E. Lee, et al. (2009). "Human cardiac development in the first trimester: a high-resolution magnetic resonance imaging and episcopic fluorescence image capture atlas." Circulation **120**(4): 343-51.

Edwards, J. E. (1953). "Malformations of the aortic arch system manifested as vascular rings." Lab Invest **2**(1): 56-75.

Edwards, J. E. and W. B. Chamberlin, Jr. (1951). "Pathology of the pulmonary vascular tree. III. The structure of the intrapulmonary arteries in cor triloculare biatriatum with subaortic stenosis." Circulation **3**(4): 524-30.

Eisenberg, B. R. and B. A. Mobley (1975). "Size changes in single muscle fibers during fixation and embedding." Tissue Cell **7**(2): 383-7.

Foster, F. S., M. Y. Zhang, et al. (2002). "A new ultrasound instrument for in vivo microimaging of mice." Ultrasound Med Biol **28**(9): 1165-72.

Garrett, W. J. and D. E. Robinson (1970). "Fetal heart size measured in vivo by ultrasound." Pediatrics **46**(1): 25-7.

Gembruch, U., C. Shi, et al. (2000). "Biometry of the fetal heart between 10 and 17 weeks of gestation." Fetal Diagn Ther **15**(1): 20-31.

Gerdes, A. M., J. Kriseman, et al. (1982). "Morphometric study of cardiac muscle: the problem of tissue shrinkage." Lab Invest **46**(3): 271-4.

Gerrits, P. O., R. W. Horobin, et al. (1992). "The effects of glycol methacrylate as a dehydrating agent on the dimensional changes of liver tissue." J Microsc **165**(Pt 2): 273-80.

Gielecki, J. S., B. Syc, et al. (2006). "Quantitative evaluation of aortic arch development using digital-image analysis." Ann Anat **188**(1): 19-23.

Goor, D. A., J. E. Edwards, et al. (1970). "The development of the interventricular septum of the human heart; correlative morphogenetic study." Chest **58**(5): 453-67.

Grant, R. P. (1962). "The embryology of ventricular flow pathways in man." Circulation **25**: 756-79.

Guihard-Costa, A. M., F. Menez, et al. (2002). "Organ weights in human fetuses after formalin fixation: standards by gestational age and body weight." Pediatr Dev Pathol **5**(6): 559-78.

Gundersen, H. J., T. F. Bendtsen, et al. (1988). "Some new, simple and efficient stereological methods and their use in pathological research and diagnosis." APMIS **96**(5): 379-94.

Hanstede, J. G. and P. O. Gerrits (1983). "The effects of embedding in water-soluble plastics on the final dimensions of liver sections." J Microsc **131**(Pt 1): 79-86.

Hegre, E. S. and A. D. Breshear (1946). "Block-surface staining." Stain Technol **21**: 161-164.

Hegre, E. S. and A. D. Breshear (1947). "The block-surface method of staining as applied to the study of embryology." Anat Rec **97**: 21-28.

Heinzer, S., T. Krucker, et al. (2006). "Hierarchical microimaging for multiscale analysis of large vascular networks." Neuroimage **32**(2): 626-36.

Heuser, C. H. and G. W. Corner (1957). Developmental horisons in human embryos: Description of age group X, 4 to 12 somites., Contrib Embryol Carnegie Inst Wash.

Hibbard, L. S., J. S. McGlone, et al. (1987). "Three-dimensional representation and analysis of brain energy metabolism." Science **236**(4809): 1641-6.

Hinton, R. B., Jr., J. Lincoln, et al. (2006). "Extracellular matrix remodeling and organization in developing and diseased aortic valves." Circ Res **98**(11): 1431-8.

Hirakow, R. (1983). "Development of the cardiac blood vessels in staged human embryos." Acta Anat (Basel) **115**(3): 220-30.

His, W. (1887). "Ueber die Methoden der plastischen Rekonstruktion und über deren Bedeutung für Anatomie und Entwicklungsgeschichte. ." Anat Anz. **II**: 382-92.

Ho, S. Y., R. H. Anderson, et al. (2002). "Atrial structure and fibres: morphologic bases of atrial conduction." Cardiovasc Res **54**(2): 325-36.

Ho, S. Y., E. J. Baker, et al. (1995). Color Atlas of Congenital Heart Disease. London, Mosby-Wolfe.

Hoffman, E. A. and E. L. Ritman (1985). "Shape and dimensions of cardiac chambers: importance of CT section thickness and orientation." Radiology **155**(3): 739-44.

Hogers, B., L. van der Weerd, et al. (2009). "Non-invasive tracking of avian development in vivo by MRI." NMR Biomed **22**(4): 365-73.

Hornberger, L. K., S. P. Sanders, et al. (1995). "Left heart obstructive lesions and left ventricular growth in the midtrimester fetus. A longitudinal study." Circulation **92**(6): 1531-8.

Huijsmans, D. P., W. H. Lamers, et al. (1986). "Toward computerized morphometric facilities: a review of 58 software packages for computer-aided three-dimensional reconstruction, quantification, and picture generation from parallel serial sections." Anat Rec **216**(4): 449-70.

Hutchins, G. M., A. Kessler-Hanna, et al. (1988). "Development of the coronary arteries in the embryonic human heart." Circulation **77**(6): 1250-7.

Hyett, J., G. Moscoso, et al. (1995). "Morphometric analysis of the great vessels in early fetal life." Hum Reprod **10**(11): 3045-8.

Johnson, G. A. and R. R. Maronpot (1989). "Magnetic resonance microscopy of chemically-induced liver foci." Toxicol Pathol **17**(4 Pt 1): 613-6.

Johnson, J. T., M. S. Hansen, et al. (2006). "Virtual histology of transgenic mouse embryos for high-throughput phenotyping." PLoS Genet **2**(4): e61.

Jouk, P. S., Y. Usson, et al. (2000). "Three-dimensional cartography of the pattern of the myofibres in the second trimester fetal human heart." Anat Embryol (Berl) **202**(2): 103-18.

Kaufman, M. H., R. M. Brune, et al. (1997). "Computer-aided 3-D reconstruction of serially sectioned mouse embryos: its use in integrating anatomical organization." Int J Dev Biol **41**(2): 223-33.

Klinkenbijl, J. and A. C. Wenink (1988). "Morphology of sections through the fetal heart." Int J Cardiol **20**(1): 87-98.

Kouchoukos, N. T., E. H. Blackstone, et al. (2003). Kirklin/Barratt-Boyes Cardiac Surgery, Churchill Livingston.

Kruithof, B. P., S. A. Krawitz, et al. (2007). "Atrioventricular valve development during late embryonic and postnatal stages involves condensation and extracellular matrix remodeling." Dev Biol **302**(1): 208-17.

Laan, A. C., W. H. Lamers, et al. (1989). "Deformation-corrected computer-aided three-dimensional reconstruction of immunohistochemically stained organs: application to the rat heart during early organogenesis." Anat Rec **224**(3): 443-57.

Lamers, W. H., A. Wessels, et al. (1992). "New findings concerning ventricular septation in the human heart. Implications for maldevelopment." Circulation **86**(4): 1194-205.

Lange, L. W., D. J. Sahn, et al. (1980). "Qualitative real-time cross-sectional echocardiographic imaging of the human fetus during the second half of pregnancy." Circulation **62**(4): 799-806.

Larsen, W. J. (2001). Human Embryology. New York, Churchill Livingstone.

Leslie, J., S. Shen, et al. (1983). "The human fetal heart in the second trimester of gestation: a gross morphometric study of normal fetuses." Am J Obstet Gynecol **145**(3): 312-6.

Licata, R. H. (1954). "The human embryonic heart in the ninth week." Am J Anat **94**(1): 73-125.

Mandarim-de-Lacerda, C. A. (1991). "Growth allometry of the myocardium in human embryos (from stages 15 to 23)." Acta Anat (Basel) **141**(3): 251-6.

Maroun, L. L. and N. Graem (2005). "Autopsy standards of body parameters and fresh organ weights in nonmacerated and macerated human fetuses." Pediatr Dev Pathol **8**(2): 204-17.

Martinez, H. G., S. I. Prajapati, et al. (2009). "Images in cardiovascular medicine: Microscopic computed tomography-based virtual histology for visualization and morphometry of atherosclerosis in diabetic apolipoprotein e mutant mice." Circulation **120**(9): 821-2.

McLean, M. and J. W. Prothero (1991). "Three-dimensional reconstruction from serial sections. V. Calibration of dimensional changes incurred during tissue preparation and data processing." Anal Quant Cytol Histol **13**(4): 269-78.

McLean, M. R. and J. Prothero (1987). "Coordinated three-dimensional reconstruction from serial sections at macroscopic and microscopic levels of resolution: the human heart." Anat Rec **219**(4): 374-7, 434-9.

Meyer, E. P. and V. J. Domanico (1988). "Three-dimensional reconstruction: a tissue embedding method for alignment of serial sections." J Neurosci Methods **26**(2): 129-32.

Mohun, T. J., L. M. Leong, et al. (2000). "The morphology of heart development in Xenopus laevis." Dev Biol **218**(1): 74-88.

Moore, K. L. (2003). The Developing Human. Clinically Oriented Embryology. Philadelphia, W.B. Saunders Company.

Moorman, A., S. Webb, et al. (2003). "Development of the heart: (1) formation of the cardiac chambers and arterial trunks." Heart **89**(7): 806-14.

Moss, V. A., D. M. Jenkinson, et al. (1990). "Automated image segmentation and serial section reconstruction in microscopy." J Microsc **158**(Pt 2): 187-96.

Nelson, T. R., D. H. Pretorius, et al. (1996). "Three-dimensional echocardiographic evaluation of fetal heart anatomy and function: acquisition, analysis, and display." J Ultrasound Med **15**(1): 1-9 quiz 11-2.

Nowak, D., J. Gielecki, et al. (2008). "Types of coronary vasculature in the human fetus: an autopsy study." Cells Tissues Organs **188**(4): 393-9.

O'Rahilly, R. (1971). "The timing and sequence of events in human cardiogenesis." Acta Anat (Basel) **79**(1): 70-5.

O'Rahilly, R. (1973). Developmental stages in human embryos, including a survey of the Carnegie collection. Part A. Embryos of the first three weeks (stage 1 to 9). Washington D.C., Carnegie Instituion of Washington.

O'Rahilly, R. (1979). "Early human development and the chief sources of information on staged human embryos." Eur J Obstet Gynecol Reprod Biol **9**(4): 273-80.

O'Rahilly, R. (1987). Developmental Stages in Human Embryos: Including a Revision of Streeter's "Horizons" and a Survey of the Carnegie Collection. Washington DC, Carnegie Institution of Washington.

O'Rahilly, R. and F. Muller (1987). Developmental Stages in Human Embryo, Carnegie Institution of Washington.

O'Rahilly, R. and F. Muller (1996). Human Embryology and Tetralogy. New York, Wiley-Liss.

Odgaard, A., K. Andersen, et al. (1990). "A direct method for fast three-dimensional serial reconstruction." J Microsc **159**(Pt 3): 335-42.

Odgaard, A. and H. J. Gundersen (1993). "Quantification of connectivity in cancellous bone, with special emphasis on 3-D reconstructions." Bone **14**(2): 173-82.

Ohayon, J., Y. Usson, et al. (1999). "Fibre Orientation in Human Fetal Heart and Ventricular Mechanics : A Small Perturbation Analysis." Comput Methods Biomech Biomed Engin **2**(2): 83-105.

Orts-Llorca, F., J. Puerta Fonolla, et al. (1982). "The formation, septation and fate of the truncus arteriosus in man." J Anat **134**(Pt 1): 41-56.

Parker, J. D. and M. C. Warner (1970). "Effects of fixation, dehydration and staining on dimensions of myxosporidan." J Wildl Dis **6**(4): 448-56.

Payne, K. T. and G. M. Hutchins (1973). "Rapid production of reconstruction drawings from serial sections." Am J Clin Pathol **60**(6): 820-2.

Petiet, A. E., M. H. Kaufman, et al. (2008). "High-resolution magnetic resonance histology of the embryonic and neonatal mouse: a 4D atlas and morphologic database." Proc Natl Acad Sci U S A **105**(34): 12331-6.

Pexieder, T., A. C. Wenink, et al. (1989). "A suggested nomenclature for the developing heart. Working Group for Embryology and Teratology of the European Society of Cardiology." Int J Cardiol **25**(3): 255-63.

Pieles, G., S. H. Geyer, et al. (2007). "microMRI-HREM pipeline for high-throughput, high-resolution phenotyping of murine embryos." J Anat **211**(1): 132-7.

Prothero, J. S. and J. W. Prothero (1986). "Three-dimensional reconstruction from serial sections. IV. The reassembly problem." Comput Biomed Res **19**(4): 361-73.

Reisner, A. H., C. A. Bucholtz, et al. (1990). "Two- and three-dimensional image reconstructions from stained and autoradiographed histological sections." Comput Appl Biosci **6**(3): 253-61.

Rosenthal, J., V. Mangal, et al. (2004). "Rapid high resolution three dimensional reconstruction of embryos with episcopic fluorescence image capture." Birth Defects Res C Embryo Today **72**(3): 213-23.

Rousselle, S. and J. Wicks (2008). "Preparation of medical devices for evaluation." Toxicol Pathol **36**(1): 81-4.

Rude, F. P., L. Anderson, et al. (1994). "Three-dimensional reconstructions of the primary palate region in normal human embryos." Anat Rec **238**(1): 108-13.

Rydmark, M., T. Jansson, et al. (1992). "Computer-assisted realignment of light micrograph images from consecutive section series of cat cerebral cortex." J Microsc **165**(Pt 1): 29-47.

Sanchez-Quintana, D., V. Garcia-Martinez, et al. (1995). "Morphological changes in the normal pattern of ventricular myoarchitecture in the developing human heart." Anat Rec **243**(4): 483-95.

Sanchez-Quintana, D., V. Garcia-Martinez, et al. (1990). "Myocardial fiber architecture in the human heart. Anatomical demonstration of modifications in the normal pattern of ventricular fiber architecture in a malformed adult specimen." Acta Anat (Basel) **138**(4): 352-8.

Scarborough, J., J. F. Aiton, et al. (1997). "The study of early human embryos using interactive 3-dimensional computer reconstructions." J Anat **191 (Pt 1)**: 117-22.

Schneider, J. E., S. D. Bamforth, et al. (2003). "Rapid identification and 3D reconstruction of complex cardiac malformations in transgenic mouse embryos using fast gradient echo sequence magnetic resonance imaging." J Mol Cell Cardiol **35**(2): 217-22.

Schneider, J. E. and S. Bhattacharya (2004). "Making the mouse embryo transparent: identifying developmental malformations using magnetic resonance imaging." Birth Defects Res C Embryo Today **72**(3): 241-9.

Schneider, J. E., J. Bose, et al. (2004). "Identification of cardiac malformations in mice lacking Ptdsr using a novel high-throughput magnetic resonance imaging technique." BMC Dev Biol **4**: 16.

Sedmera, D., T. Pexieder, et al. (2000). "Developmental patterning of the myocardium." Anat Rec **258**(4): 319-37.

Seo, J. W., N. A. Brown, et al. (1992). "Abnormal laterality and congenital cardiac anomalies. Relations of visceral and cardiac morphologies in the iv/iv mouse." Circulation **86**(2): 642-50.

Sharpe, J., U. Ahlgren, et al. (2002). "Optical projection tomography as a tool for 3D microscopy and gene expression studies." Science **296**(5567): 541-5.

Shinebourne, E. A., F. J. Macartney, et al. (1976). "Sequential chamber localization--logical approach to diagnosis in congenital heart disease." Br Heart J **38**(4): 327-40.

Sjostrand, F. S. (1958). "Ultrastructure of retinal rod synapses of the guinea pig eye as revealed by three-dimensional reconstructions from serial sections." J Ultrastruct Res **2**(1): 122-70.

Skoglund, T., R. Pascher, et al. (1993). "3D reconstruction of biological objects from sequential image planes--applied on cerebral cortex from cat." Comput Med Imaging Graph **17**(3): 165-74.

Smith, B. R. (2001). "Magnetic resonance microscopy in cardiac development." Microsc Res Tech **52**(3): 323-30.

Smith, B. R., E. L. Effmann, et al. (1992). "MR microscopy of chick embryo vasculature." J Magn Reson Imaging **2**(2): 237-40.

Smith, D. L. and I. C. Schoonover (1953). "Direct filling resins: dimensional changes resulting from polymerization shrinkage and water sorption." J Am Dent Assoc **46**(5): 540-4.

Smrcek, J. M., C. Berg, et al. (2006). "Early fetal echocardiography: heart biometry and visualization of cardiac structures between 10 and 15 weeks' gestation." J Ultrasound Med **25**(2): 173-82; quiz 183-5.

Soufan, A. T., J. M. Ruijter, et al. (2003). "Three-dimensional reconstruction of gene expression patterns during cardiac development." Physiol Genomics **13**(3): 187-95.

Spencer, T. N., K. J. Botting, et al. (2006). "Contractile and Ca2+-handling properties of the right ventricular papillary muscle in the late-gestation sheep fetus." J Appl Physiol **101**(3): 728-33.

Steigman, S., M. Weinreb, Jr., et al. (1984). "Histomorphometric evaluation of the dimensional changes in rat-incisor tissues following histological processing and embedding in paraffin wax and glycol methacrylate." Arch Oral Biol **29**(5): 395-8.

Stockley, E. W., H. M. Cole, et al. (1993). "A system for quantitative morphological measurement and electronic modelling of neurons: three-dimensional reconstruction." J Neurosci Methods **47**(1-2): 39-51.

Streeter, G. L. (1942). "Developmental horisons in human embryos: Description of age group XI, 13 to 20 somites, and age group XII, 21 to 29 somites. ." Contrib Embryol Carnegie Inst Wash **36**: 211.

Streeter, G. L. (1945). "Developmental horisons in human embryos: Description of age group XIII, embryos about 4 or 5 mm long, and age group XIV, period of indentation of the lens vesicle." Contrib Embryol Carnegie Inst Wash **31**: 27.

Streeter, G. L. (1948). "Developmental horisons in human embryos: Description of age group XV, XVI, XVII, XVIII, being the third issue of a survey of the Carnegie Collection." Contrib Embryol Carnegie Inst Wash **32**: 133.

Streeter, G. L. (1949). "Developmental horizons in human embryos; a review of the histogenesis of cartilage and bone." Contrib Embryol **33**(213-221): 149-68.

Streeter, G. L. (1951). "Developmental horisons in human embryos: Description of age group XIX, XX, XXI, XXII, and XXIII, being the fifth issue of a survey of the Carnegie Collection." Contrib Embryol Carnegie Inst Wash **34**: 165.

Streicher, J., M. A. Donat, et al. (2000). "Computer-based three-dimensional visualization of developmental gene expression." Nat Genet **25**(2): 147-52.

Streicher, J., W. J. Weninger, et al. (1997). "External marker-based automatic congruencing: a new method of 3D reconstruction from serial sections." Anat Rec **248**(4): 583-602.

Sundsten, J. W. and J. W. Prothero (1983). "Three-dimensional reconstruction from serial sections: II. A microcomputer-based facility for rapid data collection." Anat Rec **207**(4): 665-71.

Szpinda, M. (2007). "Morphometric study of the ascending aorta in human fetuses." Ann Anat **189**(5): 465-72.

Theiler, K. (1972). The House Mouse. New York, Springer-Verlag.

Thompson, P. (1907). "Description of a Human Embryo of Twenty-Three Paired Somites." J Anat Physiol **41**(Pt 3): 159-71.

Tynan, M. J., A. E. Becker, et al. (1979). "Nomenclature and classification of congenital heart disease." Br Heart J **41**(5): 544-53.

Vasudeva, G. (2009). "Monomer systems for dental composites and their future: a review." J Calif Dent Assoc **37**(6): 389-98.

Verbeek, F. J., D. P. Huijsmans, et al. (1995). "Design and implementation of a database and program for 3D reconstruction from serial sections: a data-driven approach." Microsc Res Tech **30**(6): 496-512.

Vernall, D. G. (1962). "The human embryonic heart in the seventh week." Am J Anat **111**: 17-24.

Vinals, F., R. Ascenzo, et al. (2008). "Fetal echocardiography at 11 + 0 to 13 + 6 weeks using four-dimensional spatiotemporal image correlation telemedicine via an Internet link: a pilot study." Ultrasound Obstet Gynecol **31**(6): 633-8.

Vinegoni, C., D. Razansky, et al. (2009). "Born normalization for fluorescence optical projection tomography for whole heart imaging." J Vis Exp(28).

Vinegoni, C., D. Razansky, et al. (2009). "Normalized Born ratio for fluorescence optical projection tomography." Opt Lett **34**(3): 319-21.

Webb, S., N. A. Brown, et al. (1996). "The structure of the mouse heart in late fetal stages." Anat Embryol (Berl) **194**(1): 37-47.

Webb, S., N. A. Brown, et al. (1998). "Formation of the atrioventricular septal structures in the normal mouse." Circ Res **82**(6): 645-56.

Weninger, W. J., S. H. Geyer, et al. (2006). "High-resolution episcopic microscopy: a rapid technique for high detailed 3D analysis of gene activity in the context of tissue architecture and morphology." Anat Embryol (Berl) **211**(3): 213-21.

Weninger, W. J., B. Maurer, et al. (2009). "Measurements of the diameters of the great arteries and semi-lunar valves of chick and mouse embryos." J Microsc **234**(2): 173-90.

Weninger, W. J., S. Meng, et al. (1998). "A new episcopic method for rapid 3-D reconstruction: applications in anatomy and embryology." Anat Embryol (Berl) **197**(5): 341-8.

Weninger, W. J. and T. Mohun (2002). "Phenotyping transgenic embryos: a rapid 3-D screening method based on episcopic fluorescence image capturing." Nat Genet **30**(1): 59-65.

Weninger, W. J. and T. J. Mohun (2007). "Three-dimensional analysis of molecular signals with episcopic imaging techniques." Methods Mol Biol **411**: 35-46.

Wenink, A. C. (1992). "Quantitative morphology of the embryonic heart: an approach to development of the atrioventricular valves." Anat Rec **234**(1): 129-35.

Wenink, A. C. and A. C. Gittenberger-de Groot (1982). "Left and right ventricular trabecular patterns. Consequence of ventricular septation and valve development." Br Heart J **48**(5): 462-8.

Wessels, A. and D. Sedmera (2003). "Developmental anatomy of the heart: a tale of mice and man." Physiol Genomics **15**(3): 165-76.

Whiten, S., S. D. Smart, et al. (1998). "Computer-aided interactive three-dimensional reconstruction of the embryonic human heart." J Anat **193 (Pt 3)**: 337-45.

Wong, Y. M., R. P. Thompson, et al. (1983). "Computer reconstruction of serial sections." Comput Biomed Res **16**(6): 580-6.

Yamada, S., H. Itoh, et al. (2007). "Computerized three-dimensional analysis of the heart and great vessels in normal and holoprosencephalic human embryos." Anat Rec (Hoboken) **290**(3): 259-67.

Yelbuz, T. M., X. Zhang, et al. (2003). "Images in cardiovascular medicine. Approaching cardiac development in three dimensions by magnetic resonance microscopy." Circulation **108**(22): e154-5.

Zaffran, S., R. G. Kelly, et al. (2004). "Right ventricular myocardium derives from the anterior heart field." Circ Res **95**(3): 261-8.

Zhou, Y. Q., F. S. Foster, et al. (2002). "Applications for multifrequency ultrasound biomicroscopy in mice from implantation to adulthood." Physiol Genomics **10**(2): 113-26.

Zosmer, N., D. Jurkovic, et al. (1996). "Selection and identification of standard cardiac views from three-dimensional volume scans of the fetal thorax." J Ultrasound Med **15**(1): 25-32.